University of Granada
Faculty of Science

The work presented to obtain the title of
DOCTOR OF PHILOSOPHY

Martin Jelínek
Instituto de Astrofísica de Andalucía CSIC

STUDY OF GAMMA-RAY BURSTS WITH ROBOTIC TELESCOPES

Director de la tesis: Prof. Alberto J. Castro-Tirado, PhD.
Programa del estudio: Métodos y Técnicas Avanzadas en Física

Granada 2014

Editor: Editorial de la Universidad de Granada
Autor: Martin Jelínek
D.L.: GR 2285-2014
ISBN: 978-84-9083-346-9

ꝛe ſtellam vnã. In vtroq; humero ſiñgulas. In vtraq; mãma ſin/
gulas. ſed darioꝛé dextrã: ꝛ ſub ea alterã obſcurã: ꝛ i cubito dexti ro
clarã vnã. In zona vnã clari⁹ cęteris lucentẽ. hec ſtella arctur⁹ ap/
pellaꝛ. In vtriſq; pedib⁹ ſingulas: quę oio ſunt quatuoꝛdecim.

Boetes

Coronã humero ſiniſtro prope contingere arctophi
lax videꝛ: quę ante engonaſin dextri pedis calce cõ/
iungit. hęc cancro ꝛ leone exoꝛicte occidere: cũ ſcoꝛ/

STUDY OF GAMMA-RAY BURSTS WITH ROBOTIC TELESCOPES

Martin Jelínek
Instituto de Astrofísica de Andalucía CSIC

RESÚMEN

El trabajo trata de explosiones de rayos gamma (gamma-ray bursts, GRBs), observados como breves destellos de radiación gamma de origen cósmico. El fenómeno, que es actualmente considerado como uno de los fenómenos más energéticos del universo, fue descubierto en 1967.

Actualmente, los GRBs se detectan y localizan automáticamente por satélites especializados, y las alertas se generan y envían a telescopios robóticos situados en la Tierra. De este modo, los estudios multirrango, usando datos que abarcan los rayos gamma, rayos X, el visible, infrarrojos, y las ondas de radio, permiten una visión completa de estos eventos, tras el descubrimiento en 1997 de las postluminiscencias la emisión del GRB que sigue a los rayos gamma en otras longitudes de onda.

Esta es una selección de los resultados obtenidos entre 2004 y 2014, durante el desarrollo de mi tesis en el Instituto de Astrofísica de Andalucía, situado en Granada, y en las estaciones BOOTES en Espaa.

El capítulo I ofrece una breve introducción a la física de los GRBs, los seis siguientes capítulos son estudios de explosiones de rayos gamma individuales. El capítulo VIII es un resumen de todos los seguimientos de GRBs realizados con éxito por BOOTES-1B y BOOTES-2 durante la última década. El último capítulo es esencialmente una introducción al *Compact Low Resolution Spectrograph* (COLORES), un instrumento ligero tipo FOSC que hemos desarrollado y que está operando exitosamente en BOOTES-2 desde 2012.

SUMMARY

The work talks about gamma-ray bursts (GRBs), observed as brief flashes of gamma radiation of cosmic origin. The phenomena, now considered one of the most energetic phenomena in the universe, was discovered in 1967.

Nowadays, with specialized satellites, GRBs are detected and localized automatically, and triggers are generated and sent to ground-based robotic telescopes. This way, a multi wavelength studies, employing data ranging from gamma-rays through X-rays and optical to radio wavelengths, permit a complex view onto these events, since the discovery of the afterglows – the emission on other wavelengths in 1997

This is a selection of results I obtained between 2004 and 2014, while working on my PhD thesis in the Andalusian Institute of Astrophysics in Granada and at BOOTES stations in Spain.

Chapter I provides a brief introduction into the GRB physics, the following six chapters are studies of individual gamma-ray bursts. Chapter VIII is an effort to summarize all the successful GRB follow-ups performed by BOOTES-1B and BOOTES-2 during the past decade. The last chapter is essentially a user's introduction to the Compact Low Resolution Spectrograph (COLORES), a lightweight FOSC instrument we developed and have been successfully operating at BOOTES-2 since 2012.


VRANIA
FD

INDEX

Introduction

This tesis is an amalgamation of my activities I did over the past 10 years. It could be described as a voyage from an interest about GRBs, and their observation using simple photometric observation methods, towards construction of our own specialized robotic telescope and a spectrograph. A path, which like a spectrum ranges throughout the field between theoretical and practical astronomy, or between physics and instrumentation. The ordering of the chapters intends to follow the dispersion. The thesis starts with a brief introduction to the theory of gamma-ray bursts, goes on with GRBs observed by non-BOOTES telescopes, then GRBs observed by our system, and concludes with two chapters dedicated to overall BOOTES performance and the spectrograph COLORES we constructed for BOOTES-2. From ideas to tools, from physics to design, from theory to practice. And, by chance, this order is also mostly historical.

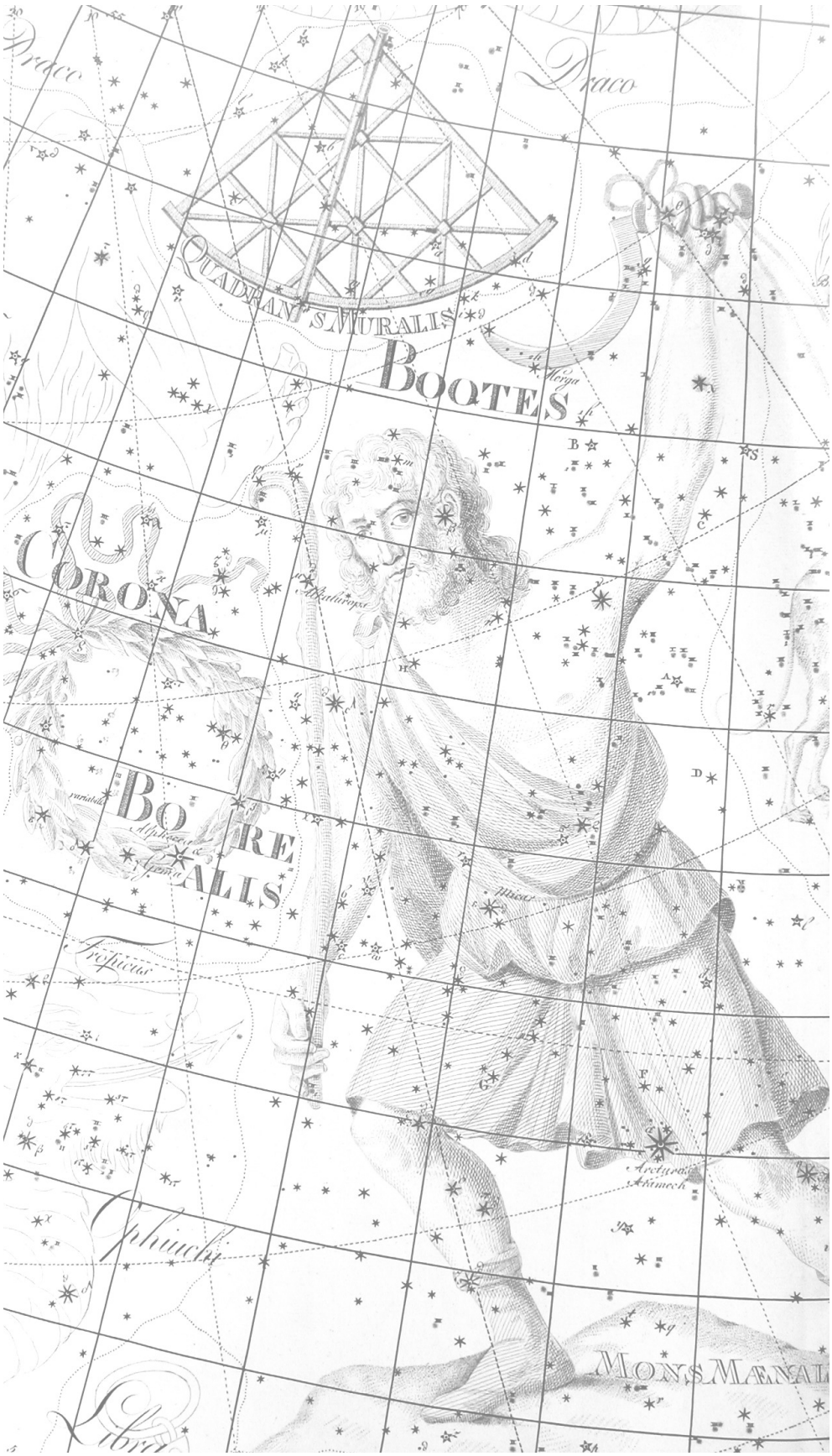
Draco
QUADRANS MURALIS
BOOTES
CORONA
BOREALIS
Arcturus
Akrimech
MONS MÆNAL

I. Cosmic Gamma-ray bursts

Gamma-ray bursts (GRB) were discovered by satellites *Vela* in 1967, as one of the most energetic phenomena of the universe, Klebesadel et al. (1973). The GRBs show up as brief pulses (from few miliseconds to several hundred seconds) (Fig 3) of high-energy gamma ray photons (in MeV range). The impossibility to focus gamma-rays made their precise localization challenging, and the data defficiency of observational data created space for an abundancy of theoretical models. Majority of these models supported their Galactic origin, but BATSE[1)] has shown that the distribution of GRBs on the celestial sphere is isotropic (Fig 2), ruling out the Milky Way as their origin and supporting the cosmological origin. With the first detection of an X-ray counterpart (Costa et al., 1997) an in optical wavelengths (van Paradijs et al., 1997) for GRB 970228, and with the first redshift ($z = 0.835$ for GRB 970508), the cosmological origin was confirmed. These counterparts are referred to as "afterglows", in general have longer duration than the gamma-ray emission, and were anticipated theoretically by Paczynski & Rhoads (1993). At present, the highest measured redshift for a gamma-ray burst is $z = 8.2$ for GRB 090423 (Tanvir et al., 2009).

The examination of GRB durations as detected by BATSE reveals a bimodal distribution (Fig 1) with GRBs *short*, with mean duration < 2 s, and *long*, that take more than 2 s (Kouveliotou et al., 1993). Nowadays it is generally accepted that the long GRBs (LGRB), are associated with massive stars and that the explosion is related to its collapse, which gives birth to a black hole (Woosley, 1993). This theory is supported by observations of supernovae superposed to the afterglow emission, and it is in agreement with their redshift distribution (Fryer et al., 1999). Studies of host galaxies revealed a strong affinity to star-forming regions, additionally supporting this theory (Gorosabel et al., 2006).

Starting ten years ago, thanks to the rapid and precise localizations by satelite *Swift*, also counterparts of the short GRBs (SHB[2)]). As well as the

[1)] Burst and Transient Source Explorer, an experiment onboard the satellite *Compton*, 1991 – 2001

[2)] *Short hard burst*, although nowadays the hardness is believed to be rather an observational artefact.

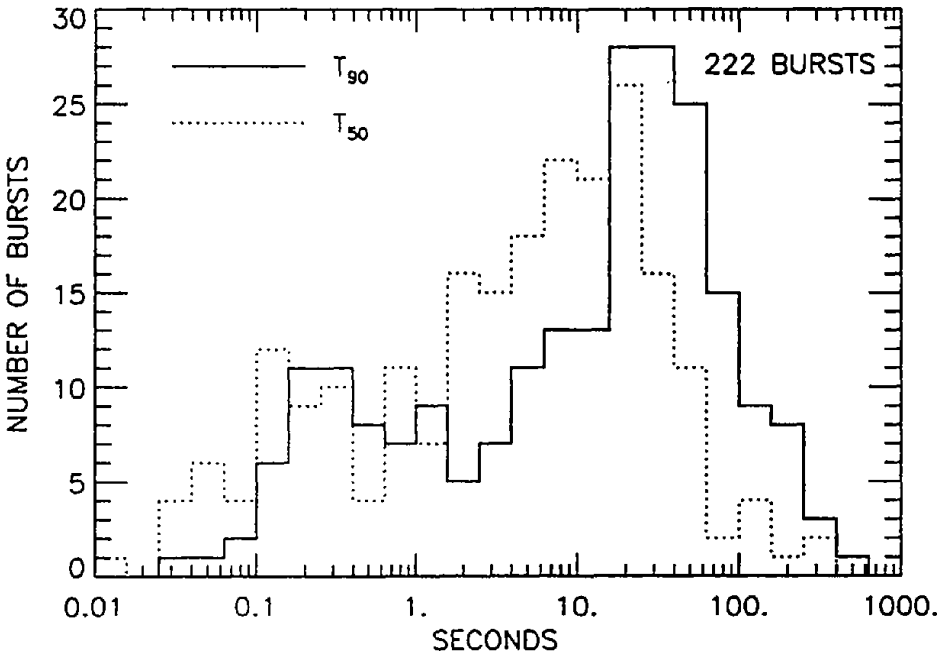

Figure 1 GRB bimodality.

long GRBs, the short GRBs are at cosmological distances, although the redshifts tend to be lower. This seems to be in agreement with the model of a neutron star[3)] pair merging, which need timescale of 10^9 years – comparable with the age of the universe – to form, and then to lose the orbital energy via gravitational waves to reach the moment of coalescence. Observations of the short GRB host galaxies show these to be of late, more evolved types than those hosting LGRBs, further supporting this scenario.

The penetration power of the gamma-ray emission, together with the enormous released energy, causes GRBs to be observable across a great range of redshifts. This makes them an interesting tool to study the Universe on a high redshift scale. If the LGRBs are indeed related to the massive star deaths, they can be used to trace star formation history of the universe. Also, GRBs can be used as a mechanism to select distant galaxies for statistical purposes, which has an advantage against other selection mechanisms, practically removing the tendency to select bright galaxies and the low-light tail of the luminosity function.

GRBs can be used as more than mere identifiers for other studies, but also their properties can be useful for cosmological studies. Before this is made

[3)] Or in general black hole + neutron star, neutron star + neutron star, neutron star + white dwarf etc.

possible, a distance estimation has to be established, preferrably based only on the high-energy emission. Various such indicators have been proposed, including Lag-Luminosity correlation (Norris, 2002), varibility-luminosity relation (Fenimore & Ramirez-Ruiz, 2000), and the relation of Amati et al. (2002) (Fig 6), relating the equivalent isotropic energy and the peak of high energy spectrum. These correlations are not very strong and it is difficult to use them to obtain precise estimations of cosmological parameters (Bloom et al., 2003).

1.1 Theoretical models

The observations provided a complete multiwavelength spectrum of a GRB, but the mechanism to produce it is still a little enigmatic. Not to surprise, until 1994 there had been more than 150 theoretical models published (see Nemiroff, 1994). The fact that nowadays we know that most – if not all – GRBs happen in other galaxies, descarted most of these models but the few which are able to produce 10^{51-54} erg in a few seconds:

Merger: a merging binary of neutron stars, a neutron star and a white dwarf, or a neutron star and a black hole (Narayan et al., 1992). Neutron stars may take $\sim 10^9$ years to produce the event, they are produced during supernovae, which may give them powerfu kicks so that they have enough time and speed to be found far away from the regions of their origin. This

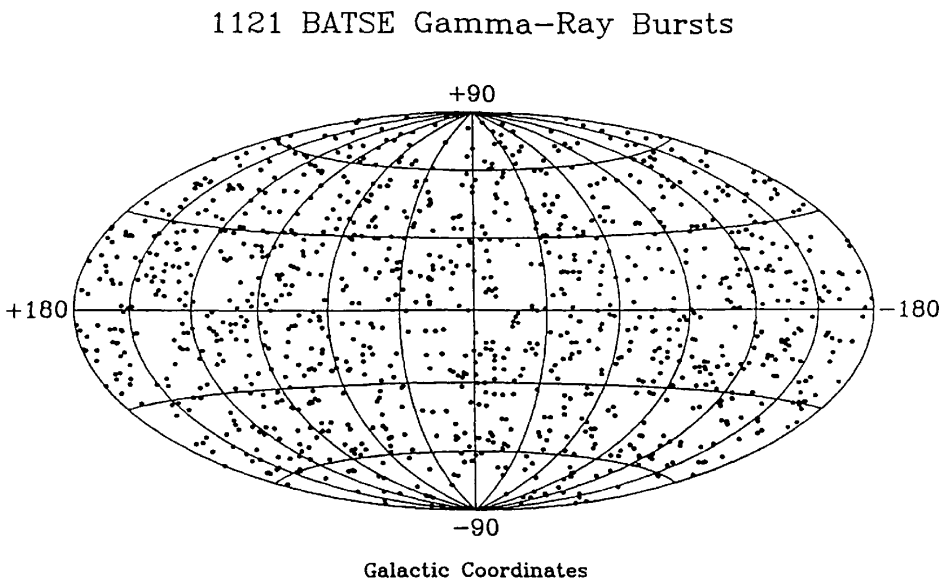

Figure 2 GRB distribution.

model is often mentioned with short GRBs, although there is no direct proof.

Supernova: A failed or high-rotation speed supernova, in which a massive star produces a "dirty fireball" with a luminosity up to 300× greater than a normal supernova. The end of such stars happens in $\sim 10^6$ years, and a natural consequence of this model is that the GRBs would be associated with dense, gas and dust rich regions and regions with active star formation. Given that there have been detected supernova signatures in spectra and light curved of the nearby GRBs, this is the model expected to apply to the long GRBs.

In this model, a series of relativistic internal shocks within the ejecta, is expected to be responsible for the γ-ray emission and a small fraction of other wavelength short-lived ($\sim$seconds) emission, while a shock of the ejecta against the surrounding interstellar material is responsible for the X-ray and optical emission of the long-lived ($\sim$days) afterglow (see Meszaros et al.,

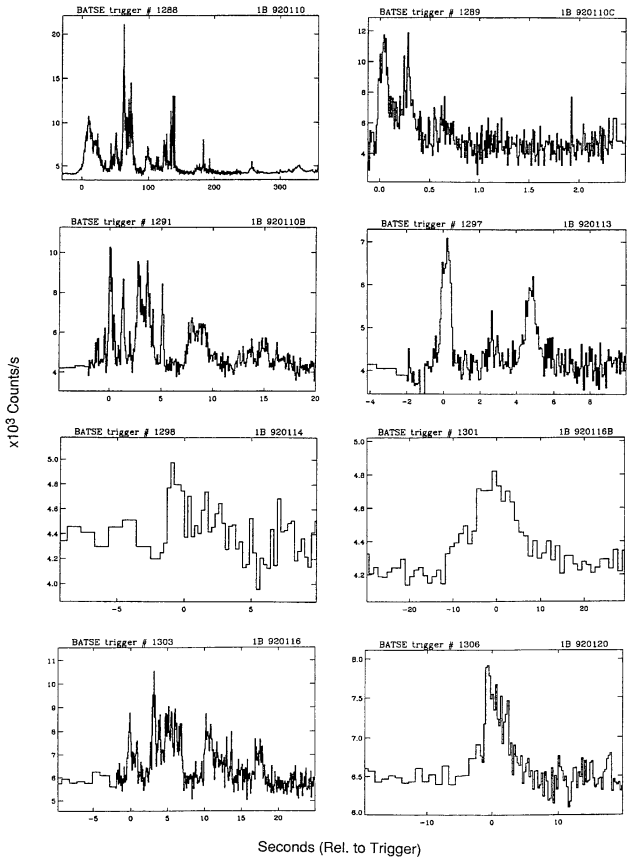

Figure 3 GRB lightcurves.

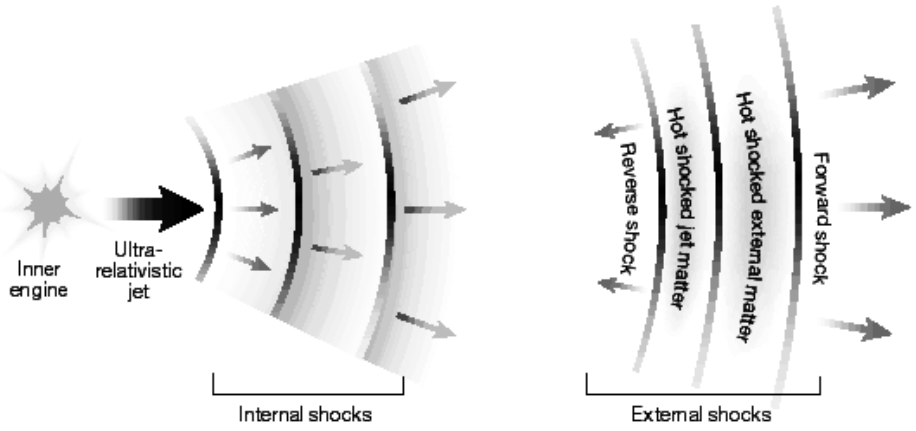

Figure 4 GRB shock.

1994).

The observational characteristics of the counterparts of GRBs have accommodated within models called "fireball" (eg. Meszaros et al., 1994). In them, a compact source releases $\sim 10^{53}$ erg in a few seconds. The plasma is accelerated to relativistic speeds (forming the so-called fireball) and the emitted radiation is because of electrons with very high Lorentz factors. The spherical shock wave moves ahead of the fireball, decelerates hitting and sweeping out the interstellar medium it finds in its way, producing synchrotron emission observed – almost always – from the X-ray up to the radio waves (the already outlined *afterglow*).

The properties of such a fireball can be derived form the spectral characteristics of the sinchritron radiation (Sari et al., 1998). The multiwavelength spectrum is then described by three basic parameters: the *synchrotron frequency* $\nu_{\rm m}$: the electron population has some initial distribution of lorenz factors $\gamma_{\rm e}$ in a form of a power las $\mathrm{d}M\mathrm{d}\gamma_e \sim \gamma_e^- p$ for values larger than the minimum lorentz factor $\gamma_e > \gamma_{\rm m}$ (i.e. above the synchrotron frecuency $\gamma_{\rm m}$), which corresponds to the lowest energy electrons. The *cooling frecuency* $\nu_{\rm c}$: associated to the electron cooling: slow ($\nu_{\rm c} > \nu_{\rm m}$) or fast ($\nu_{\rm c} < \nu_{\rm m}$); and the *maximum flux* $F_{\nu,\rm max}$.

Althoug initially $\nu_{\rm c} < \nu_{\rm m}$, at the time t_0, $\nu_{\rm c} = \nu_{\rm m}$. The characteristic frecuencies evolve as $\nu_{\rm c} \sim t^{-\frac{1}{2}}$ and $\nu_{\rm m} \sim t^{-\frac{3}{2}}$. At this moment, the shock wave evolution starts to be adiabatic, with $\nu_{\rm c} > \nu_{\rm m}$ and the spectrum changes as $F_\nu \sim \nu^{-\frac{p-1}{2}}$ for $\nu_{\rm m} < \nu < \nu_{\rm c}$; $F_\nu \sim \nu^{-\frac{p}{2}}$ for $\nu > \nu_{\rm c}$ and $F_\nu \sim \nu^{\frac{1}{3}}$ for $\nu > \nu_{\rm m}$. See Fig 5.

The evolution of flux for a given frequency as a function of time then

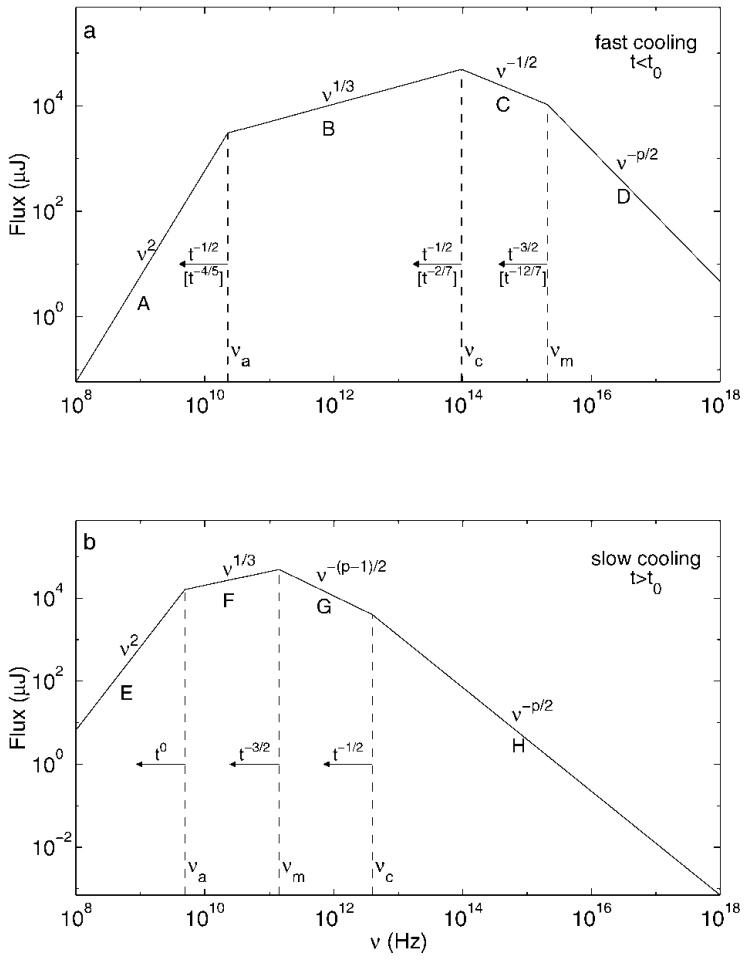

Figure 5 GRB spectrum.

comes as a function of evolution of $\nu_{\rm c}(\sim t^{-\frac{1}{2}})$ and $\nu_{\rm m}(\sim t^{-\frac{3}{2}})$. For $\nu < \nu_{\rm c}$ the flux decays as a power law of an exponent α, $F \sim t^{\alpha}$ with $\alpha = \frac{2-3p}{4}$, which allows for an independent determination of p.

Analogically to the forward shock, also reverse shock could be derived. Its contribution is expected to be of importance t optical wavelengths during the first seconds after the explosion (Sari & Piran, 1999). See Fig 7. first seconds after

The behaviour described in the previous paragraphs is indeed being observed for many afterglows, many poits, however, are left to be resolved.

1.2 Optical afterglows: a chronology

History of GRB discoveries is a history of singular events, making emphasis on the most important ones, the history is described here.

GRB 970228 was the first afterglow undoubtedly related to a GRB in both X-rays (Costa et al., 1997) and optical. The optical afterglow was detected 20 hours after the explosion was detected in γ-rays (van Paradijs et al., 1997), thanks to a precise localization of the X-ray emission by *Beppo-SAX*.

GRB 980425 was a GRB associated to a type Ic supernova discovered soon after in its errorbox. It is the first hint of a SN-GRB connection (Galama et al., 1998).

GRB 990123 was very bright and was accompanied with an exceptional, bright afterglow. It was interpreted as a reverse shock (Akerlof et al., 1999; Sari & Piran, 1999).

GRB 030329 This GRB happened so near that a transition from an afterglow spectrum to a spectum of a supernova could be observed. The relation

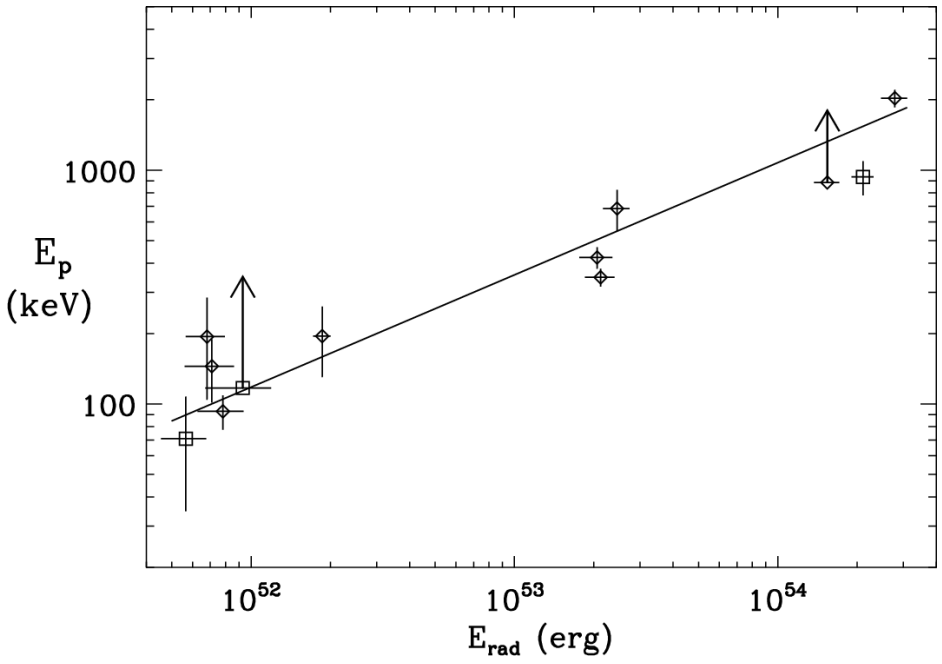

Figure 6 GRB amati relation.

of supernovas and gamma-ray burst is accepted (Hjorth et al., 2003; Stanek et al., 2003).

GRB 041227 = SGR 1806-20 within the Milky Way produced an explosion so huge that a lunar echo could be detected. The lightcurve in X-rays is similar to some short GRBs (Hurley et al., 2005).

GRB 050509B was a short GRB localized in X-rays with precision so good that a host galaxy could be identified. Although the optical counterpart remained undetected, permitted the first distance measurement for a shot GRB.

GRB 050709 was a short GRB with the first optical afterglow discovered in a galaxy with redshift $z = 0.1$: although also cosological, the energy released in short GRBs is much smaller than that of the long GRBs (Fox et al., 2005).

GRB 050904 was a very high redshift GRB. The first GRB where the Lyman-α blanketing prevented th optical afterglow to be detected bluewards of ~ 7000 Å, rendering it completely invisible to the human eye (Haislip et al., 2006).

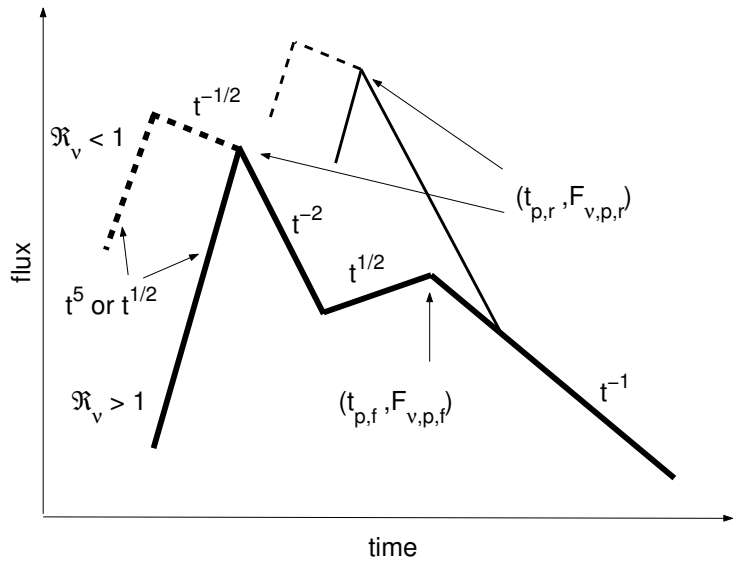

Figure 7 GRB zhang.

GRB 060121 was a short-duration GRB with many confusing properties, which opened the discussion on what really makes the "short" and "long" two different groups (de Ugarte Postigo et al., 2006).

GRB 060218 was a very peculiar GRB, very nearby and weak, associated to a bright supernova. It revived the discussion about how are really associated the GRBs and supernovas (Campana et al., 2006).

1.3 Present and future

Nowadays, *Swift* detects about a hundred GRBs per year, and of these, an optical afterglow is detected for about 40%. With the quantity, there are more questions than answers surfacing. The old image of a single explosion has to be joined with *X-ray flares*, the "restarts" of the internal engine, which were discovered by *Swift* (Burrows et al., 2005; Chincarini et al., 2005).

Another large amount of GRBs is being discovered by the satelite *Fermi* - a larger number by its Gamma-rey Burst Monitor (GBM), providing good spectral coverage but relatively poor localizations, and a much smaller number of GRBs is detected by its main instrument LAT, providing for both great data and localizations. Detections by *Fermi* permit observations of very high energy gamma-rays, up to GeV, a window which was inaccessible since the end of *CGRO*.

Combining this with the existence of advanced robotic telescopes on ground, as a new generation of BOOTES, we may be sure that in the near future many of the still perduring mysteries in this enigmatic field will be figured out.

References

Akerlof, C., Balsano, R., Barthelmy, S., et al. 1999, Nature, 398, 400
Amati, L., Frontera, F., Tavani, M., et al. 2002, A&A, 390, 81
Bloom, J. S., Frail, D. A., & Kulkarni, S. R. 2003, ApJ, 594, 674
Burrows, D. N., Hill, J. E., Nousek, J. A., et al. 2005, Space Science Reviews, 120, 165
Campana, S., Mangano, V., Blustin, A. J., et al. 2006, Nature, 442, 1008
Chincarini, G., Moretti, A., Romano, P., et al. 2005, `astro-ph/0506453`
Costa, E., Frontera, F., Heise, J., et al. 1997, Nature, 387, 783
de Ugarte Postigo, A., Castro-Tirado, A. J., Guziy, S., et al. 2006, ApJ, 648, L83
Fenimore, E. E. & Ramirez-Ruiz, E. 2000, ArXiv Astrophysics e-prints
Fox, D. B., Frail, D. A., Price, P. A., et al. 2005, Nature, 437, 845
Fryer, C. L., Woosley, S. E., & Hartmann, D. H. 1999, ApJ, 526, 152
Galama, T. J., Vreeswijk, P. M., van Paradijs, J., et al. 1998, Nature, 395, 670
Gorosabel, J., Castro-Tirado, A. J., Guziy, S., et al. 2006, A&A, 450, 87

Haislip, J. B., Nysewander, M. C., Reichart, D. E., et al. 2006, Nature, 440, 181
Hjorth, J., Sollerman, J., Møller, P., et al. 2003, Nature, 423, 847
Hurley, K., Boggs, S. E., Smith, D. M., et al. 2005, Nature, 434, 1098
Klebesadel, R. W., Strong, I. B., & Olson, R. A. 1973, ApJ, 182, L85+
Kouveliotou, C., Meegan, C. A., Fishman, G. J., et al. 1993, ApJ, 413, L101
Meszaros, P., Rees, M. J., & Papathanassiou, H. 1994, ApJ, 432, 181
Narayan, R., Paczynski, B., & Piran, T. 1992, ApJ, 395, L83
Nemiroff, R. J. 1994, Comments on Astrophysics, 17, 189
Norris, J. P. 2002, ApJ, 579, 386
Paczynski, B. & Rhoads, J. E. 1993, ApJ, 418, L5+
Sari, R. & Piran, T. 1999, ApJ, 520, 641
Sari, R., Piran, T., & Narayan, R. 1998, ApJ, 497, L17+
Stanek, K. Z., Matheson, T., Garnavich, P. M., et al. 2003, ApJ, 591, L17
Tanvir, N. R., Fox, D. B., Levan, A. J., et al. 2009, Nature, 461, 1254
van Paradijs, J., Groot, P. J., Galama, T., et al. 1997, Nature, 386, 686
Woosley, S. E. 1993, ApJ, 405, 273

II. GRB 051028: an intrinsically faint GRB at high redshift?

The question whether a significant fraction of gamma ray bursts (GRBs) are intrinsically faint or true dark events remains unsolved (see Filliatre et al., 2005; Castro-Tirado et al., 2007, and references therein). For instance, GRB 000418 was detected in the near-IR (Klose et al., 2000) and it is one of the reddest (R-K = 4) together with GRB 980329 (Reichart et al., 1999), GRB

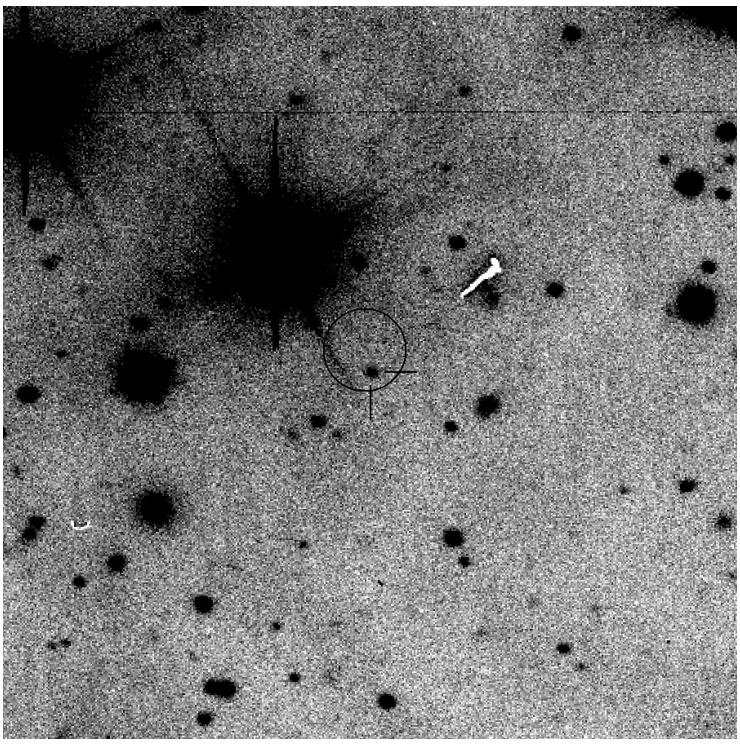

Figure 8 The deep R band image of the GRB 051028 field taken at the 4.2WHT on 28 Oct 2005. The optical afterglow within the $3\farcs8$ *Swift*/XRT error box (circle) is depicted. The field is $2\farcm5 \times 1\farcm9$ with North up and East to the left.

030115 (Levan et al., 2006) and the recent GRB 050915A (Bloom & Alatalo, 2005). In most cases, it has been suggested that the cause of the reddening was dust extinction in the host galaxy. On the other hand, GRB 021211 was found to be very dim at 24 hours, as a scaled-down version of GRB 990123 (Pandey et al., 2003).[4)]

With the launch of *Swift* in Nov 2004, which has the ability to follow-up the events detected by the GRB detector onboard (BAT) or by other satellites like *HETE-2* and *INTEGRAL*, it is possible to zoom in on this population of optically faint events in order to disentangle their nature.

GRB 051028 was one of such event. It was discovered by *HETE-2* on 28 Oct 2005, lying (90% confidence) on a $33' \times 18'$error box centred at coordinates: RA (J2000) = $01^{\rm h}48^{\rm m}38\overset{\rm s}{.}6$ Dec (J2000) = $+47°48'30\overset{''}{.}0$ (Hurley et al., 2005). The burst started at T_0 = 13:36:01.47 UT and a value of T_{90} = 16 s is derived, putting it in the "long-duration" class of GRBs. It had a fluence of 6 $\times 10^{-7}$ erg cm^{-2} in the 2-30 keV range and 6 $\times 10^{-6}$ erg cm^{-2} in the 30-400 keV range (Hurley et al., 2005). This event was also detected by *Konus*/WIND in the 20 keV - 2 MeV range, with a duration of $\approx$ 12 s, a fluence of $(6.78^{+0.61}_{-1.08}) \times 10^{-6}$ erg cm^{-2} in the 20 keV - 2 MeV range and a peak energy $E_p = 298^{+73}_{-50}$ keV (Golenetskii et al., 2005). *Swift*/XRT started to observe the field $\sim$ 7.1 hours after the event and detected the X-ray afterglow $5.2'$ away from the center of the initial $HETE-2$ error box (Racusin et al., 2005).

We report here results of multi-wavelength observations in optical and X-ray waveband and discuss the reasons for the apparent optical faintness of GRB 051028 in comparison with other bursts.

2.1 X-ray observations

We availed ourselves of the public X-ray observations from *Swift*/XRT which consists of four observations starting $\sim$ 7.1, 120, 150 and 230 hours after the event respectively. The detection in the first observation is significant (signal-to-noise ratio S/N$\sim$13.5), but in later observations the X-ray afterglow is weaker and it is detected with a signal-to-noise of 3.3, 2.9 and 2.7.

The XRT data is in photon counting mode and were reduced using the standard pipeline for XRT data using *Swift* software version 2.2[5)] and using the most recent calibration files. The data were analysed with the XSPEC version 11.3 (Arnaud, 1996) . Source and background regions were extracted using a circular aperture. Spectra were selected to have at least

[4)] Based on observations taken with the 1.34m Tautenburg telescope in Germany, with the 2.0 m Himalayan Chandra Telescope in India and with the 4.2 m William Herschel telescope at the Spanish Observatorio del Roque de los Muchachos in Canary Islands.

[5)] http://swift.gsfc.nasa.gov/docs/software/lheasoft/ /download.html

Table 1. Journal of optical observations of the GRB 051028 field.

Date of 2005 UT midtime	Telescope (instrument)	Filter	Exp. time (s)	Magnitude
Oct 28, 16:18	2.0 HCT (HFOSC)	R_c	300	20.63±0.04
Oct 28, 16:32	2.0 HCT (HFOSC)	R_c	300	20.72±0.05
Oct 28, 16:47	2.0 HCT (HFOSC)	R_c	300	21.14±0.07
Oct 28, 17:03	2.0 HCT (HFOSC)	R_c	300	21.27±0.07
Oct 28, 17:43	1.34 Taut (CCD)	R_c	1 080	21.23±0.13
Oct 28, 17:47	2.0 HCT (HFOSC)	R_c	300	21.17±0.08
Oct 28, 21:42	4.2 WHT (PFC)	R	300	21.97±0.05
Oct 29, 05:47	4.2 WHT (PFC)	R	120	22.8±0.3
Oct 29, 20:15	4.2 WHT (PFC)	R	720	>23.7
Oct 31, 22:14	4.2 WHT (PFC)	R	2 700	>25.1
Oct 28, 16:25	2.0 HCT (HFOSC)	I_c	300	19.79±0.11
Oct 28, 16:39	2.0 HCT (HFOSC)	I_c	300	19.94±0.06
Oct 28, 16:55	2.0 HCT (HFOSC)	I_c	300	20.29±0.09
Oct 28, 17:09	1.34 Taut (CCD)	I_c	1 080	20.5 ± 0.3
Oct 28, 17:10	2.0 HCT (HFOSC)	I_c	300	20.38±0.08
Oct 28, 17:55	2.0 HCT (HFOSC)	I_c	300	20.35±0.09
Oct 28, 19:12	1.34 Taut (CCD)	I_c	1 800	20.67±0.23
Oct 28, 20:33	1.34 Taut (CCD)	I_c	3 600	20.75±0.13
Oct 28, 22:50	1.34 Taut (CCD)	I_c	5 400	21.16±0.16
Oct 28, 18:28	1.34 Taut (CCD)	V	1 080	22.08±0.20

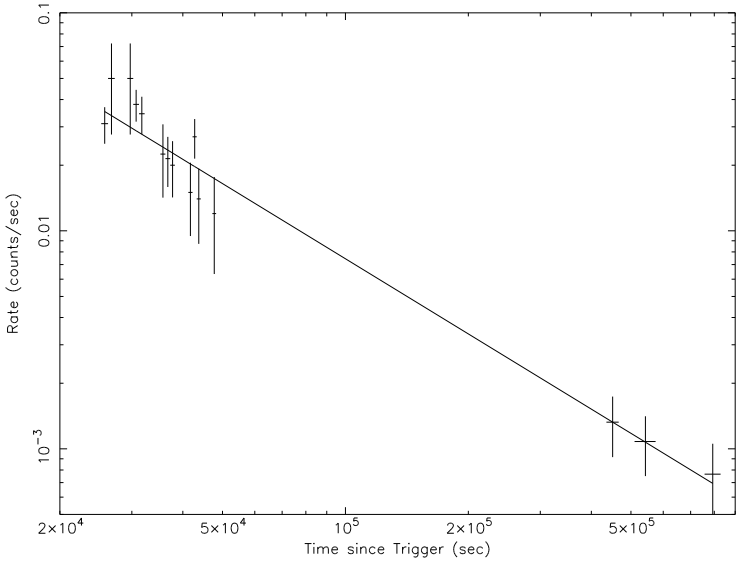

Figure 9 The X-ray lightcurve obtained by *Swift*/XRT starting 7.1 hours after the event onset and continuing up to 10 days later. The data are fit by a power-law decline exponent $\alpha_X = -1.1^{+0.1}_{-0.2}$.

20 counts/bin.

2.2 Optical observations

Target of Opportunity (ToO) observations in the optical were triggered starting 2.7 hours after the event at the 2.0 m Himalayan Chandra Telescope (HCT) at Indian Astronomical Observatory (HCO). $10'\times\ 10'$ frames were taken in imaging mode with the Himalaya Faint Object Spectrograph (HFOSC), covering only the central part of the large ($33'\times\ 18'$) *HETE-2* error box. Additional observations were conducted at the 1.34m Schmidt telescope in Tautenburg (providing a $42'\times\ 42'$ FOV and thus covering the large error box) and at the 4.2 m William Herschel Telescope (WHT + Prime Focus Camera) at Observatorio del Roque de los Muchachos in La Palma (Spain). A mosaic of 2 images ($15'\times\ 15'$ FOV) were taken in order to cover the entire *HETE-2* error box. Subsequently, follow-up observations were taken on the following days at the 4.2 m WHT. Table **??** displays the observing log. The optical field was calibrated using the calibration files provided by Henden (2005).

2.3 The X-ray afterglow

The X-ray data confirm the presence of a decaying X-ray source in the fraction (70 %) of the *HETE-2* error box covered by the *Swift*/XRT, as previously reported by Racusin et al. (2005). The X-ray position is RA(J2000) = $01^{\rm h}48^{\rm m}15\overset{\rm s}{.}1$, Dec(J2000) = $+47°45'12\overset{''}{.}9$ (l^{II} = 132°.72, b^{II} = -14°.03), with an estimated uncertainty of $3\overset{''}{.}8$ (Page et al., 2005, 90% containment).

The X-ray light curve in the energy range 0.3 to 10 keV is shown in Fig. 1. The early X-ray light curve (2×10^4 to 5×10^4 s) can be fit by a power-law decay $F_X \propto t^{\alpha_X}$ with exponent $\alpha_X = -1.43\pm0.60$ with a χ^2/d.o.f = 9.3/10. The data were also fit including the late time data up to 10 days ($\sim8.6\times10^5$ s) and resulted in a exponent $\alpha_X = -1.1^{+0.15}_{-0.2}$ with χ^2/d.o.f = 10.7/13) compatible with the power-law index obtained considering only the early observations. The value of α_X is dominated by the late time data and a break or flattening of the light curve at intervening times is possible and cannot be excluded by the observations.

A spectrum was extracted for the first observation starting at 7.1 hours consisting of 5 *Swift* orbits. The X-ray spectrum was fit by an absorbed power-law with photon index $\Gamma=2.3^{+0.30}_{-0.25}$ with a column density $N_H = 0.40^{+0.30}_{-0.25}$ $\times$ 10^{22} cm^{-2} (with χ^2/d.o.f = 9.1/9) (Fig. 2). The galactic column density, $N_{H,GAL}$, was estimated to be 1.2×10^{21}cm^{-2} using the weighted average of 6 points within 1°of the source location [6] (Dickey & Lockman, 1990). The

[6] http://heasarc.gsfc.nasa.gov/cgi-bin/Tools/w3nh/w3nh.pl

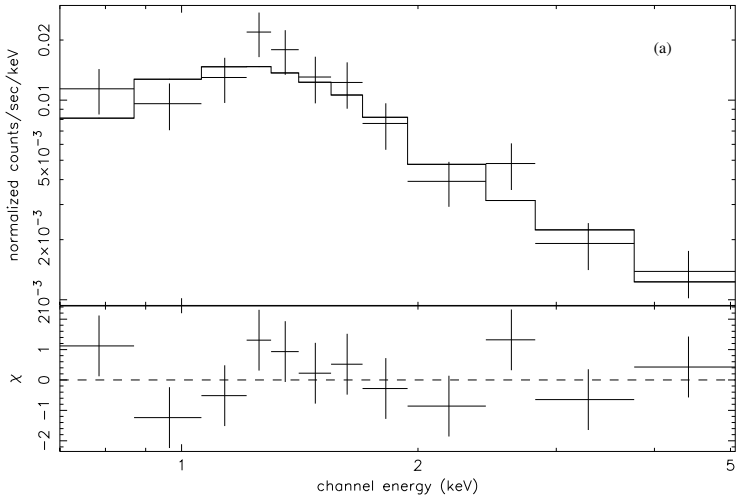

Figure 10 The X-ray spectrum obtained by *Swift*/XRT for the time interval T_0 + 7.1 hours to T_0 + 13.2 hours. The data can be fitted by a power-law with photon index $\Gamma = 2.3^{+0.30}_{-0.25}$.

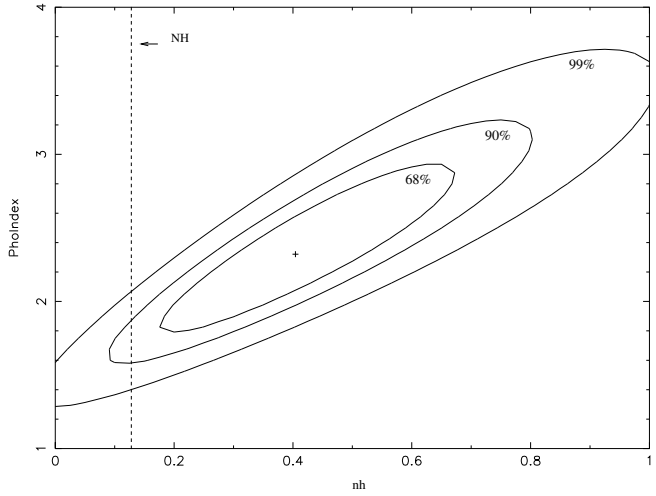

Figure 11 Contour plot of column density versus photon index for the absorbed power law model shown in Figure 2. The dashed line shows the estimated Galactic column density value 1.2×10^{21} cm^{-2} and the contours denote 68%, 90% and 99% confidence levels respectively. The spectrum is compatible (90% confidence) with Galactic absorption.

values used to estimate $N_{H,GAL}$ range from 1.01×10^{21}cm^{-2} to 1.33×10^{21}cm^{-2}. The fitted spectrum is compatible at 90% confidence level with Galactic absorption of 1.2×10^{21}cm^{-2} (Fig. 3). A power-law index of $\Gamma = 1.7 \pm 0.2$ (χ^2/d.o.f = 12.8/10) (i.e. a spectral X-ray index $\beta_X = -0.7 \pm 0.2$ with $F(\nu) \propto \nu^{\beta}$) is obtained if only Galactic absorption $N_{H,GAL}$ of 1.2×10^{21}cm^{-2} is considered in agreement with Page et al. (2005). Alternatively, if we assume that all of the extra absorption originates in the host galaxy and freeze the $N_{H,GAL}$ at 1.2×10^{21}cm^{-2} then the intrinsic absorption in the host at the pseudo-z (see below) of z=3.7 is $N_{H,z=3.7}$ of $12.2^{+18.5}_{-12.1}\times10^{22}$cm^{-2}.

2.4 The optical afterglow

The optical counterpart was discovered on our R-band images taken at the 4.2m WHT telescope starting 7.5 hours after the onset of the gamma-ray event. A faint $R = 21.9$ object was detected inside the *Swift*/XRT error circle (Jelinek et al., 2005; Pandey et al., 2005). Astrometry against USNO-B yielded the coordinates: RA(J2000) = $01^{\rm h}48^{\rm m}15\overset{\rm s}{.}00$, Dec(J2000) = $+47^{\circ}45'09\overset{''}{.}4$, with $0\overset{''}{.}2$ uncertainty (1σ, see Fig. 4).

With E(B-V) = 0.21 in the line of sight (Schlegel et al., 1998), $A_V = 0.71$ is derived (which translates into $A_V = 0.6$ if the correction factor proposed by Dutra et al. (2003) is taken into account). A value of $A_V = 0.7$ is obtained

using the fit from Predehl & Schmitt (1995) for the Galactic H column. We choose $A_V \sim 0.7$ for the rest of this paper, which implies $A_R = 0.53$ and $A_I = 0.37$.

From the analysis of the full VRI dataset available obtained at Hanle, Tautenburg and La Palma, we have obtained the optical afterglow lightcurve plotted in Fig. 5. The data between T_0 + 4 hours and T_0 + 15 hours can be fitted by a shallow power-law decline with decay index $\alpha_{opt} = -0.9 \pm 0.1$. The upper limits obtained at 1.5 and 3.5 day (>23.7 and >25.1 respectively) may suggest the existence of a break in the lightcurve after $\sim$ 1 day.

The data prior to 4 hours (i.e. in the range T_0 + 2.7 hours and T_0 + 4 hours) show a bumpy behaviour very similar to the one seen in other events like GRB 021004 (de Ugarte Postigo et al., 2005), GRB 030329 (Guziy et al. 2006 and references therein) and GRB 050730 (Pandey et al., 2006). In fact, the similarity with GRB 050730 is very remarkable, if GRB 051028 is shifted up by 3 magnitudes (Fig. 6). There is evidence for at least two of such bumps taking place, superimposed on the power-law decline. This could be explained in the framework of multiple energy injection episodes (Björnsson et al., 2004). GRB 050730 is an optically bright afterglow (see Fig. 12 of Nardini et al., 2006) whereas GRB 051028 seems an optically faint event if at redshift $z \sim$ 3-4. Unfortunately there is no X-ray data available at this epoch to allow a more complete modelling being carried out.

2.5 A high redshift event

We have extrapolated the optical and X-ray fluxes of the GRB 051028 afterglow to T_0 + 11 hours and derived a value of $\beta_{opt-X} = -0.55 \pm 0.05$. Thus GRB 051028 is located in the "gray" or "potentially dark" GRB locus on the dark GRB diagram by Jakobsson et al. (2004). How can the optical faintness of GRB 051028 be explained ?

Although the redshift of this event could not be properly measured due to its faintness at the time of the discovery, we are able to constrain it on the basis of the VRI-band data presented in this paper. Using the magnitudes derived here and correcting them for the Galactic extinction in the line of sight, we determine a spectral optical index $\beta_{opt} = -2.1 \pm 0.4$. In the simplest fireball models (Sari et al., 1998), $F_\nu \propto \nu^\beta$ with $\beta = -p/2$ for $\nu > \nu_c$ and $\beta = -(p\text{-}1)/2$ for $\nu < \nu_c$. Thus, for a typical range of p values in the range $1.5 < p < 3$ (Zeh et al., 2006), β_{opt} should be in the range $-1.5 < \beta_{opt} < -0.25$. In fact, the GRB 051028 X-ray data before T_0 + 0.5 day are well fitted by a jet model with $p = 2.4$ in the slow cooling case, moving through the ISM (with ρ = constant) prior to the jet break time and with a cooling frequency ν_c still above the X-rays. A value of $\Gamma = 1.7$ is favoured (as $\Gamma = 2.3$ is giving high, unrealistic values of p) and thus we can consider that

all the absorption is Galactic in origin (and ruling out dust along the line of sight in the host galaxy). The X-ray data (both values of Γ) are also eventually fitted for a value of $p = 2.1$ if ν_c would have already crossed the X-ray band at that time (0.5 d), as it seems to be derived from a sample of events studied by *BeppoSAX* (Piro, 2005), but this is unlikely in the light of the recent *Swift*/XRT results for a sample of (presumably higher-z) events (Panaitescu et al., 2006). In any of the above mentioned cases, the observed value of α_{opt} can be reproduced and therefore β_{opt} should be ~ -0.7. What is the reason for the discrepancy in the observed and expected values of β_{opt} ?

Fig. 7 shows the derived β_{opt} when using *only* VRI magnitudes for a sample of bursts in the range $3.3 < z < 4.5$. As can be seen the derived values are in the range of the one found for GRB 051028, well above the $\beta_{opt} = 1.5$ value mentioned previously. This is naturally explained by the fact that at $z \sim 3.2$ and $\sim$4.0, the Lyman-α break begins affecting the V

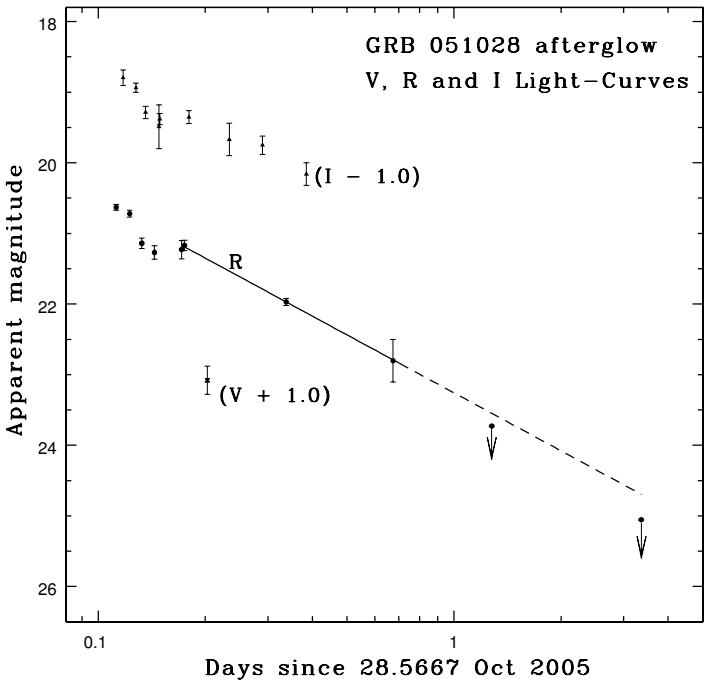

Figure 12 The R and I-band lightcurves (including the V-band single detection) obtained at Hanle (HCT), Tautenburg and La Palma (WHT) starting 2.7 hours after the event onset and continuing up to 3.5 days later. The data after 4.0 hours are fit by a power-law decline exponent $\alpha_{opt} = -0.9 \pm 0.1$.

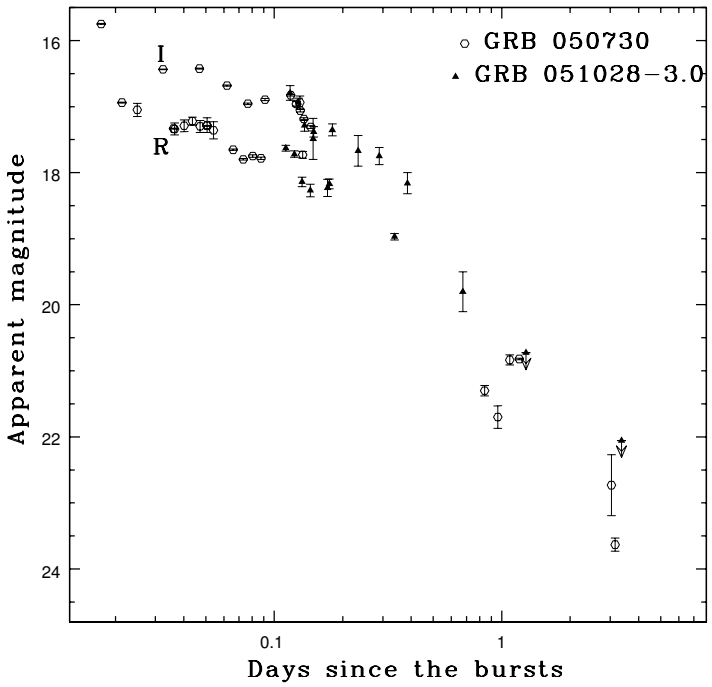

Figure 13 The GRB 051028 R and I-band light curves shifted by ~ 3 mag in order to match the GRB 050730 R-band lightcurve (from Pandey et al. 2006). No shift in the T-T_0 values has been performed. These combined data strengthen the evidence of a "bumpy" behaviour of the GRB 051028 afterglow.

and R passbands respectively. Therefore, one *natural* explanation for the β_{opt} value found for GRB 051028 is that it also arose at a $z \approx 3{-}4$, a value to be compared with that of GRB 050730 ($z = 3.967$), a burst which has a suprisingly similar optical afterglow lightcurve, as we have shown in Section 3.2. This $z \approx 3{-}4$ value is in fact in agreement with the pseudo-z = 3.7 $\pm$ 1.8 derived for this burst using the recent pseudo-z estimator developed by Pélangeon et al. (2006) on the basis of the observed peak energy and the bolometric luminosity in the 15 sec long interval containing the highest fluence. This would be in agreement with the fact that no host galaxy is detected down to $R = 25.1$. This high-redshift is also supported by the late break time, as typical afterglows undergo a jet break episode before $T_0 + 1$ day in the rest frame (Zeh et al., 2006). In fact, the Ghirlanda et al. (2004) $E_p - E_\gamma$ relation is satisfied for GRB 051028 when considering the pseudo-z = 3.7.

The fact that the afterglow of GRB 051028 is not unusual in the *Swift*/XRT

sample may indicate that the density of the surrounding medium where the progenitor has taken place should be closer to the the typical value of $\approx$ 1 cm^{-3} derived for several long-duration GRBs. So a low density environment is not the reason for its faintness at optical wavelengths. It could be that GRB 051028 could be an underluminous GRB similar to GRB 980613, GRB 011121 and GRB 021211 (see Nardini et al. and references therein), in contrast to GRB 050730.

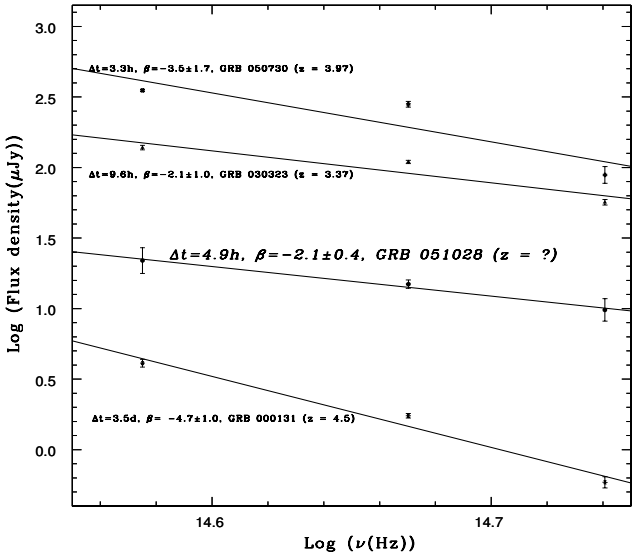

Figure 14 The β_{opt} spectral indexes obtained for GRB optical afterglows in the redshift range $3 < z < 4.5$ based solely on the VRI data. The β_{opt} value derived for GRB 051028 is in the range of those derived for this high-z sample and therefore supports that GRB 051028 also arose at a z = 3-4.

2.6 Conclusions

We have presented multiwavelength observations of the long duration GRB 051028 detected by *HETE-2* between 2.7 hours and $\sim$ 10 days after the event. The X-ray afterglow of GRB 051028 can be compared to other GRB afterglows in the sense that its flux at 11 hours is typical, i.e., one can assume that the burst has occurred on a classical n $\sim$ 1 cm^{-3} environment. The optical afterglow, on the other hand, is dim at a similar epoch (and comparable for instance to GRB 030227, citetct03. We also noticed the remarkable similarity to the optical afterglow of GRB 050730, a burst lasting

$\sim$ 10 times longer with comparable gamma-ray fluence[7)] at $z = 3.967$ (see Pandey et al. 2006 and references therein). This indicates that the faintness of the optical emission is not due to a low-density environment as in the case of some short GRBs, such as GRB 050509b (Castro-Tirado et al., 2005). Instead, we propose that GRB 051028 occurred in a faint galaxy (with R >25.1) at a high redshift consistent with the pseudo-$z = 3.7 \pm 1.8$.

Thanks to the extraordinary repointing capabilities of *Swift*, the accurate localisations for future events and the corresponding multiwavelength follow-up will shed more light on the origin of this faint optical afterglow population.

References

Arnaud, K. A. 1996, in Astronomical Society of the Pacific Conference Series, Vol. 101, Astronomical Data Analysis Software and Systems V, ed. G. H. Jacoby & J. Barnes, 17

Björnsson, G., Gudmundsson, E. H., & Jóhannesson, G. 2004, ApJ, 615, L77

Bloom, J. S. & Alatalo, K. 2005, GRB Coordinates Network, 3984

Castro-Tirado, A. J., Bremer, M., McBreen, S., et al. 2007, A&A, 475, 101

Castro-Tirado, A. J., de Ugarte Postigo, A., Gorosabel, J., et al. 2005, A&A, 439, L15

de Ugarte Postigo, A., Castro-Tirado, A. J., Gorosabel, J., et al. 2005, A&A, 443, 841

Dickey, J. M. & Lockman, F. J. 1990, ARA&A, 28, 215

Dutra, C. M., Ahumada, A. V., Clariá, J. J., Bica, E., & Barbuy, B. 2003, A&A, 408, 287

Filliatre, P., D'Avanzo, P., Covino, S., et al. 2005, A&A, 438, 793

Ghirlanda, G., Ghisellini, G., & Lazzati, D. 2004, ApJ, 616, 331

Golenetskii, S., Aptekar, R., Mazets, E., et al. 2005, GRB Coordinates Network, 4183

Henden, A. 2005, GRB Coordinates Network, 4184

Hurley, K., Ricker, G., Atteia, J.-L., et al. 2005, GRB Coordinates Network, 4172

Jakobsson, P., Hjorth, J., Fynbo, J. P. U., et al. 2004, ApJ, 617, L21

Jelinek, M., Pandey, S. B., Guziy, S. S., et al. 2005, GRB Coordinates Network, 4175

Klose, S., Stecklum, B., Masetti, N., et al. 2000, ApJ, 545, 271

Levan, A., Fruchter, A., Rhoads, J., et al. 2006, ApJ, 647, 471

Nardini, M., Ghisellini, G., Ghirlanda, G., et al. 2006, A&A, 451, 821

Page, K. L., Goad, M. R., Burrows, D. N., et al. 2005, GRB Coordinates Network, 4205

Panaitescu, A., Mészáros, P., Burrows, D., et al. 2006, MNRAS, 369, 2059

Pandey, S. B., Anupama, G. C., Sagar, R., et al. 2003, A&A, 408, L21

[7)] The scarcity of the available X-ray data for GRB 051028 does not allow to make a straight comparison with respect to the GRB 050730 X-ray afterglow.

Pandey, S. B., Castro-Tirado, A. J., McBreen, S., et al. 2006, A&A, 460, 415
Pandey, S. B., Jelinek, M., Guziy, S. S., et al. 2005, GRB Coordinates Network, 4176
Pélangeon, A., Atteia, J.-L., Lamb, D. Q., & Hete-2 Science Team. 2006, in American Institute of Physics Conference Series, Vol. 836, Gamma-Ray Bursts in the Swift Era, ed. S. S. Holt, N. Gehrels, & J. A. Nousek, 149–152
Piro, L. 2005, Nuovo Cimento C Geophysics Space Physics C, 28, 473
Predehl, P. & Schmitt, J. H. M. M. 1995, A&A, 293, 889
Racusin, J., Page, K., Kennea, J., et al. 2005, GRB Coordinates Network, 4174
Reichart, D. E., Lamb, D. Q., Metzger, M. R., et al. 1999, ApJ, 517, 692
Sari, R., Piran, T., & Narayan, R. 1998, ApJ, 497, L17+
Schlegel, D., Finkbeiner, D., & Davis, M. 1998, ApJ, 500, 525
Zeh, A., Klose, S., & Kann, D. A. 2006, ApJ, 637, 889

III. The bright optical flash from GRB 060117

A bright long-soft GRB 060117 was detected by *Swift* satellite on January 17, 2006, at 6:50:01.6 UT. It showed a multi-peak structure with T_{90}=16±1 s with maximum peak flux $48.9 \pm 1.6\,\mathrm{ph\,cm^{-2}s^{-1}}$. Coordinates computed by *Swift* were available within 19 s and immediately distributed by GCN (Cummings et al., 2006).

FRAM received the notice at 06:50:20.8 UT, 19.2 s after the trigger and immediately started the slew. The first exposure started at 06:52:05.4, 123.8 s after the GRB. Eight images with different exposures were taken before the observation was terminated. A bright, rapidly decaying object was found, and its presence was reported by Kubánek et al. (2006) and Jelínek et al. (2006) soon after the discovery. The point-spread function of the object is similar to the stars in the image, and the object did not move more than 2″ over the course of our observation, ruling out a near-Earth object crossing the field of view. The weather conditions during the observation were very good, but the Moon was nearly full (93 %) and the GRB location was only slightly more than 5° above the horizon. Consequently, the magnitude limits of our observation were $\sim$ 2.5 mag worse than the technical limit of the FRAM instrument in the optimal conditions. Table 1 displays the log of our observations (see also Fig 1), where the magnitude errors do not include systematic error of the USNO-B1.0 R1 magnitude, which should be <0.1 mag.

An optical counterpart to GRB 060117 was found 128.8 s after the burst at

$$\alpha = 21^{\mathrm{h}}51^{\mathrm{m}}36\overset{\mathrm{s}}{.}23 \quad \delta = -59°58'39\overset{''}{.}3 \quad \pm 1\overset{''}{.}5 \quad \text{(J2000)}.$$

The error amounts to a 1-σ uncertainty including systematic errors.

3.1 Follow-up

Swift itself could not observe the GRB with its X-ray and optical instruments, because of the Sun observing constraint (Campana et al., 2006). One month later on Feb 14 and 15, 2006, *Swift* XRT (Burrows et al., 2005) pointed to the burst position and did not detect any source at the corresponding position with a 3-σ limit of $1.0\times10^{-3}\,\mathrm{counts\,s^{-1}}$, corresponding to an unabsorbed 0.2 – 10 keV flux upper limit of $2.3\times10^{-14}\,\mathrm{erg\,cm^{-2}\,s^{-1}}$. The burst was also

detected by Konus-Wind (Golenetskii et al., 2006) and by Suzaku WAM (Terada et al., 2006).

Unfortunately, the later optical follow-up was unsuccessful due to cloudy weather in both New Zealand and South Africa. The limits reported by PROMPT (Nysewander et al., 2006) (observations beginning 18.0 h after the burst), however, suggest a surprisingly rapid decay. The search for a radio afterglow was also unsuccessful (Schmidt et al., 2006).

The lag-luminosity pseudo-redshift estimation from *Swift* data yields $z \simeq 1.3 \pm 0.3$ (Cummings et al., 2006). The redshift estimate based on the γ-ray data from Konus-Wind gives $z \simeq 0.45 \pm 0.2$ (Pelangeon & Atteia, 2006).

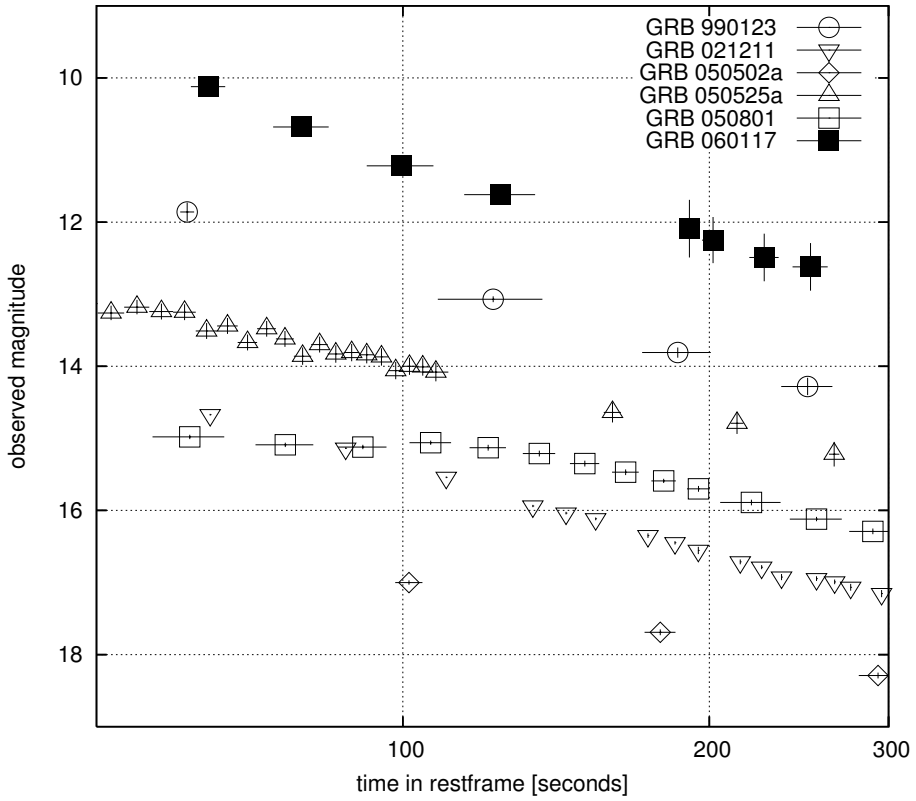

Figure 15 The optical light curve of GRB 060117 in comparison with other well-covered early GRB optical emissions: GRB 990123 (Akerlof et al., 1999), GRB 021211 (Li et al., 2003), GRB 050502a (Guidorzi et al., 2005), GRB 050525a (Blustin et al., 2006), and GRB 050801 (Rykoff et al., 2006). In this figure we use $z \approx 1.0$ for GRB 060117. Observed R-band magnitudes are shown, except for GRB 050525a, where the V-band values are plotted.

Table 2. Optical R-band photometric observations of the optical flash GRB 060117.

UT Date of exp. start	$T - T_0[s]$	$T_{\rm exp}[s]$	R	δR
2006 Jan. 17.786169	128.8	10	10.12	0.13
2006 Jan. 17.786833	159.1	20	10.68	0.12
2006 Jan. 17.786343	199.3	30	11.22	0.14
2006 Jan. 17.787583	249.7	40	11.62	0.18
2006 Jan. 17.789109	382.4	10	12.09	0.45
2006 Jan. 17.789410	403.4	20	12.25	0.36
2006 Jan. 17.789815	452.9	30	12.49	0.37
2006 Jan. 17.790336	502.9	40	12.62	0.37

Note. — The magnitudes are not corrected for Galactic extinction ($A_R \sim 0.01$ mag). $T - T_0$ is mean exposure time since the GRB.

3.2 Host galaxy identification and redshift estimation

Further observation was performed on the field of GRB060117 during the following year, leading to the discovery of the host galaxy and, this being observed in multiple filters could lead to the redshift estimation. TBF

3.3 Data acquisition and reduction

FRAM is part of the Pierre Auger cosmic-ray observatory (Pierre Auger Collaboration, 2005), and its main purpose is to immediately monitor the atmospheric transmission. FRAM works as an independent, RTS2-driven (Kubánek et al., 2004), fully robotic system, and it performs a photometric calibration of the sky on various UV-to-optical wavelengths using a 0.2 m telescope and a photoelectric photomultiplier. As a primary objective, FRAM observes a set of chosen standard stars and a terrestrial light source. From these observations it obtains instant extinction coefficients and the extinction wavelength dependence. Additionally, FRAM is able to follow GCN alerts, using its wide-field camera with a fixed R-band filter.

The wide-field camera consists of a Carl Zeiss Sonnar 200 mm $f/2.8$ telephoto lens, SBIG ST7 imager, and Bessel R-band filter. The ST7 camera has a 768×512 Kodak KAF-0402E CCD that covers a field of view of $120' \times 80'$

with a scale of $9\farcs6$/pixel. The effective diameter of the lens is 57 mm and the 3σ limiting magnitude under optimum conditions reaches $R \sim 15.0$ for a 30 s exposure.

The raw images were dark-frame subtracted using a median of several dark-frame exposures. Given the significant dark current of the camera, the darks were treated separately for each exposure time. The flat-field correction was then applied using the median of 40 normalized 1s exposures obtained while mosaicing through the twilight sky. The aperture photometry was done using the `phot` routine in IRAF[8)] with the aperture diameter of 2 pixels. To get a precise astrometric position of the source, we used the four most significant images and computed the average position.

The images were astrometrically and photometrically calibrated on the fly using the `past` program in the context of JIBARO (de Ugarte Postigo et al., 2005), using all sources with more than 10-σ significance from the image compared to USNO-B1.0 (Monet et al., 1998) positions and *R1* magnitudes. `Past` employs a sigma-clipped third-degree polynomial surface fit. For the astrometry, an error-weighted mean of the zero point is used. Systematic errors of USNO-B1.0 should be less than $0\farcs2$ in the astrometry and less than 0.1 mag for the photometry. Since the Galactic extinction, taken from the maps published by Schlegel et al. (1998) is very low ($E_{B-V} = 0.038$), we neglect this value in the following discussion.

3.4 Discussion

In the search for the interpretation of the lightcurve, we assume a uniform ISM, and that the influence of the internal shock emission on the lightcurve is negligible because our observation starts ∼100 s after the end of the gamma-ray burst.

In the simplest case, the lightcurve can be fitted and a single power law with a temporal flux-decay index $\alpha = -1.73 \pm 0.12$. The $\chi^2/d.o.f.$ for this fit is 1.296. If we assume this decay to be a signature of a pure forward shock, we get the value of the electron energy distribution power-law index $p = 3.3 \pm 0.1$. This value is very high in comparison with other known optical transients, but it is consistent with $p = 3.82^{+1.0}_{-0.5}$ as computed from the Konus-Wind spectra of the GRB (Golenetskii et al., 2006) (cf. Shen et al., 2005). In contrast, if the linear decay is a signature of a pure reverse shock, we get $p = 2.0 \pm 0.1$ – close to the typical value for the optical transients observed so far. We should note that such a reverse shock emission should be accompanied by a forward shock with $\alpha_F \simeq$-0.7.

[8)] IRAF is distributed by the National Optical Astronomy Observatory, which is operated by the Association of Universities for Research in Astronomy, Inc., under co-operative agreement with the National Science Foundation.

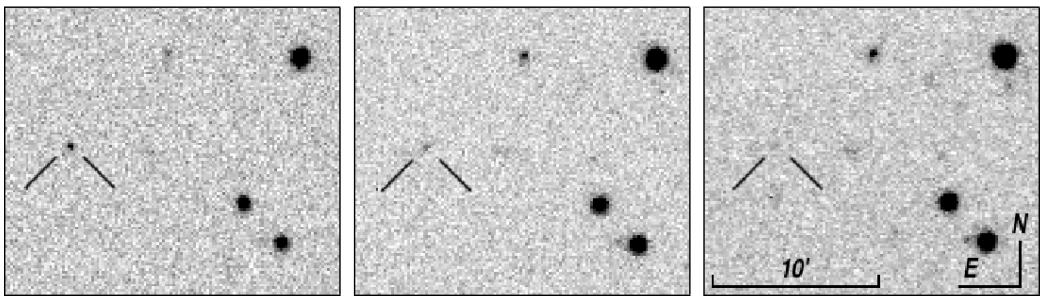

Figure 16 Details of the surroundings of the optical flash of GRB 060117 as observed by FRAM. Images taken 129, 249, and 480s after the trigger.

Another possibility (after Shao & Dai, 2005) is to interpret the data as a Type I lightcurve (as given by Zhang et al., 2003), which depicts a transition between the reverse and the forward shock with the passage of the typical frequency break ν_m through the observed passband at time $t_{m,f}$. We assume the lightcurve is initially dominated by a rapidly falling reverse-shock emission with $F_{\nu,r} \sim t_d^{-(27p+7)/35}$, followed by a forward-shock emission that rises as $F_{\nu,r} \sim t_d^{+1/2}$ before $t_{m,f}$ and then decays with $F_{\nu,f} \sim t_d^{-(3p-3)/4}$. Using a χ^2 minimization fit to this scenario, we obtain $p = 2.96 \pm 0.06$, a magnitude of forward shock maxima $m_{m,f} = 11.82 \pm 0.04$, a time of the maxima $t_{m,f} = 301 \pm 4\,\mathrm{s}$ (after trigger), and a magnitude of the reverse shock at $t = t_{m,f}$ $m_{m,r} = 12.43 \pm 0.05$ ($\chi^2/d.o.f.$ for this fit is 0.015). Corresponding decay indices are α_R=2.49±0.05 and α_F=1.47±0.03 (see Fig 3). If the crossing time $t_\times$ (Zhang et al., 2003) coincides with the end of the GRB (i.e. $\sim 20\,\mathrm{s}$), then we can estimate the peak magnitude of this OT as $R \sim 5\,\mathrm{mag}$ by backward extrapolation.

Note, that this is only one of the plausible interpretations. There may be other possible explanations for this behaviour including density jump in the media (Lazzati et al., 2002) or energy injection (Björnsson et al., 2004). Without a multiwavelength observation it is impossible to distinguish which of these possibilities actually took place.

The position of the burst and its distance from the Sun made the object difficult to observe. PROMPT (Nysewander et al., 2006) shows that the bright OT decayed very fast, and 20 hours after the burst its magnitude was already $I > 21.2$. Using the procedure of Šimon et al. (2001) we transform this limit to the filter of our observation: $R \gtrsim 21.5$ From this limit we then get the estimate of an average late decay as $\alpha_\mathrm{late} < -1.62$. Among the three interpretations we have shown, only the pure forward shock scenario is compatible with this limit without introducing an unusually early jet break, which is required to explain the other two scenarios.

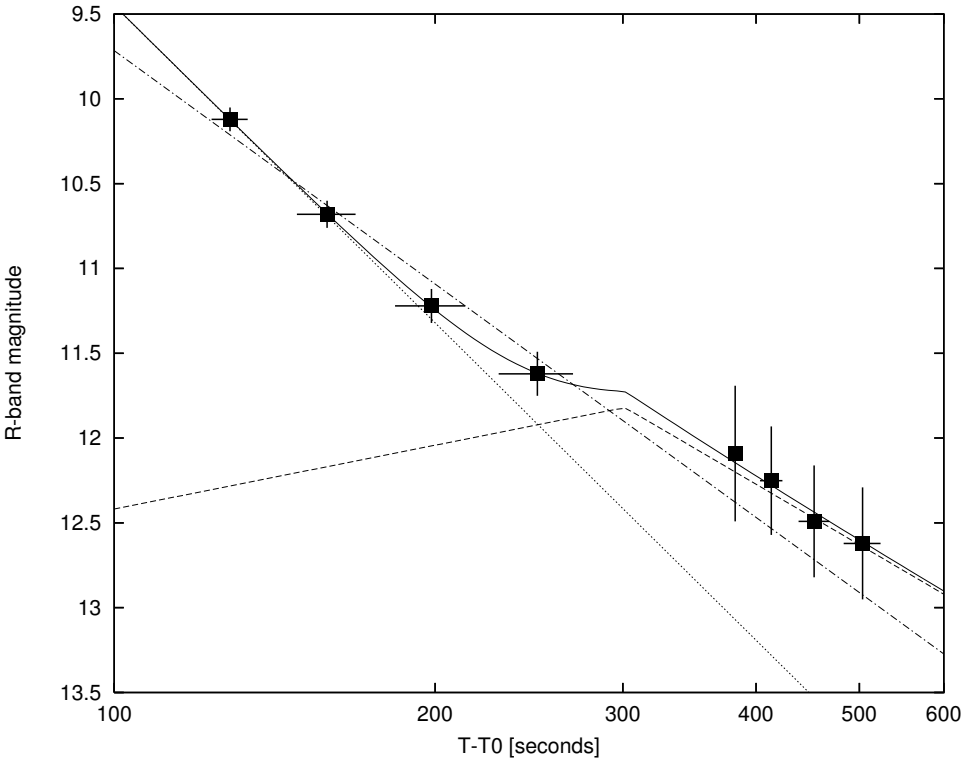

Figure 17 The R-band afterglow lightcurve of GRB 060117. The lightcurve is fitted as a superposition of reverse shock (dotted line) and forward shock (dashed line). The linear fit is plotted by a dot-and-dash line.

Soon after the *Swift* trigger, a suspicion of an extremely low-redshift GRB was raised (Tanvir, 2006) due to the presence of a nearby galaxy PGC 128172 with $z = 0.04$ in the *Swift* errorbox. However, this discovered transient lies $3\overset{\mathrm{m}}{.}1$ from this galaxy, accordingly the projected distance – 160 kpc – is approximately four times larger than the visible major diameter of this galaxy. Furthermore, the position angle of the transient with respect to the PGC 128172, which we observe practically edge-on, is 97°. The association of the OT with this galaxy is, therefore, quite unlikely.

3.5 Conclusions

The GRB 060117 is the most intense (in terms of peak flux) GRB detected so far by Swift. With the maximum brightness of $R = 10.1$ mag, FRAM has discovered one of the optically brightest prompt optical emissions ever detected. The initial optical decay was found to be one of the steepest of an early GRB optical afterglow observed.

We have presented 3 scenarios for explaining the lightcurve. The apparent change in its slope is neglected in two simple scenarios, where we suppose the observed lightcurve to only be the trace of a forward, resp. reverse, shock. In the third (preferred) scenario, the shape of the lightcurve is explained as a transition between reverse and forward shock emission. The forward-shock-only interpretation is flawless regarding the PROMPT limit, but shows rather spurious value of p. The other two scenarios (i.e. those involving reverse shock) result in a relatively slowly decaying forward shock, and later limits require an early jet break $t_{\mathrm{j}} \sim 0.2\,\mathrm{d}$. The detailed analysis of this problem is beyond the scope of this letter.

Progress in further study of the particular case of GRB 060117 depends on the measurement of its distance. Therefore the follow-up and identification of host galaxy with a large telescope is of high importance.

A larger sample of GRB rapid follow-ups is needed to decide whether this kind of transition, already suggested for other bursts, is common.

References

Akerlof, C., Balsano, R., Barthelmy, S., et al. 1999, Nature, 398, 400

Björnsson, G., Gudmundsson, E. H., & Jóhannesson, G. 2004, ApJ, 615, L77

Blustin, A., Band, D., Barthelmy, S., et al. 2006, ApJ, 637, 901

Burrows, D. N., Hill, J. E., Nousek, J. A., et al. 2005, Space Science Reviews, 120, 165

Campana, S., Barthelmy, S., Gehrels, N., et al. 2006, GCN 4533

Cummings, J., Barbier, L., Barthelmy, S., et al. 2006, GCN Circular, 4538

de Ugarte Postigo, A., Jelínek, M., Gorosabel, J., et al. 2005, in Astrofísica Robótica en España, ed. A. Castro-Tirado, B. de la Morena, & J. Torres, Madrid, 35–50

Golenetskii, S., Aptekar, R., Mazets, E., et al. 2006, GCN Circular, 4542

Guidorzi, C., Monfardini, A., Gomboc, A., et al. 2005, ApJ, 630, L121

Jelínek, M., Kubánek, P., Prouza, M., Nekola, M., & Hudec, R. 2006, GCN Circular, 4536

Kubánek, P., Jelínek, M., Nekola, M., et al. 2004, in AIP Conf. Proc. 727: Gamma-Ray Bursts: 30 Years of Discovery

Kubánek, P., Jelínek, M., Prouza, M., Nekola, M., & Hudec, R. 2006, GCN 4535

Lazzati, D., Rossi, E., Covino, S., Ghisellini, G., & Malesani, D. 2002, A&A, 396, L5

Li, W., Filippenko, A. V., Chornock, R., & Jha, S. 2003, ApJ, 586, L9

Monet, D. B. A., Canzian, B., Dahn, C., et al. 1998, VizieR Online Data Catalog, 1252, 0

Nysewander, M., LaCluyze, A., Reichart, D., et al. 2006, GCN Circular, 4548

Pelangeon, A. & Atteia, J. L. 2006, GCN Circular, 4544

Pierre Auger Collaboration. 2005, in Proceedings of the 29th International Cosmic Ray Conference, Pune, India

Rykoff, E., Mangano, V., Yost, S., et al. 2006, ApJ, 638, L5
Schlegel, D., Finkbeiner, D., & Davis, M. 1998, ApJ, 500, 525
Schmidt, B., Wieringa, M., Frail, D. A., & Soderberg, A. 2006, GCN Circular, 4546
Shao, L. & Dai, Z. G. 2005, ApJ, 633, 1027
Shen, R., Kumar, P., & Robinson, E. 2005, astro-ph/0512489
Šimon, V., Hudec, R., Masetti, N., & Pizzichini, G. 2001, in ESA SP-459: Exploring the Gamma-Ray Universe, 441–444
Tanvir, N. 2006, GCN 4534
Terada, Y., Yamaoka, K., Sugita, S., et al. 2006, GCN Circular, 4573
Zhang, B., Kobayashi, S., & Mészáros, P. 2003, ApJ, 595, 950

IV. An intense X-ray flare and a refreshed shock observed may share a common origin in a GRB 060904B

4.1 Introduction

GRB 060904B was detected at T_0 = 02:31:03 UT on September 9, 2006 by the BAT instrument aboard the *Swift* mission (Grupe et al., 2006a). The position of the gamma-ray event was distributed using the GRB Coordinates Network (GCN)(Barthelmy et al., 1995). The GRB had a duration of ∼80 s which, together with a spectrum that could be fitted with a power-law of index 1.7(Markwardt et al., 2006), classifies it as a member of the long/soft group of events. The high-energy light curve (Gamma + X-rays) was found to have two main emission episodes, with the second one starting 120 s after the main one at T_0. The rapid dissemination of the X-ray position helped to identify the optical afterglow soon (Rykoff et al., 2006; Fugazza et al., 2006). In optical wavelenghts, the afterglow showed an interesting variability at the level of ∼17–18 mag for about 90 minutes, when it started to decay rapidly. Assuming a flat cosmology with $\Omega_\Lambda = 0.73$, $\Omega_M = 0.27$ and $H_0 = 71\,\mathrm{km\,s^{-1}\,Mpc^{-1}}$ (Spergel et al., 2003), the redshift of $z = 0.703$ measured by (Fugazza et al., 2006) implies luminosity distance 4.281 Gpc, the scale of 7.154 kpc/″ and a look-back time 6.31 Gyr (Wright, 2006).

We present the optical and milimetric observations of the optical afterglow performed by several instruments around the globe. The lightcurve shows a complicated structure, which we are trying to explain with two different models.

4.2 Observations

Gamma and X-rays For the γ-ray fluence of $1.7^{+0.2}_{-0.2} \times 10^{-6}\,\mathrm{erg\,cm^{-2}}$ (Markwardt et al., 2006) we obtain a isotropic-equivalent energy release in γ-rays of $E_{\gamma,\mathrm{iso}} = 2.2^{+0.75}_{-0.75} \times 10^{51}$ erg. The fact that no break time is seen on the X-ray light curve ($t_j > 7$ days) implies $\theta_j > 0.18$, i.e. a geometry-corrected $E_\gamma > 3.5 \times 10^{49}$ erg in agreement with other E_γ values determined

for long-duration GRBs (Frail et al., 2001).

Swift XRT (Burrows et al., 2005) observed the object starting 69 s after the trigger but had to cease 240 s later due to Earth ocultation (Grupe et al., 2006a,b). Later, the GRB was reobserved several times, as shown in the the Table 1.

We found the analysis of Swift X-ray data tricky due to suspiction for low-energy X-ray breaks present in the spectra. Therefore we started fitting the late ($2^{\rm nd}$ orbit) data with a fixed spectral slope to it's optical-to-x-rays value of $\beta = 0.871 \pm 0.017$. As there is apparently no break in the SED (cf. fig. 20), this way of getting β is providing the most reliable value of all the methods available. While fixing the Galactic neutral hydrogen column density to the value $n_{{\rm H},z=0}$ given by (Schlegel et al., 1998) we obtain the host galaxy value $n_{{\rm H},z=0.703} = (0.2 \pm 0.2) \times 10^{-22} {\rm cm}^{-2}$ in agreement with (Butler & Kocevski, 2007). We use this value later, while fitting the early X-ray data to avoid confusion with the X-ray breaks. (Note that $n_{\rm H}$ should decrease with exposure due to ionization, while any free fit to the given data yields it's rise with flare intensity (cf. (Butler & Kocevski, 2007), fig. 11.)

Detailed fitting of the X-ray data is provided by (Butler & Kocevski, 2007), we concentrated on the simultaneous X-ray to optical fits of optical points we have.

The X-ray lightcurve and spectrum were derived from the *Swift*/XRT data (Grupe et al., 2006b). A giant X-ray flare is observed starting at T_0 + 85 s and lasting for 400 s. The flare data were fitted with a single power-law plus with a photon index $\Gamma = 2.16$ and a fixed Galactic hydrogen column

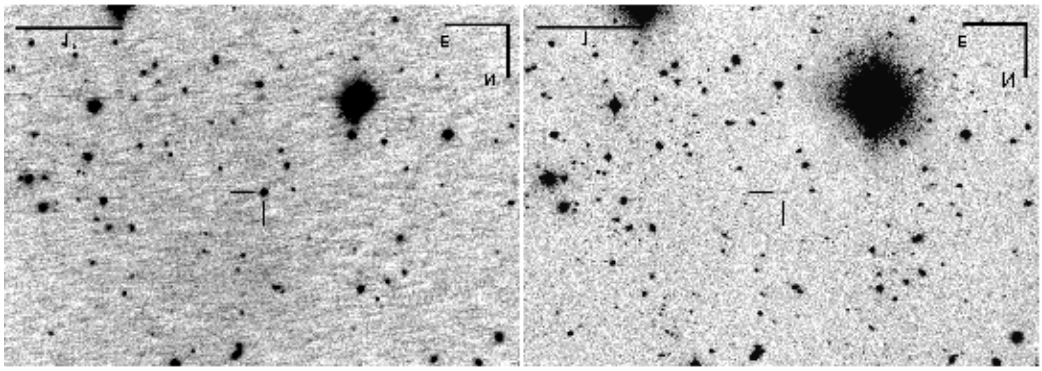

Figure 18 The bright GRB 060904b optical afterglow superimposed to a bright underlying host galaxy. A combination of UBVRI optical images taken at 1.5 hr after the onset of the event (right) can be compared with the frames taken 2.5 months later, showing the location of the host galaxy. An offset of $\sim 1''$ (TBC) is shown when detailed astrometry is performed. This corresponds to $\sim$7 kpc at $z = 0.703$.

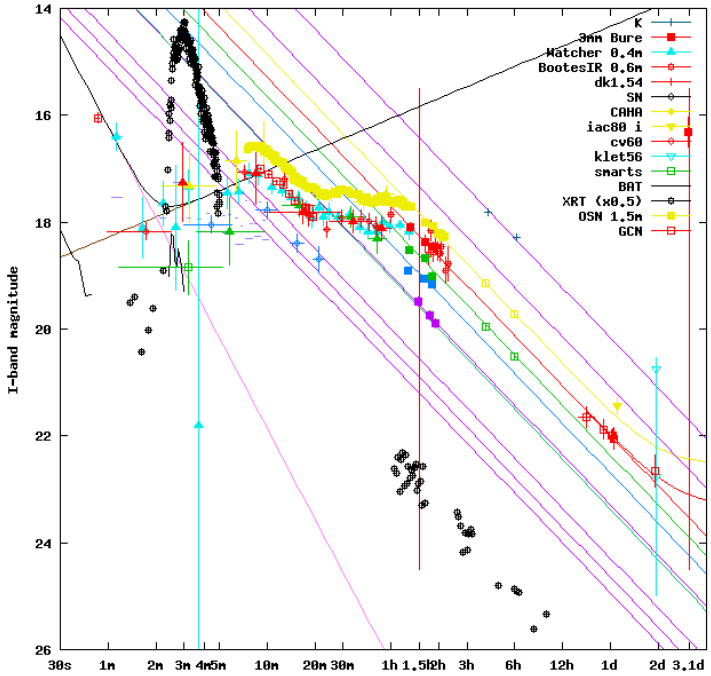

Figure 19 Light curve of the afterglow in near infrared (J & K), visible (R & I) and X-ray bands. The resulting afterglow light curves starting at T_0 + 5 min have been simultaneously fitted with a model based on the standard fireball model for which N energy injection have been included at 0.X and 0.Y days (Björnsson et al., 2004). Filled symbols are data presented in this article whereas empty ones are data from the literature^{GCN06}. A blow up is inserted in order to show the detailed structure seen in the I-band light curve.

density $N_{H,gal}$= (4.09 ± 0.13) $\times 10^{21}$ cm^{-2} and an intrinsic column density $N_{H(host)}$ (7.6 ± 0.4) $\times 10^{21}$ cm^{-2}at fixed redshift of z = 0.703 (χ^2/d.o.f. = 1.1).

The X-ray data, together with the detections in the optical/near-IR pass-bands, allowed to construct a spectral flux distribution (SFD) at various epochs during the GRB, the X-ray flare, and then 90 minutes and 3.1 days after the burst (Figure 20).

Optical follow-up Immediately on receipt of the initial alert by *Swift* images were triggered at the 0.4 m WATCHER telescope in South Africa (de Ugarte Postigo et al., 2006b), 0.6 m telescope at Črni Vrh(Skvarc, 2006), 0.6 m BOOTES-IR (de Ugarte Postigo et al., 2006a) and 1.5 m telescopes (the later two at Observatorio de Sierra Nevada, OSN), in order to monitor

the varying optical afterglow lightcurve, confirming the earlier detections (Rykoff et al., 2006) (Fig. 4.1). Later, the GRB was monitored by the 1.2 m SMARTS telescope (Grupe et al., 2006b), the 0.8 m photometric telescope at Canary Islands and the 0.57 m telescope at Kleť. Very late observations were performed by the Danish 1.54 m telescope at La Silla and with the 2.2 m telescope of the Calar Alto Observatory (CAHA).

We performed the astrometry solution for 404 I-band images obtained at the OSN. We derived the median location of the optical afterglow

$$\alpha = 3^h52^m50.521^s, \quad \delta = -0°43'30.55'' \quad \text{(J2000)}$$

with the (1σ) dispersion of $0.06''$ against the reference of USNO-B1.0, whose reported systematic error (Monet et al., 1998) – $0.2''$ – dominates the uncertainity.

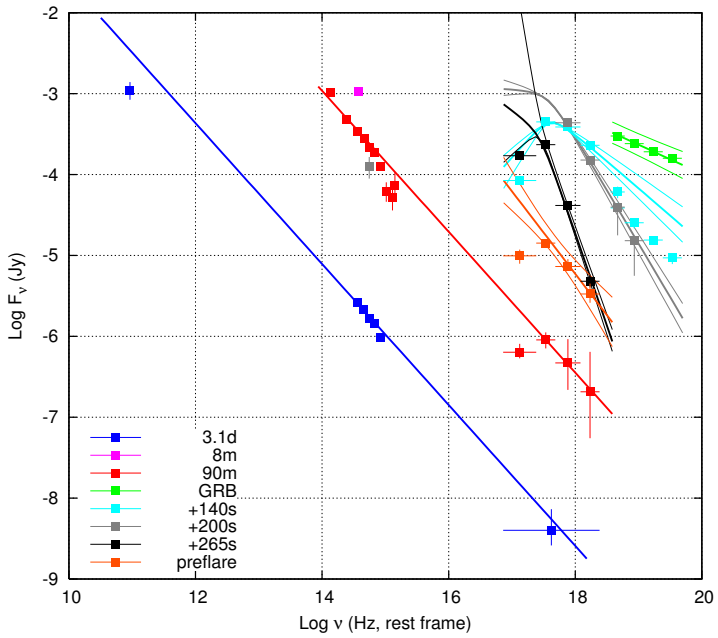

Figure 20 Spectral flux distribution: The afterglow is detected in all passbands (mm, near-IR, optical and X-rays). The detection of the afterglow in the nIR K band is extrapolated from a near epoch using as reference a quasi-simultaneous R passband detection. The spectral flux distribution (SFD) built with this photometric data allows us to study the redshift and intrinsic extinction of the afterglow. Multicolour information has been used to construct a spectral flux distribution at different times after the burst (T_0 + 1.5 hr, T_0 + 3.1 d).

Optical images have been photometrically calibrated against Sloan Digital

Sky Survey applying the corresponding transformations for our photometric system. For nIR images we have used field stars from the 2 Micron All Sky Survey catalogue. A galactic extinction correction of E(B-V)=0.173 (Schlegel et al., 1998) is applied and magnitudes have been converted to Jansky for clarity.

To construct the lightcurves, we make use of the optical data publeished by Klotz (2008), Rykoff (2009).

4.3 Discussion

The first optical peak The early peak observed by ROTSE-III, and supported by observations from Watcher and TAROT peaks at ∼54 s after the trigger. The observation by *Swift*/XRT reveal a short pre-flare period, when the X-ray emission has an afterglow-compatible spectra. In contrast with later data, where a the afterglow spectra seems to be a simple power-law, this peak would suggest a break in the spectra between X-rays and optical. Optical points are ∼ one order of magnitude weaker than the extrapolation of the X-ray spectra. There are several possible explanations.

Spectral break: as there is no color information within the dataset, we cannot disprove that at this early time after the GRB, the characteristic frequency ν_m of the fireball wasn't passing through the optical band.

Change of extinction: there might have happened a dust sweep-out during the second high-energy emission (X-ray flare) which might have changed the extinction properties withn the line-of-sight.

Something else: while the X-ray afterglow resembles the later X-ray afterglow, the mechanism of it's emission may be different - for example the X-rays may come from the latest phases of the first GRB pulse, while the optical emission may be due to a reverse shock emission.

The second optical peak The second optical peak happens soon after the second period of high-energy emission of this GRB. It rises approximately as a power-law, peaks at 480 s and can be fitted as a Beugermannn function (hyperbola in the log-log space) with $\alpha_{\rm rise}$=+3.0±0.8 and $\alpha_{\rm decay}$=-1.03±0.03. The top and decay part of this peak are covered with fast-photometry observations of the OSN 1.5 m. The peak seems to have a small bump on it's decaying side. This peak seems to have a similar relation to the X-ray flare as does the first optical peak to the GRB, refreshing the already decaying afterglow by several magnitudes on optical by a factor of 10.

The plateau The observation of the OSN 1.5 m telescope clearly resolve the plateau as a series of two bumps, which, with less resolution, form a flat-looking feature. Letting ourself on a thin ice of speculation, the mentioned

bump on the second optical peak might have been a signature of just another high-energy phase, which would have the same relation to the first bump of the plateau, as has the GRB to the first and X-ray flare to the second optical peak. This single well-resolved plateau rises a question, whether the other GRBs with observed plateaus are cases of not well sampled data to see the bumpy structure of the plateau or if they are plateau-like intrinsically.

Power-law decay At about 90 min after the GRB, the lightcurve starts to decay steadily as a power-law with a decay index $\alpha = -1.03$. During this period, most of color information has been obtained and, too, the X-ray data are available again to form a complete spectral energy distribution (SED) of the GRB. This SED shows a simple power-law spectra across its range - should there have been any spectral break, it should lay below 5 μm in the near infrared or above some 2 keV in the X-rays.

The host galaxy At about 3 days after the GRB, the host galaxy starts to emerge in the optical bands. At the same period, the Plateau de Bure (PdB) *mm* detection of the afterglow was achieved. The SED constructed for this period from the late X-ray point, the PdB radio data and host galaxy subtracted optical point reveals no significant change in the wide-band spectra of the afterglow.

Comparing the images from OSN from the early phase to the late images taken at Danish 1.54m, we derive the offset of $0.484\pm0.026''$ (With the OT being $0.315\pm0.024''$ east and $0.340\pm0.027''$ north from the host barycenter). This corresponds to 3.5 ± 0.9 kpc distance from the center of the host.

Supernova search Imaging of the GRB continued for several weeks with the hope to discover a supernova component by the NOT 2.5m and CAHA 2.2m telescopes. The supernova search has been unsuccessfull, with the limit (given mostly by the cross-calibration error between different telescopes) R>23.5 m.

In the standard fireball model scenario, the observed prompt gamma-ray emission is due to internal shocks, and as the fireball is decelerating by the circumburst medium, a pair of shocks develop (Meszaros & Rees, 1997). A prompt reverse shock can be responsible of prompt, concurrent emission at all wavelengths, whereas the late afterglow emission is produced as a consequence of the forward shock impinging on the interstellar medium. All these physical mechanisms are contributing to the overall light curve observed at X-rays, optical, near-IR and millimetre wavelengths: a reverse shock, an internal shock and a forward shock.

Early optical emission One minute after the GRB, an early optical flash was observed. We detect it on a 10 s exposure centered at $T_0 + 68$ s, i.e. 25 s after the end of the GRB prompt emission (and also in TAROT data at $T_0 + 56$ s. The light observed in this interval could be a low-energy tail of a γ-ray prompt emission. It could be also a signature of a reverse shock, but we would need to shift $T_{0,R}$ towards the end of a prompt gamma-ray emission to obtain a result compatible with predictions (Sari & Piran, 1999). Fig. 20 shows that this optical emission is the tail of the higher energy emission towards shorter wavelengths.

Refreshed internal shock The intense X-ray flare, coincident with a concurrent weak optical flare can be interpreted as a consequence of a late internal shock. With a fluence of $(5.0 \pm 0.5) \times 10^{-7}\,\mathrm{erg\,cm^{-2}}$ in the 0.3–10 keV range, we obtain an isotropic-equivalent energy release in X-rays of $E_{\mathrm{X,iso}} 6.4^{+0.5}_{-0.8} \times 10^{50}$ erg and a geometry-corrected $E_{\mathrm{X}} > 1.0 \times 10^{49}$ erg. This X-ray flare was also detected in gamma-rays by the BAT instrument, and a fluence of $4.0 \pm 0.5) \times 10^{-7}\,\mathrm{erg\,cm^{-2}}$ in the 15–200 keV range was derived, implying an isotropic-equivalent energy release in γ-rays of $E_{\gamma,,iso} = 5.1^{+0.4}_{-0.3} \times 10^{50}$ erg and a geometry-corrected $E_\gamma > 0.8 \times 10^{49}$ erg.

The forward shock We have modelled the GRB 060904B afterglow following the prescription of Björnsson et al. (2004) on the basis of the standard fireball model (Sari & Piran, 1999), for which 2 energy injections have been included at 0.014 and 0.022 days after the onset of the burst. These energy injections, which amount to 1.3 x 10^{50} erg and 1.1 x 10^{50} erg respectively are needed in order to explain the bumpy behaviour seen during the first hours (Fig. 19).

The fact that the derived energies for both the intense flare seen in both gamma-rays and X-rays ($\sim 5 \times 10^{48}$ erg if we assume $\theta = 5.6°$) cannot be compared with the energy deposited on the refreshed forward shock by the energy injections ($\sim 2.4 \times 10^{50}$ erg) can not considered as strong evidence of a relationship. The energy injection is also supported by the shift in the preflare versus postflare X-ray light curve.

4.4 Conclusions

The observational data of this GRB are not consistent with the model of multiple energy injections. The brightness changes within the afterglow are simply too fast.

The data are also not consistent with Molinari et al. `astro-ph/0612607`, as we cannot interpret this GRB without stating that the peak of the afterglow was with 99% confidence NOT associated with the GRB main peak.

Whether we happen to have a strong conclusion upon the injection time and energy is yet to be seen and depends how the modelling will look like.

References

Barthelmy, S. D., Butterworth, P., Cline, T. L., et al. 1995, Ap&SS, 231, 235
Björnsson, G., Gudmundsson, E. H., & Jóhannesson, G. 2004, ApJ, 615, L77
Burrows, D. N., Hill, J. E., Nousek, J. A., et al. 2005, Space Science Reviews, 120, 165
Butler, N. R. & Kocevski, D. 2007, ApJ, 663, 407
de Ugarte Postigo, A., Aceituno, F., Castro-Tirado, A. J., & Kubánek, P. 2006a, GCN 5509
de Ugarte Postigo, A., French, J., & Kubánek, P. 2006b, GCN 5510
Frail, D. A., Kulkarni, S. R., Sari, R., et al. 2001, 562, L55
Fugazza, D., D'Avanzo, P., Malesani, D., et al. 2006, GCN 5513
Grupe, D., Barthelmy, S. D., Chester, M. M., et al. 2006a, GCN 5505
Grupe, D., Godet, O., & Barthelmy, S. 2006b, GCN 5517
Markwardt, C., Barbier, L., Barthelmy, S. D., et al. 2006, GCN 5520
Meszaros, P. & Rees, M. J. 1997, 476, 232
Monet, D. B. A., Canzian, B., Dahn, C., et al. 1998, VizieR Online Data Catalog, 1252, 0
Rykoff, E. S., Rujopakarn, W., & Yuan, F. 2006, GRB Coordinates Network
Sari, R. & Piran, T. 1999, ApJ, 520, 641
Schlegel, D., Finkbeiner, D., & Davis, M. 1998, ApJ, 500, 525
Skvarc, J. 2006, GCN 5511
Spergel, D., Verde, L., Peiris, H., et al. 2003, ApJ, 148, 175
Wright, E. L. 2006, PASP, 118, 1711

Table 3. GRB 060904B Optical Photometry

Telescope	Filter	$t_{\rm start}$ (s)	$t_{\rm end}$ (s)	mag	$f_{\nu,{\rm O}}$ (mJy)
Watcher 0,4 m	C_R	63.3	73.3	17.38 ± 0.35	
		187.8	197.8	17.36 ± 0.41	
		314.8	324.8	17.22 ± 0.40	
		343.3	353.3	17.54 ± 0.47	
		378.2	388.2	17.33 ± 0.41	
		410.8	420.8	17.07 ± 0.27	
		438.4	448.4	17.08 ± 0.41	
		470.9	480.9	16.82 ± 0.23	
		502.8	512.8	17.08 ± 0.26	
		532.5	542.5	17.29 ± 0.47	
		566.7	576.7	16.71 ± 0.21	
		597.9	607.9	16.79 ± 0.26	
		626.9	656.9	17.24 ± 0.17	
		729.0	759.0	17.12 ± 0.13	
		830.6	860.6	17.30 ± 0.15	
		929.0	959.0	17.17 ± 0.16	
		1033.6	1063.6	17.48 ± 0.16	
		1137.1	1167.1	17.45 ± 0.18	
		2784.5	3021.5	18.15 ± 0.15	
		3092.2	3329.2	17.94 ± 0.13	
		3398.7	3633.7	17.47 ± 0.12	
		1241.3	1475.3	17.92 ± 0.10	
		1546.4	1780.4	17.83 ± 0.11	
		1856.2	2086.2	17.81 ± 0.12	
		2166.7	2401.7	17.85 ± 0.11	
		2470.6	2703.6	17.95 ± 0.14	
		3868.9	4382.9	17.89 ± 0.10	
		4388.4	4898.4	18.14 ± 0.18	
	V	765.0	1129.0	17.44 ± 0.22	
		1684.1	2367.1	17.64 ± 0.20	
		2607.1	3290.1	18.09 ± 0.28	
	R	454.0	558.0	16.84 ± 0.35	
		663.0	1340.0	17.76 ± 0.17	
		1581.1	2566.1	17.97 ± 0.15	
		2824.1	3495.1	18.05 ± 0.16	
	I	1171.1	1848.1	17.46 ± 0.13	
		2089.1	2766.1	17.63 ± 0.14	
		3024.1	3697.1	17.47 ± 0.15	

Note. — Magnitudes are not corrected for Galactic extinction.

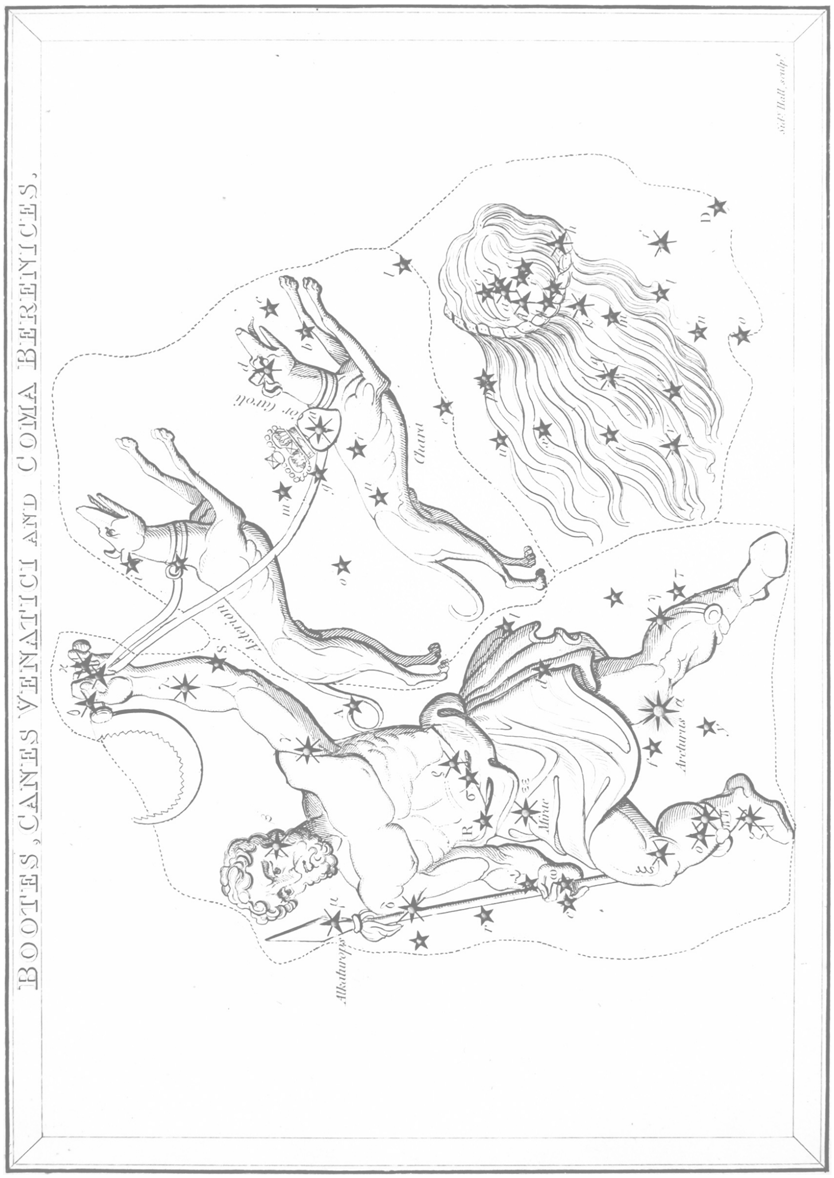
BOOTES, CANES VENATICI AND COMA BERENICES.

V. An early detection of the optical transient of the GRB 080413A

We present results of our early follow-up of the bright optical afterglow of the GRB 080413A with the 30 cm telescope BOOTES-1B, together with the later photometry and spectroscopy by various larger telescopes. We found a bright, slowly decaying optical afterglow with magnitude 13.3, fading slowly with a temporal power law decay index of $\alpha_1 = (0.30 \pm 0.16)$. This early decay gradually steepened at ~ 16 min after the GRB trigger steepened to a fireball-model-typical slope of $\alpha_2 = (1.33 \pm 0.05)$. We fit the afterglow lightcurve as a forward shock afterglow with an energy injection, expanding in the stellar wind density profile. The NOT observation reveal a positionally coincident, bright host galaxy with $r' = 22.8 \pm 0.1$. [9)]

5.1 Introduction

A bright long-soft GRB 080413A was detected by *Swift* (Mangano et al., 2008a) satellite on friday April 13, 2008, at 2:54:19.3 UT (Mangano et al., 2008b). It showed a triple-peak structure with $T_{90}=46 \pm 1$ s with maximum peak flux 48.9 ± 1.6 ph cm^{-2}s^{-1}. Coordinates computed by *Swift* were available within 14 s and immediately distributed by GCN.

The burst was also detected by *Suzaku* Wide-band All-sky Monitor (WAM) (Enoto et al., 2008), allowing for a joint spectral fit of *Swift*/BAT and *Suzaku*/WAM data (Ohno et al., 2008).

At optical wavelengths, a bright, rapidly decaying object was found, and its presence was reported by various teams (Rykoff & Rujopakarn (2008), Beardmore et al. (2008), Klotz et al. (2008)) soon after the discovery.

Two independent groups – Thoene et al. (2008) from the VLT and Cucchiara et al. (2008) from Gemini-South – reported Spectroscopic observation with large telescopes, fixing the GRB redshift at $z = 2.433$.

[9)] The data presented here were obtained in part with ALFOSC, which is provided by the Instituto de Astrofisica de Andalucia (IAA) under a joint agreement with the University of Copenhagen and NOTSA.

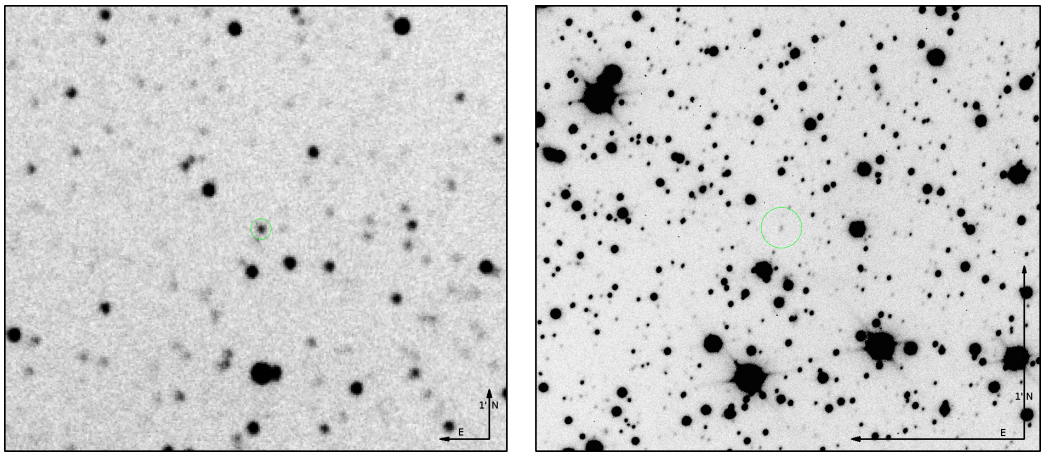

Figure 21 The neighborhood of the optical afterglow of GRB080413A taken by BOOTES-1B 60.7s after the GRB (left) and NOT 1 day after (right). North is up, east is left.

Swift itself observed the GRB position with its optical (UVOT) and an X-ray (XRT) telescopes Evans et al. (2008).

5.2 Observations

BOOTES-1B did receive the notice at 02:54:33.7 UT, 14.4 s after the trigger and immediately started the slew. The first exposure started at 02:55:20.0, 60.7 s after the GRB. The robotic telescope automatically obtained a set of 60× 6 s, 48× 20 s and 90× 60 s unfiltered exposures. These exposures were automatically dark-frame and flat-field corrected. Later, to obtain a good signal-to-noise ratio, some of the exposures were combined.

The weather conditions during the observation were fine, with the Moon about 7° below the horizon at the time of trigger, and the GRB about 11° (airmass=5.2) above the horizon, rising slowly to about 18° during the first hour after the GRB.

Following the detection by BOOTES, the 2.54 m Nordic Optical Telescope was triggered. Although the weather at La Palma was not perfect (thick cirrus passing), several exposures with a good detection of the OT were obtained. The first 300 s was errorneously obtained in a narrow-band NII filter. Then a 300 s R-band image was obtained. Further, a series of unfiltered spectroscopical acquisition images was taken, but the worsening weather did not allow for a good spectrum to be taken. By the end of the night, another series of unfiltered images was obtained. NOT kept observing the position for the two following nights. The optical afterglow was further observed by

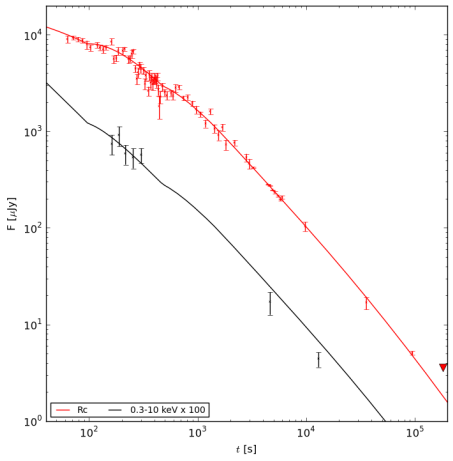

Figure 22 The optical and X-ray lightcurve of the afterglow fitted with two energy injections.

the 0.6 m B&C telescope at Mt. John, New Zealand. One month after the GRB, the position was reimaged and photometrically calibrated with the 2.54 m Isaac Newton Telescope in the r' band.

All images were astrometrically calibrated using the `past` program from the JIBARO effort (de Ugarte Postigo et al., 2005), using all sources with more than 10-σ significance from the image compared to USNO-B1.0 (Monet et al., 1998) positions. `Past` employs a sigma-clipped third-degree polynomial surface fit.

The celestial coordinates of the optical counterpart of the GRB 080413A, determined from our best resolution 2.5m NOT images are

$$\alpha = 19^{\rm h}09^{\rm m}11\overset{\rm s}{.}76 \quad \delta = -27^\circ 40' 40\overset{''}{.}6 \quad \pm 0\overset{''}{.}3 \quad \text{(J2000)},$$

about 0.6°E from τ Sgr. The error amounts to a 1-σ uncertainty including systematic errors.

Table 5 displays the log of our photometric observations (see also Fig 1), where the magnitude errors do not include systematic error of the USNO-B1.0 R1 magnitude, which are expected to be <0.1 mag.

Photometric calibration was done by establishing secondary standards in the vicinity of the optical afterglow. Two stars were calibrated in SDSS-r' band using the AB magnitudes obtained from SDSS DR7 web page. NOT and B&C images were calibrated against these standards, as well. BOOTES-1B unfiltered images needed brighter calibration stars. These were obtained from unfiltered, cloud-affected NOT images. (In any other images these stars were saturated.)

The difference between r′ and R band filters is expected to cause a constant offset in the measured brightness of the afterglow. However, the size of this offset seems to be small enough and we decided to ignore it.

Lightcurve The optical lightcurve has a rather simple layout – there seems to be a plateau, with a smooth transition to a steeper decay. This decay seems to be common with the slope observed in X-rays. During the transition, there is an indication of steps, suggesting weak re-energization of the ejecta.

The X-ray afterglow lightcurve, as mentioned by Mangano et al. (2008b) has two phases: an early steep decay, which is supposedly associated with an internal shock emission of the gamma-ray burst itself, and a later, rather more shallow lightcurve of the afterglow emission.

Mangano et al. (2008b) also mentions the detection of an X-ray flare at T0+5000s. We examined the data obtained by the 2.5 m Nordic Optical Telescope, by coincidence taken at the same time interval for a possible optical counterpart of such a flare without positive detection. The optical emission follows a smooth power law with no sign of a bump.

Lightcurve modelling The optical lightcurve data recorded by BOOTES show, apart from the general transition between two decay phases, two less prominent bumps. We show that they can be modelled as energy injections, following Jóhannesson et al. (2006). Our optical afterglow data is fitted simultaneously together with the X-ray data from *Swift*/XRT. The model only reproduces the afterglow, so the optical points affected by the host galaxy (from the second night on), as well as the flaring-phase X-ray data (i.e. until 176 s) are not used. The fit was performed in both ISM and wind density profiles, and for different numbers of injections. The best fit was reached with an initial shock followed by 2 refreshed shocks in the stellar wind profile. Parameters of this best fit are shown in Table 4.

Note that we did not use any color information - all the optical data used were unfiltered. The model, however, closely repeats the observed multicolor behaviour measured by (Cobb, 2008).

Photometry of the host galaxy By the second day after the GRB detection, the optical lightcurve starts to flatten, and a more careful analysis unveils slight positional offset of the source detected at later times. Careful analysis of the best resolution images reveals its extended nature, making it a candidate host galaxy.

The measured brightness of this object is $r' = 22.81 \pm 0.10$ and $U = 23.2 \pm 0.2$. Using two images taken by NOT (one from the first night, and the second 30 days later), we measured the positional offset between the afterlow and the supposed host galaxy as 0.94±0.02".

Table 4. The 2-injection, wind profile model parameters.

Parameter	Value
E_0	$0.8 \times 10^5 0$ erg
E_1 (1.6 min)	0.5 E_0
E_2 (8.3 min)	0.9 E_0
θ_0	1°
p	1.92
ϵ_i	0.002
ϵ_B	0.02
A_*	0.4

Note. — The injection energies E_1 and E_2 are in units of E_0, the initial energy. Other model parameters are: the half opening angle θ_0, the electron density index p, the fraction of internal energy stored in electrons after acceleration ϵ_i, the fraction of internal energy stored in the form of magnetic field ϵ_B and the wind parameter A_*.

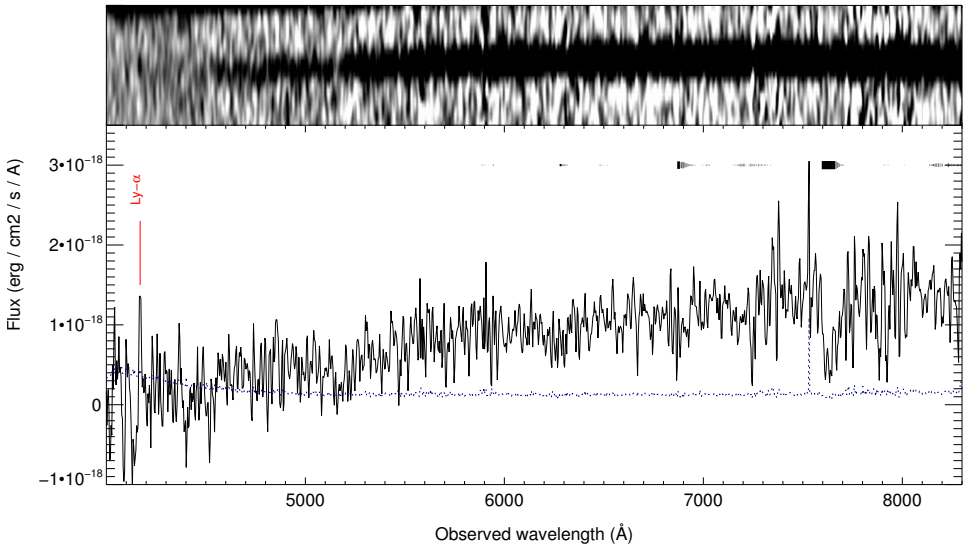

Figure 23 The spectrum of the GRB 080413A host galaxy. Note the Ly-α line on the far ultraviolet (left) side of the spectrum.

Applying the chance probabilities of Bloom et al. (2002) that a galaxy not associated with the GRB (σ_{gx} ∼0.5 %) and of (cite star density study) that any object would be found (σ_{sx} ∼1.0 %), implies a likelihood of σ ∼99.0 % that the object is a galaxy related to the GRB. We therefore consider this object the putative host galaxy.

Using (Kobulnicky, 2012) we estimate a distance modulus $D_m = 46.5 \pm 0.2$ for the GRB redshift ($z = 2.433$, $H_0 = 71 \pm 7$, $\Omega_M = 0.27$, $\Omega_\Lambda = 0.73$). For a roughly estimated host galaxy spectral slope of $\alpha = -1.0 \sim -3.0$ we derive a k-correction of $\sim 1.8 \pm 0.6$. Further, the (local) Galactic extinction is $A_r = 0.435$ Schlegel et al. (1998). The redshift of z=2.433 thus implies an absolute magnitude -22.3±0.6 for such a host, a brightness corresponding to a large elliptical galaxy, with a projected distance GRB-host 6.9 kpc.

While a large portion of GRB host galaxies are blue subluminous star forming objects (Savaglio et al., 2009), it is not impossible for a large galaxy to be found, especially in case of dark GRBs (Rossi et al., 2012).

Spectroscopy of the host galaxy We used the Gran Telescopio Canarias equipped with OSIRIS to obtain a spectrum of the host galaxy (see Fig.23), which shows a flat continuum without prominent spectral features except for a single emission spectral line which we identify as the Lyman-α line at the redshift of 2.433.

We used the spectral data to estimate the star formation rate of the galaxy, using the prescriptions of Dijkstra & Westra (2010). For the measured intensity of Ly-α line

$$F_{\mathrm{Ly}\alpha} = 1.8 \times 10^{-17} \mathrm{erg\,s^{-1}m^{-2}}$$

we obtain a lower limit (because of the limited Ly-α escape fraction cf. Atek et al. 2008)

$$\mathrm{SFR}_{\mathrm{Ly}\alpha} > 0.5 M_{\odot}\mathrm{yr}^{-1}.$$

For the estimation based on the ultraviolet continuum flux. (we used the flux estimation in the middle of the region suggested by Kennicutt 1998)

$$L_{\mathrm{UV,1900\AA}} = 1.3 \times 10^{-29} \mathrm{erg\,s^{-1}m^{-2}Hz^{-1}}$$

we get the

$$\mathrm{SFR}_{\mathrm{UV,1900\AA}} = 1.7 M_{\odot}\mathrm{yr}^{-1}.$$

Our measured Ly-*alpha* flux and star-formation rate falls well within the sample of Milvang-Jensen et al. (2012).

5.3 Conclusions

An early GRB optical lightcurve was observed with an initially shallower (plateau) and a later steeper (α 1.33 ± 0.05) decay, which fits with two energy injections. Profile seems to be a stellar wind. No optical emission related to the X-ray flare detected. While it seems that many GRBs happen in rather small galaxies (cite a general GRB host study), GRB 080413A seems to have happened in the outskirts of a large spiral or an elliptical galaxy with a relatively low star forming rate.

References

Atek, H., Kunth, D., Hayes, M., Östlin, G., & Mas-Hesse, J. M. 2008, A&A, 488, 491

Beardmore, A. P., Burrows, D. N., Evans, P. A., et al. 2008, GCN Circular, 7594

Cobb, B. E. 2008, GCN Circular, 7609

Cucchiara, A., Fox, D. B., & Cenko, S. B. 2008, GCN Circular, 7616

de Ugarte Postigo, A., Jelínek, M., Gorosabel, J., et al. 2005, in Astrofísica Robótica en España, ed. A. Castro-Tirado, B. de la Morena, & J. Torres, Madrid, 35–50

Dijkstra, M. & Westra, E. 2010, MNRAS, 401, 2343

Enoto, T., Nakagawa, Y. E., Tamagawa, T., et al. 2008, GCN Circular, 7624

Evans, P. A., Page, K. L., Beardmore, A. P., Starling, R. L. C., & Marshall, F. E. 2008, GCN Circular, 7605

Jóhannesson, G., Björnsson, G., & Gudmundsson, E. H. 2006, ApJ, 647, 1238
Kennicutt, Jr., R. C. 1998, ARA&A, 36, 189
Klotz, A., Boer, M., & Atteia, J. L. 2008, GCN Circular, 7595
Kobulnicky, C. 2012, http://faraday.uwyo.edu/ chip/misc/Cosmo2/-cosmo.cgi
Mangano, V., Barthelmy, S., Beardmore, A., et al. 2008a, GCN Circular 7794
Mangano, V., Parsons, A., Sakamoto, T., et al. 2008b, GCN Report 144
Milvang-Jensen, B., Fynbo, J. P. U., Malesani, D., et al. 2012, ApJ, 756, 25
Monet, D. B. A., Canzian, B., Dahn, C., et al. 1998, VizieR Online Data Catalog, 1252, 0
Ohno, M., Kokubun, M., Suzuki, M., et al. 2008, GCN Circular, 7630
Rossi, A., Klose, S., Ferrero, P., et al. 2012, ArXiv e-prints
Rykoff, E. S. & Rujopakarn, W. 2008, GCN Circular, 7593
Savaglio, S., Glazebrook, K., & Le Borgne, D. 2009, ApJ, 691, 182
Schlegel, D., Finkbeiner, D., & Davis, M. 1998, ApJ, 500, 525
Thoene, C. C., Malesani, D., Vreeswijk, P. M., et al. 2008, GCN Circular, 7602

Table 5. Optical photometric observations of the optical afterglow of the GRB 080413A.

UT Date of mid exp.	$T - T_0[s]$	$T_{\rm exp}[s]$	filter	mag	δ mag	tel.
2008 Apr 13.121793	63.7	6	C	14.02	0.09	B-1
2008 Apr 13.121886	71.7	6	C	13.98	0.05	B-1
2008 Apr 13.121977	79.6	6	C	14.02	0.06	B-1
2008 Apr 13.122069	87.5	6	C	14.05	0.06	B-1
2008 Apr 13.122165	95.8	6	C	14.16	0.11	B-1
2008 Apr 13.122255	103.6	6	C	14.24	0.08	B-1
2008 Apr 13.122439	119.5	6	C	14.17	0.07	B-1
2008 Apr 13.122524	126.8	6	C	14.23	0.07	B-1
2008 Apr 13.122628	135.8	6	C	14.29	0.09	B-1
2008 Apr 13.122718	143.6	6	C	14.23	0.06	B-1
2008 Apr 13.122926	161.6	6	C	14.08	0.08	B-1
2008 Apr 13.123019	169.6	6	C	14.54	0.10	B-1
2008 Apr 13.123124	178.7	6	C	14.51	0.08	B-1
2008 Apr 13.123216	186.6	6	C	14.32	0.10	B-1
2008 Apr 13.123436	205.6	6	C	14.32	0.10	B-1
2008 Apr 13.123528	213.6	6	C	14.27	0.05	B-1
2008 Apr 13.123746	232.4	6	C	14.54	0.10	B-1
2008 Apr 13.123830	239.7	6	C	14.52	0.09	B-1
2008 Apr 13.123936	248.8	6	C	14.40	0.11	B-1
2008 Apr 13.124026	256.6	6	C	14.33	0.06	B-1
2008 Apr 13.124165	268.6	6	C	14.78	0.09	B-1
2008 Apr 13.124259	276.7	6	C	15.05	0.13	B-1
2008 Apr 13.124350	284.6	6	C	14.88	0.13	B-1
2008 Apr 13.124445	292.8	6	C	14.69	0.09	B-1
2008 Apr 13.124536	300.7	6	C	14.77	0.12	B-1
2008 Apr 13.124755	319.6	6	C	14.83	0.09	B-1
2008 Apr 13.124848	327.6	6	C	15.17	0.14	B-1
2008 Apr 13.124938	335.4	6	C	14.97	0.12	B-1
2008 Apr 13.125157	354.3	6	C	15.36	0.12	B-1
2008 Apr 13.125242	361.7	6	C	14.95	0.13	B-1
2008 Apr 13.125357	371.6	6	C	15.14	0.16	B-1
2008 Apr 13.125451	379.7	6	C	15.00	0.11	B-1
2008 Apr 13.125546	387.9	6	C	15.18	0.15	B-1
2008 Apr 13.125636	395.7	6	C	15.09	0.09	B-1
2008 Apr 13.125731	403.9	6	C	15.02	0.13	B-1
2008 Apr 13.125821	411.7	6	C	15.05	0.11	B-1
2008 Apr 13.125925	420.7	6	C	15.13	0.14	B-1
2008 Apr 13.126018	428.7	6	C	14.99	0.10	B-1
2008 Apr 13.126108	436.5	6	C	15.33	0.14	B-1
2008 Apr 13.126204	444.8	6	C	15.75	0.29	B-1
2008 Apr 13.126308	453.8	6	C	15.51	0.16	B-1

Table 5 (cont'd)

UT Date of mid exp.	$T - T_0[s]$	$T_{\rm exp}[s]$	filter	mag	δ mag	tel.
2008 Apr 13.126562	475.7	3×6	C	15.25	0.10	B-1
2008 Apr 13.126840	499.7	3×6	C	15.40	0.09	B-1
2008 Apr 13.127129	524.7	3×6	C	15.47	0.11	B-1
2008 Apr 13.127660	570.6	3×6	C	15.41	0.08	B-1
2008 Apr 13.127937	594.5	3×6	C	15.47	0.11	B-1
2008 Apr 13.128344	629.7	3×6	C	15.28	0.10	B-1
2008 Apr 13.128910	678.6	6+2×20	C	15.26	0.06	B-1
2008 Apr 13.129656	743.0	3×20	C	15.54	0.06	B-1
2008 Apr 13.130463	812.8	3×20	C	15.52	0.07	B-1
2008 Apr 13.131452	898.2	3×20	C	15.68	0.07	B-1
2008 Apr 13.132340	974.9	3×20	C	15.84	0.10	B-1
2008 Apr 13.133412	1067.6	4×20	C	15.96	0.07	B-1
2008 Apr 13.134764	1184.4	5×20	C	16.20	0.10	B-1
2008 Apr 13.136250	1312.8	5×20	C	15.89	0.07	B-1
2008 Apr 13.137690	1437.2	5×20	C	16.33	0.11	B-1
2008 Apr 13.139134	1561.9	5×20	C	16.50	0.13	B-1
2008 Apr 13.140774	1703.6	5×20	C	16.30	0.09	B-1
2008 Apr 13.142179	1825.0	5×20	C	16.75	0.13	B-1
2008 Apr 13.146529	2200.9	10×60	C	16.70	0.07	B-1
2008 Apr 13.153694	2819.9	10×60	C	17.08	0.10	B-1
2008 Apr 13.155857	3006.8	180	NII	17.24	0.13	NOT
2008 Apr 13.158959	3274.8	180	R	17.34	0.02	NOT
2008 Apr 13.172279	4425.7	90	C	17.78	0.01	NOT
2008 Apr 13.174941	4655.7	90	C	17.81	0.01	NOT
2008 Apr 13.177962	4916.7	40	C	17.93	0.01	NOT
2008 Apr 13.180533	5138.8	40	C	17.98	0.03	NOT
2008 Apr 13.185452	5563.8	40	C	18.08	0.02	NOT
2008 Apr 13.188367	5815.7	40	C	18.17	0.03	NOT
2008 Apr 13.190763	6022.7	40	C	18.11	0.04	NOT
2008 Apr 13.234727	9821.2	2x300	C	18.86	0.12	NOT
2008 Apr 13.535831	35835	0	R	20.84	0.16	B & C
2008 Apr 14.221936	95116	5×200	R	22.14	0.05	NOT
2008 Apr 15.218093	181184	5×300	R	22.52	0.07	NOT
2008 May 13.121056	2592000	5×600	r′	22.81	0.10	INT
2011 Aug 29.916324	1.06×10^8	13×1200	U	23.2	0.2	NOT

VI. BOOTES observation of GRB 080603B

GRB 080603B was a long gamma-ray burst detected on June 3, 2008, at 19:38:13 UT by *Swift*-BAT (Mangano et al., 2008b). The burst was also detected by *Konus*-WIND (Golenetskii et al., 2008) and *INTEGRAL*-SPI/ACS (Rau, 2012).

In X-rays, the afterglow was detected by *Swift*-XRT, providing a rapid and precise localization (Mangano et al., 2008a).

The optical afterglow was observed by several telescopes - ROTSE III (Rujopakarn et al., 2008), TAROT (Klotz et al. (2008b), Klotz et al. (2008a), Klotz et al. (2009)), TLS Tautenburg (Kann et al., 2008), RTT150 (Zhuchkov et al., 2008), the Liverpool Telescope (Melandri et al., 2008), Xinglong EST (Xin et al., 2008), the 1.0m telescope at CrAO (Rumyantsev & Pozanenko, 2008; Rumyantsev et al., 2008), the 1.5 m telescope of Sayan observatory (Klunko & Pozanenko, 2008) and from Maidanak (Ibrahimov et al., 2008). In infrared by PAIRITEL (Miller et al., 2008), spectroscopy was obtained by the NOT (Fynbo et al., 2008) and the Hobby-Eberly Telescope (Cucchiara & Fox, 2008), providing a redshift of z=2.69.

An upper limit on radio emission was set by the VLA (Chandra & Frail, 2008).

6.1 Observations

At both BOOTES stations, the GRB happened during twilight, delaying follow-up by $\sim$ 1h. Despite the delay, the optical afterglow is well detected in the data from both telescopes.

The 60 cm telescope BOOTES-2/TELMA, in La Mayora, Málaga, Spain, started taking data at 20:29:19 UT, i.e. 51 minutes after the GRB trigger. A sequence of r′-band exposures was taken, and later, after confirming the detection of the optical transient, i′, g′ and Y band images were obtained. In the near infrared Y band, despite 600 s of integration, the afterglow was not detected.

The 30 cm telescope BOOTES-1B, located in El Arenosillo, Huelva, Spain, (Jelínek et al., 2010) obtained 368 unfiltered images totalling more than 6 hours of integrated light until the end of the night. The images were combined

Table 6. Calibration stars used.

ID.	g′	r′	i′	Clear
1	18.00	17.50	17.32	17.52
2	18.80	17.35	16.04	17.35
3	19.88	18.42	17.09	18.47

to improve signal-to-noise, to yield 11 data points for the period between 1.2 and 5.2 hours after the GRB. One point has a large error due to clouds crossing the field of view.

Best fit astrometric position of the afterglow, obtained from the weighted average of all available images from BOOTES-2 is

$$\alpha = 11:46:07.73 \quad \delta = +68:03:39.9 \quad (J2000),$$

about 1.6° SE from star λ Dra.

Photometry was done in the optimal aperture using IRAF/Daophot. Calibration was performed against three SDSS (DR8)(Eisenstein et al., 2011) stars. The stars are marked on the identification chart (Fig. 26) and their brightnesses are in the Table 6. Our unfiltered, "Clear", best fit magnitude Clear=$A_1 * g' + A_2 * r'$ used for BOOTES-1B calibration is mentioned as well.

For the summary of our observations, see Table 7.

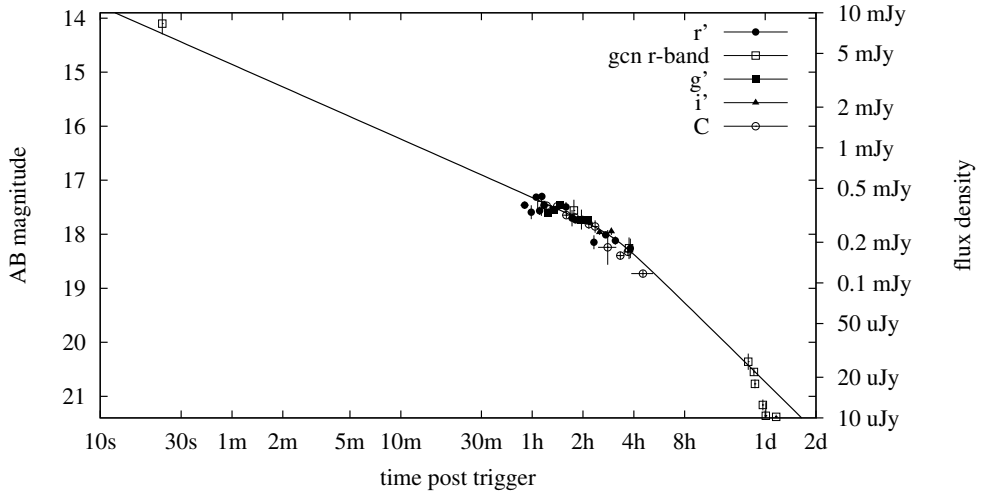

Figure 24 The overall view of the light curve of GRB 080603B.

Table 7. Optical photometric observations of the optical afterglow of the GRB 080603B.

UT Date of mid exp.	$T - T_0[h]$	tel.	filter	$T_{\rm exp}[s]$	mag	δ mag
Jun 3.855805	0.902	B-2	r′	3×120 s	17.46	0.07
Jun 3.859348	0.987	B-2	r′	2×120 s	17.59	0.13
Jun 3.862188	1.056	B-2	r′	2×120 s	17.31	0.05
Jun 3.864311	1.107	B-2	r′	120 s	17.57	0.08
Jun 3.865747	1.141	B-2	r′	120 s	17.30	0.07
Jun 3.867151	1.175	B-2	r′	120 s	17.46	0.06
Jun 3.868946	1.218	B-1B	Clear	10×60 s	17.53	0.07
Jun 3.870011	1.243	B-2	g′	3×120 s	18.29	0.04
Jun 3.874248	1.345	B-2	g′	3×120 s	18.24	0.04
Jun 3.876758	1.405	B-1B	Clear	10×60 s	17.54	0.06
Jun 3.879225	1.465	B-2	g′	4×120 s	18.14	0.03
Jun 3.884248	1.585	B-2	r′	3×120 s	17.50	0.09
Jun 3.884664	1.595	B-1B	Clear	10×60 s	17.70	0.06
Jun 3.889912	1.721	B-2	r′	3×120 s	17.70	0.15
Jun 3.892654	1.787	B-1B	Clear	10×60 s	17.75	0.06
Jun 3.893455	1.806	B-2	r′	4×120 s	17.74	0.06
Jun 3.899839	1.959	B-2	g′	5×120 s	18.42	0.19
Jun 3.900620	1.978	B-1B	Clear	10×60 s	17.79	0.06
Jun 3.906961	2.130	B-2	g′	5×120 s	18.42	0.04
Jun 3.908509	2.167	B-1B	Clear	10×60 s	17.87	0.09
Jun 3.914867	2.320	B-2	r′	4×120 s	18.15	0.13
Jun 3.916482	2.359	B-1B	Clear	10×60 s	17.91	0.11
Jun 3.922694	2.508	B-2	i′	5×120 s	17.89	0.05
Jun 3.931774	2.726	B-2	r′	7×120 s	18.01	0.06
Jun 3.934988	2.803	B-1B	Clear	35×60 s	18.30	0.32
Jun 3.940845	2.943	B-2	i′	5×120 s	17.88	0.07
Jun 3.947882	3.112	B-2	r′	5×120 s	18.12	0.08
Jun 3.956941	3.330	B-1B	Clear	20×60 s	18.45	0.07
Jun 3.971736	3.685	B-1B	Clear	21×60 s	18.38	0.06
Jun 3.977109	3.814	B-2	r′	5×120 s	18.26	0.18
Jun 4.006997	4.531	B-1B	Clear	78×60 s	18.79	0.07

6.2 Fitting The Lightcurve

The lightcurve, as already shown by Zhuchkov et al. (2008) shows a smooth transition between two decay slopes $\alpha_1 = -0.55 \pm 0.16$ and $\alpha_2 = -1.23 \pm 0.22$. The break occurs at $t_b = 0.129 \pm 0.016$ days.

There is no hint of chromatic evolution within the lightcurve so all filters were scaled and fitted together with the r'-band. The fitting of the lightcurve was performed in $\log t / \log f$ space, where power law functions, typical for gamma-ray bursts, show as straight lines. We used a hyperbolic transition between two slopes (smoothly broken power-law):

$$h(a, b) = a + \frac{b}{2}\sqrt{1 + \frac{a^2}{b^2}}$$

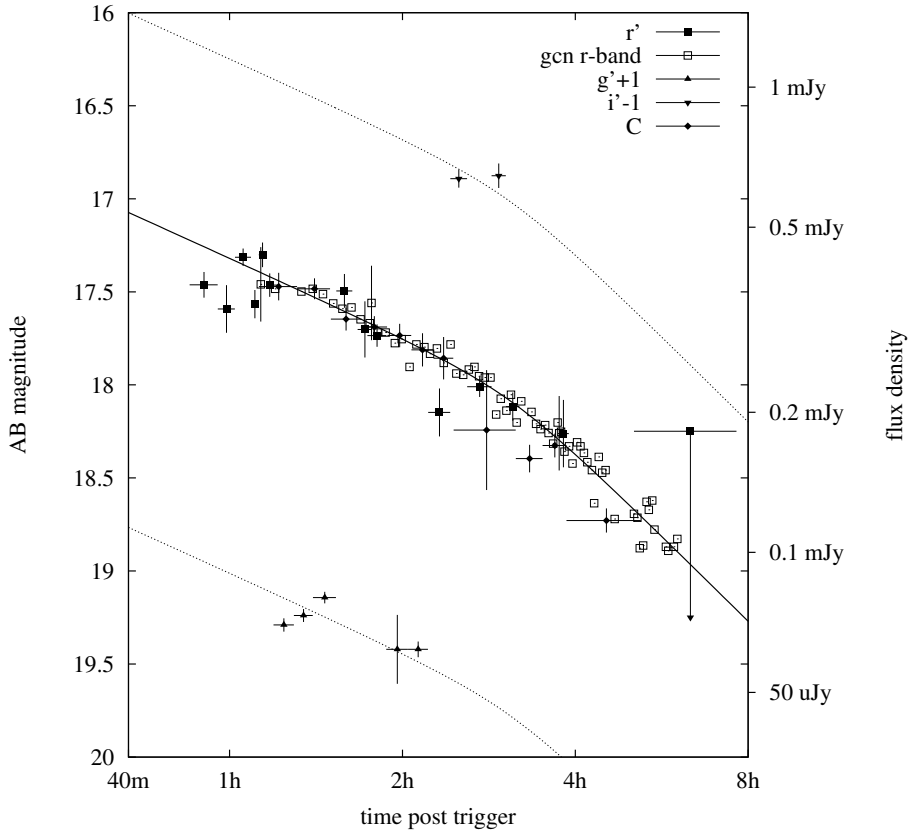

Figure 25 The detail of the optical light curve of GRB 080603B showing the observations by BOOTES (filled symbols) and from literature (empty symbols).

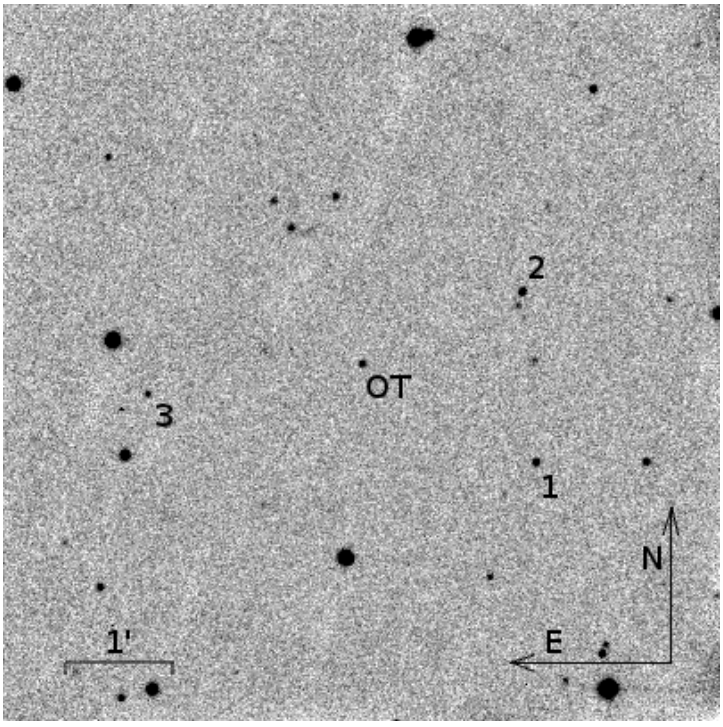

Figure 26 The finding chart of the afterglow of GRB080603B. Combination of images taken by BOOTES-2.

$$m(t) = m_0 - 2.5\alpha_2 \log \frac{t}{t_b} \ + h(-2.5(\alpha_1 - \alpha_2) \log \frac{t}{t_b}, G)$$

Where α_1 and α_2 are pre-break and post-break decay indices, t_b is the break time, m_0 is an absolute scaling parameter of the brightness and G expresses smoothness of the break.

Although the early point by ROTSE (Rujopakarn et al., 2008) was not used, it agrees with the backward extrapolation of the α_1 slope and so supports this simple interpretation.

We constructed a spectral energy distribution (SED) by fitting the needed magnitude shift of the R-band lightcurve model to the photometric points from BOOTES, UVOT (Mangano et al., 2008b) and PAIRITEL (Miller et al., 2008) obtained in other filters. While the points from UVOT are practically contemporaneous to BOOTES, PAIRITEL observed rather later (0.32 days after trigger), so the SED is therefore model-dependent in its infrared part. The synthetic AB magnitudes equivalent to $t = 0.1$ days are in Table 8.

The SED shows a clear supression of radiation above $4500\mathring{A}$, i.e. redshifted Ly-α line. No radiation is detected above the Lyman break at $3365\mathring{A}$. A rather shallow power law with an index $\beta = -0.53 \pm 0.06$ was found red-

Table 8. The spectral energy distribution in AB magnitudes equivalent to 0.1 days after the trigger. († UVOT, ‡ PAIRITEL)

Filter	$m_{\rm AB}$	$\Delta m_{\rm AB}$
W†	20.98	0.56
U†	19.83	0.23
B†	19.22	0.14
g'	18.57	0.07
r'	17.88	0.05
i'	17.81	0.09
J‡	17.44	0.10
H‡	17.19	0.10
K‡	17.22	0.10

wards from r' band. The fit was performed using the E(B-V) = 0.013 mag (Schlegel et al., 1998).

The strong suppression of light for wavelengths shorter than r' band is likely due to the Ly-α absorption within the host galaxy and Ly-alpha line blanketing for z=2.69.

6.3 Discussion

The values of $\alpha_2 = -1.23 \pm 0.22$ and $\beta = -0.53 \pm 0.06$ both point to a common electron distribution parameter $p = 2.05 \pm 0.20$ ($\alpha = (3 * p - 1)/4$, $\beta = (p - 1)/2$) (Piran, 2004). Such a combination suggests a stellar wind profile expansion and a slow cooling regime.

The pre-break decay rate $\alpha_1 = -0.55 \pm 0.16$ remains unexplained by the standard fireball model. It is unlikely that the break at $t_b = 0.129 \pm 0.016$ would be a jet break. It is quite possible that the plateau is not really a straight power law, and that some late activity of the inner engine may be producing bumping of hydrodynamic origin.

We note that the literature contains a number of observations suggesting a rapid decay by about one day after the GRB. Without having all the images, it is, however, impossible to decide whether this is a real physical effect or a zero-point mismatch.

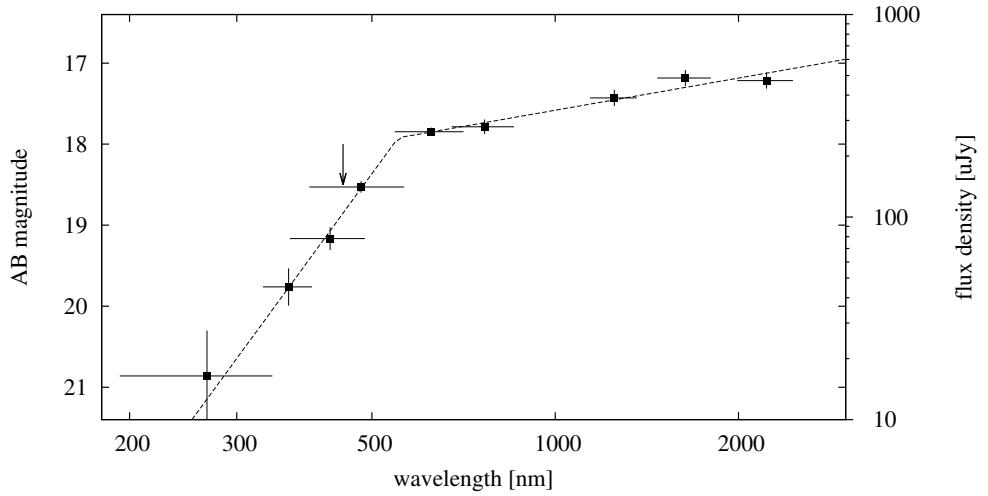

Figure 27 The spectral energy distribution of the afterglow in rest frame. The small arrow marks Ly-α position for $z = 2.69$.

6.4 Conclusions

The 0.6 m telescope BOOTES-2 in La Mayora observed the optical afterglow of GRB 080603B in three filters. The 0.3 m BOOTES-1B in El Arenosillo observed the same optical afterglow without filter.

Using the data we obtained at BOOTES and from the literature, we construct the lightcurve and broadband spectral energy distribution.

Our fit of the obained data provides the decay parameters $\alpha_2 = 1.23 \pm 0.22$ and $\beta = -0.53 \pm 0.06$, which suggest a slow cooling expansion into a stellar wind.

References

Chandra, P. & Frail, D. A. 2008, GCN Circular 7827
Cucchiara, A. & Fox, D. 2008, GCN Circular 7815
Eisenstein, D. J., Weinberg, D. H., Agol, E., et al. 2011, AJ, 142, 72
Fynbo, J., Quirion, P.-O., Xu, D., et al. 2008, GCN Circular 7797
Golenetskii, S., Aptekar, R., Mazets, E., et al. 2008, GCN Circular 7812
Ibrahimov, M., Karimov, P., Rumyantsev, A., & Pozanenko, A. 2008, GCN Circular 7975
Jelínek, M., Castro-Tirado, A. J., de Ugarte Postigo, A., et al. 2010, Advances in Astronomy, 2010
Kann, D., Laux, U., & Ertel, S. 2008, GCN Circular 7823
Klotz, A., Boer, M., & Atteia, J. 2008a, GCN Circular 7799
Klotz, A., Boer, M., & Atteia, J. 2008b, GCN Circular 7795

Klotz, A., Boër, M., Atteia, J., & Gendre, B. 2009, The Astronomical Journal
Klunko, E. & Pozanenko, A. 2008, GCN Circular 7890
Mangano, V., La Parola, B., & Sbarufatti, B. 2008a, GCN Circular 7806
Mangano, V., Parsons, A., Sakamoto, T., et al. 2008b, GCN Report 144
Melandri, A., Gomboc, A., Guidorzi, C., et al. 2008, GCN Circular 7813
Miller, A., Bloom, J., & Perley, D. 2008, GCN Circular 7827
Piran, T. 2004, Reviews of Modern Physics, 76, 1143
Rau, A. 2012, http://www.mpe.mpg.de/gamma/science/grb/1ACSburst.html
Rujopakarn, W., Guver, T., & Smith, D. 2008, GCN Circular 7792
Rumyantsev, A., Antoniuk, K., & Pozanenko, A. 2008, GCN Circular 7974
Rumyantsev, V. & Pozanenko, A. 2008, GCN Circular 7869
Schlegel, D., Finkbeiner, D., & Davis, M. 1998, ApJ, 500, 525
Xin, L., Feng, Q., Zhai, M., et al. 2008, GCN Circular 7814
Zhuchkov, R., Bikmaev, I., Sakhibullin, N., et al. 2008, GCN Circular 7803

VII. Photometric observations of GRB 080605 by BOOTES-1B and BOOTES-2

BOOTES-1B and BOOTES-2 were the world-first telescopes to follow-up the *Swift* GRB 080605. Observations started 44 s after the GRB trigger, discovering the optical afterglow with the brightness ot $R = 14.7$. The early, fast decay of the optical afterglow can only be detected on BOOTES images.

7.1 Introduction

A power-law decay with an $\alpha = 1.27 \pm 0.04$ was observed during the first $\sim$ 600 s after the trigger, in contrast to the later, shallower decay.

The GRB in question was a long burst detected by Swift on June 5, 2008 at 23:43:57 UT Sbarufatti et al. (2008). The best known position is

$$\alpha = 17:28:30.05 \quad \delta = +04:00:56.2 \quad \text{(J2000)}$$

from *HST* imaging. The host was found to be a metal enriched star forming galaxy at redshift 1.64 (Krühler et al., 2012). Zafar et al. (2012) analyzed the SED of GRB 080605 to show that its host galaxy exhibits the 2175Å extinction feature.

In the vicinity of the afterglow location, there are several stars complicating the photometry with small and medium size telescopes Kann et al. (2008). From photometric points from *GROND* (Zafar et al., 2012), a power-law decay index of $\alpha_{\rm late} = 0.72$ can be derived.

7.2 Observation by BOOTES

BOOTES-1B reacted to the burst trigger and started to take images 44 s after the GRB. A series of 2 s unfiltered exposures were acquired. The pixel scale of 2"/pixel does not permit us to spatially separate the optical transient from the nearby, 17. 8 m star. About 10 minutes after the trigger, the OT+star flux is dominated by the star and getting the OT brightness from then on becomes impossible. To obtain photometry, images were combined, resulting in longer exposure times. Eventually, 28 photometric points were

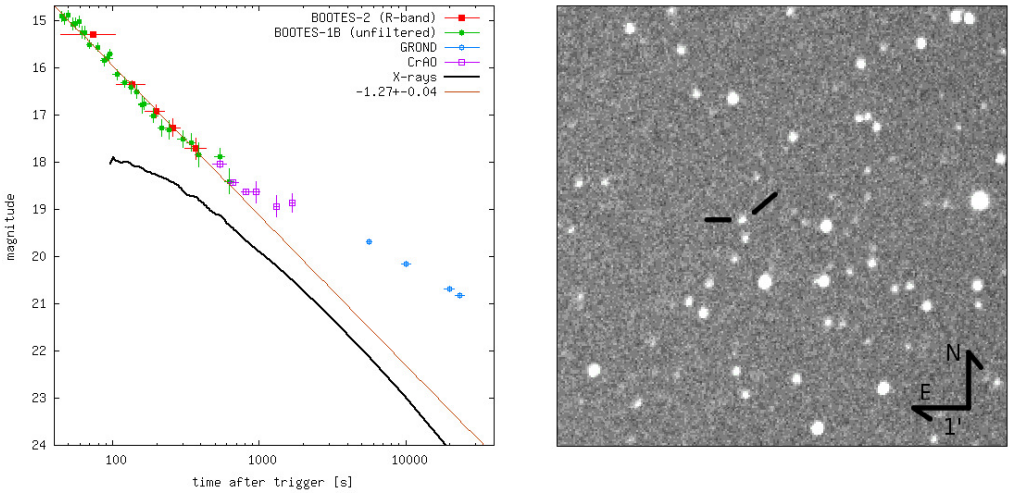

Figure 28 Left: the optical and XRT lightcurve lightcurve of the GRB 080605, X-rays (Sbarufatti et al., 2008) have been scaled up by an arbitrary constant. Right: Details of the surroundings of the optical afterglow of GRB 080605 as observed by BOOTES-1B. Image taken 45 s after the trigger.

obtained between 45 and 630 s after the GRB trigger. By a simultaneous fit of the decay rate α and the nearby star brightness

$$m_{\mathrm{measured}} = -2.5 log_{10}(10^{-0.4 m_\star} + 10^{-0.4 m_{\mathrm{OT},t_0} + 2.5 \alpha log_{10} \frac{t}{t_0}})$$

we obtained $\alpha = 1.27 \pm 0.04$ and the brightness $m_\star = 17.81 \pm 0.03$. The photometric points obtained are in the Table 9 with the nearby star flux subtracted.

BOOTES-2/TELMA reacted in 44 s and obtained a series of 60 s R-band exposures. The images have the same problem as those from BOOTES-1B: it is impossible to distinguish the star and the OT. Five photometric points were obtained by flux subtraction of the star with $m_{\mathrm{R}} = 17.42 \pm 0.07$.

7.3 Discussion

BOOTES-1B and BOOTES-2 data were independently fitted and both provided the same decay index $\alpha = 1.27$ during the first 10 minutes after the trigger. A nearby star prevented prolonged follow-up with the coarse spatial sampling provided by BOOTES. X-ray lightcurve (Sbarufatti et al., 2008), seems to undergo a transition from a plateau into a power-law decay with

T [s]	exp	mag	dmag	tel	T [s]	exp	mag	dmag	tel
44.7	2.0	14.68	0.11	B-1B	158.5	15.0	16.55	0.18	B-1B
47.3	2.0	14.73	0.11	B-1B	164.7	27.0	16.53	0.13	B-1B
49.6	2.0	14.65	0.10	B-1B	190.7	24.0	16.79	0.15	B-1B
53.3	2.0	14.84	0.13	B-1B	215.7	25.0	17.05	0.18	B-1B
55.9	2.0	14.83	0.12	B-1B	241.9	26.0	17.08	0.20	B-1B
59.3	2.0	14.79	0.12	B-1B	300.1	43.0	17.28	0.18	B-1B
61.9	2.0	15.02	0.13	B-1B	343.3	43.0	17.35	0.19	B-1B
64.5	2.0	15.02	0.14	B-1B	386.1	39.0	17.62	0.26	B-1B
69.8	7.0	15.27	0.08	B-1B	428.9	42.0	17.80	0.28	B-1B
78.9	6.0	15.34	0.09	B-1B	537.0	84.0	17.66	0.17	B-1B
87.4	8.0	15.61	0.12	B-1B	627.3	94.0	18.18	0.27	B-1B
91.8	16.0	15.57	0.08	B-1B					
95.8	8.0	15.47	0.10	B-1B	74.1	60.0	15.28	0.03	B-2
107.2	14.0	15.91	0.11	B-1B	135.5	60.0	16.35	0.08	B-2
121.1	13.0	16.08	0.12	B-1B	196.7	60.0	16.91	0.14	B-2
133.7	13.0	16.19	0.13	B-1B	258.0	60.0	17.27	0.19	B-2
146.2	11.0	16.28	0.15	B-1B	371.4	121.0	17.70	0.23	B-2

Table 9 Photometric observations of the GRB 080605 optical afterglow, as obtained by BOOTES-1B and BOOTES-2. The brightness shown is after subtracting the flux of the nearby star. The first column shows the time in seconds since the burst trigger.

$\alpha_{\rm X} = 1.47$. The optical lightcurve decay as seen by Zafar et al. (2012) between 1.5 and 6.5 h after the trigger is $\alpha_{\rm late} = 0.72$. There might be some trace of a transition between the two optical decay rates detected by Rumyantsev & Pozanenko (2008) at about 700 s after the trigger.

References

Kann, D. A., Laux, U., & Ertel, S. 2008, GRB Coordinates Network, 7864
Krühler, T., Fynbo, J. P. U., Geier, S., et al. 2012, AAP, 546, A8
Rumyantsev, V. & Pozanenko, A. 2008, GRB Coordinates Network, 7857
Sbarufatti, B., Parsons, A., Sakamoto, T., et al. 2008, GCN Report, 142, 1
Zafar, T., Watson, D., Elíasdóttir, Á., et al. 2012, APJ, 753, 82

VIII. A decade of GRB follow-up by BOOTES in Spain (2003-2013)

Since 1997, the BOOTES network has been part of the effort to follow-up gamma-ray burst events. As of now (August 2014), the network of robotic telescopes BOOTES consists of five telescopes around the globe, dedicated primarily to GRB afterglow follow-up. We present the results of our GRB follow-up programme by two telescopes of the network - BOOTES-1B and BOOTES-2. This text covers eleven years of GRB follow-ups: 71 follow-ups providing 21 detections. Follow-ups by BOOTES-1B from 2005 to 2008 were given a special attention, and are used to study the efficiency of the system. The All-sky monitor cameras (CASSANDRA) have not yet detected any GRB optical afterglows, but limits are reported where available.

Different instruments have been part of BOOTES during the years in question: two all-sky cameras, ASM1 at BOOTES-1 and ASM2 at BOOTES-2, a 30 cm telescope which was used for most of the time at BOOTES-1 station but at periods also at BOOTES-2, and the fast-moving 60 cm telescope at BOOTES-2 (Telma).

This chapter is a merging of two articles: Jelínek et al. (2010a) provided detailed description of evolution of BOOTES-1B, and analysis of efficiency of a system dedicated to GRB follow-up based on real data obtained during four years between 2005 and 2008, sections 8.1 and 8.4 are based on this article. Jelinek & Castro-Tirado (2014) is a catalogue of BOOTES-1B and BOOTES-2 GRB observations between 2003 and 2013; it is complete in providing information about successfully followed-up events, but does not provide analysis of missed triggers as the previous article.

8.1 BOOTES-1B

The telescope is built mostly from commercially available components — a Paramount ME from Software Bisque and a D=30 cm Schmidt-Cassegrain optical tube assembly from Meade. Over time, four distinct system configurations were used, including also two 8 inch S-C telescopes.

Figure 29 Four historic BOOTES-1B configurations.

8.1.1 Original Meade — stereoscopic system

The original BOOTES project idea of a new generation of robotic telescopes was very simple, BOOTES-1B would — simultaneous with an identical setup at BOOTES-2 for parallax ability — look for optical transients in an extended area of the sky with wide field cameras. Both systems would use a commercial 12-inch Meade LX-200 "robot". The wide-field cameras were considered a primary instrument, while the ability to follow-up with a large telescope was an option. Between 1998 and 2002 the wide-field system provided simultaneous limits for several *CGRO*/BATSE and *BeppoSAX* GRBs, most notably the candidate afterglow for the short GRB 000313 (Castro-Tirado et al., 2002). The 30 cm telescope was successfully used to follow-up GRB 030329.

Although we made the original system able to observe, it kept having problems. It required an operator presence several times per week and, despite a notable effort, the fork mount's electronics had to be exchanged several times. Because of that, we decided to purchase another mount.

Figure 30 The building of ESAt with domes of BOOTES-1A and BOOTES-1B (2002).

8.1.2 The Prototype

The new incarnation of BOOTES-1B was in preparation since mid-2002, and the first prototype was put together in November 2002 in order to follow-up *INTEGRAL* bursts. The most important change was the mount to be used — the Paramount ME from Software Bisque. The system was still carrying a wide field camera, but a shift had been made in priorities — the wide field camera performed monitoring of satellite field of view and the telescope pointed when a trigger was received. The early stage was, however, plagued with technical and organizational problems which eventually delayed the first real-time real-GRB follow-up until early 2005.

The prototype carried three instruments on a large aluminium base plate: The 30 cm telescope with a field spectrograph (de Ugarte Postigo, 2007) plus an SBIG-ST8 camera, the 20 cm Meade (originally BOOTES-1A) telescope with an SBIG-ST9 camera observing in a fixed V-band filter, and an unfiltered wide-field 18 mm/1:2.8 with an SBIG ST-8 CCD (43°×29°).

BOOTES-1B was operating with this setup for about a year — on June 2004 it was dismounted and sent to the Workshop in Ondřejov for a definitive solution.

8.1.3 Triple Telescope

The prototype was very heavy and from the beginning had some problems. In September 2004 BOOTES-1B finally received an upgrade — together with

the 30 cm telescope, there were also two 20 cm telescopes[10] for direct imaging in different filters. The system was completely redesigned with many mechanical improvements and was built to be as light as possible to allow the mount working at its maximum slewing speed. In belief that the rapid dissemination and fast followup after the launch of *Swift* would lead into relatively frequent detections of bright optical counterparts, the 30 cm telescope was equipped with a field spectrograph and two 20 cm telescopes with fixed V&I-band filters. The limiting magnitude of all three instruments was V $\sim$ 16 for a 60 s exposure. The wide-field cameras were moved from BOOTES-1B to BOOTES-1A.

Later, during the telescope operation it became clear that the GRB optical transients were not as bright as had been expected and so the spectrograph on the 30 cm telescope was replaced with a direct imaging CCD with R-band filter — improving the limiting magnitude but losing the spectroscopic ability.

On April 23, 2006, The ESAt building was struck by lightning during a storm, destroying a major part of BOOTES-1B electronics. It took more than a year to get BOOTES-1B definitively back online.

8.1.4 Single 30 cm telescope

During the lengthy reconstruction of BOOTES-1B, the followup strategy was reconsidered: in the interest of detecting more optical transients the filter(s) were abandoned ($\sim$2.5$\times$ or 1 magnitude gain in sensitivity). The limiting

[10] One of them lent personally by AJCT

Configuration changes of BOOTES-1B

date	configuration
ix/2003	30 cm + SBIG ST-8 + spectrograph + 20 cm + SBIG ST-9, V-band
ix/2004	30 cm + SBIG ST-8 + spectrograph + 20 cm + SBIG ST-9, V-band + 20 cm + SBIG ST-9, I-band
viii/2005 – – iv/2006	30 cm + SBIG ST-8, R-band + 20 cm + SBIG ST-9, V-band + 20 cm + SBIG ST-9, I-band
ix/2006 – – xii/2006	30 cm telescope + FLI, R-band
ix/2007 – – now	30 cm telescope + andor iXon, unfiltered

magnitude of an unfiltered 120 s exposure would be about 18.0 — effectively doubling the likelihood of getting an optical transient in comparison with the R-band imaging (cf. Fig. 45). Both 20 cm telescopes were dropped because of lack of suitable CCD cameras available for them. Since then, BOOTES-1B has only a single 30 cm telescope.

Any observations obtained after June 15, 2007 have been obtained without filter (W for white). We calibrate them against R-band, which, in in the case of no color evolution of the optical counterpart, is expected to result in a small constant offset in magnitude.

8.2 BOOTES-2

BOOTES-2 is located at CSIC's experimental station La Mayora (Instituto de Hortofruticultura Subtropical IHSM-CSIC) (at lat: 36°45′33″N, long: 04°02′ 27″W), 240km from BOOTES-1. It was originally equipped with an identical 30 cm Schmidt-Cassegrain telescope to that at BOOTES-1. In 2007 the telescope was upgraded to a lightweight 60 cm Ritchey-Chrètien telescope on a fast-slewing NTM-400 mount, both provided by Astelco. The camera was upgraded at the same time to an Andor iXon 1k×1k EMCCD, and in 2012 the capabilities were extended yet again to low resolution spectroscopy, by the installation of the spectrograph (FOSC) COLORES of our own design and construction (Rabaza et al. (2013), see also chapter IX. , page 111).

8.3 Follow-up of GRB events

Hereafter we will detail the individual results for each of the 71 events followed-up in 2003 – 2013. Each GRB is given a short introductory paragraph as a reminder of the basic optical properties of the event. Although we do not discuss the properties in other wavelengths, we try to include a

Configuration changes of BOOTES-2

date	configuration
ix/2003	30 cm + SBIG ST-9, V-band
	50 mm/f1.2 + SBIG ST-8, V-band
xi/2006 –	
– vi/2007	30 cm + andor iXon, unfiltered
vi/2007 –	
– xi/2012	60 cm telescope + andor iXon (+griz filters)
xi/2012 –	
– now	60 cm telescope + andor iXon, COLORES

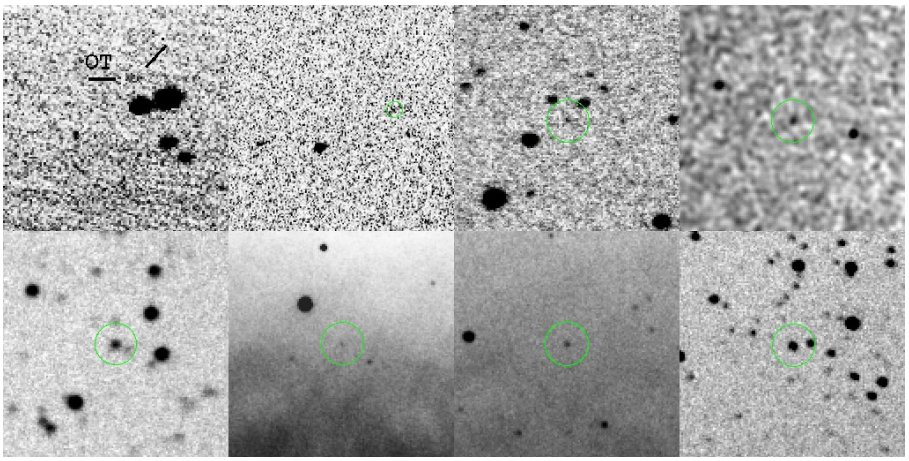

Figure 31 GRB optical transient detections by BOOTES-1B: first row: GRB 050824, GRB 050922C, GRB 051109A, GRB 080330. Second row: GRB 080413B, GRB 080430, GRB 080602B, GRB 080605.

comprehensive reference of literature relevant to each burst. As GCN reports usually summarise the relevant GCN circular traffic, we have omitted the raw GCN circulars except for events for which a GCN report or other more exhaustive paper is unavailable.

One by one, we show all the successful follow-ups that these telescopes have performed during the first ten years of the *Swift*era, and since the transition of the BOOTES network to the RTS-2 (Kubánek et al., 2004) observatory control system, which was for the first time installed at BOOTES-2 in 2003, and during the summer of 2004 at BOOTES-1.

GRB 030913 A weak *HETE2* burst (Donaghy et al., 2003). The first localization was retracted before definitive confirmation. An extensive follow-up did not reveal any optical counterpart.

The follow-up of the *HETE2* trigger by GRB 030913 belongs in the "new era" of BOOTES. BOOTES-2, then recently equipped with an early version of RTS2. It responded automatically to the trigger and observed the position just after twilight in 122 minutes. With the data taken by the 30 cm telescope, a limiting magnitude of 17.5 could be derived for 70% of the errorbox, and a limiting magnitude of 12 on 100% of the field with the wide-field camera (de Ugarte Postigo et al., 2004).

GRB 030913 was, however, the only GRB followed-up successfully at that time, given the scarcity of localizations and unreliability of the system – particularly the telescope mount then used by BOOTES-2.

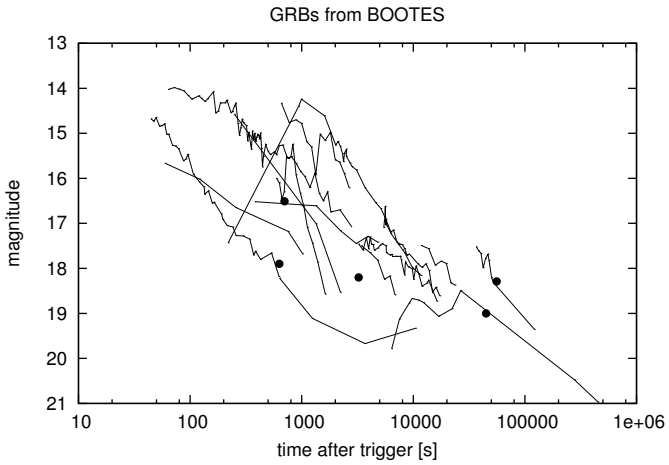

Figure 32 All the optical light curves and single detection points of BOOTES.

GRB 041016 This was a *HETE2* burst (trigger 3578). Its errorbox was covered in realtime by ASM2, providing a limit of ~ 7 during the gamma-ray emission (Jelínek et al., 2004).

GRB 041224 and GRB 041226 Two of the first bursts detected by *Swift* (Barthelmy et al., 2004; Krimm et al., 2004). Their positions were covered by the ASM2 camera (Castro-Tirado et al., 2005).

GRB 050215B This GRB was discovered by *Swift* (Barthelmy et al., 2005), was also observed by *HETE2*, and was classified as an X-ray flash (Nakagawa et al., 2005). A K-band afterglow was seen by UKIRT (Tanvir et al., 2005) and by UVOT in V-band (Mason et al., 2005).

BOOTES-1B received the notice, but a software error caused it to wait for $\sim$22 minutes before slewing to the target. We coadded 600 s exposures taken by both 20 cm telescopes to obtain limits of $V > 16.5$ and $I > 15.0$ (Jelínek et al., 2005g).

The burst was also covered during the gamma-ray emission by the All Sky Monitor at BOOTES-2 (ASM2), which provided an unfiltered limit of 10.0 (Jelínek et al., 2005c).

GRB 050421 A rather short and dim, FRED-like burst localized by *Swift* (Barbier et al., 2005; Sakamoto et al., 2005) Suggested as "naked burst" by Godet et al. (2006), discussed also by Hascoët et al. (2011).

ASM2 provided a limit of 9.0 simultaneous to the gamma-ray emission (Jelínek et al., 2005d).

GRB 050505 A bright *Swift*-discovered burst (Hurkett et al., 2006), for which Keck+LRIS detected the afterglow and calculated a redshift of $z = 4.275$ (Berger et al., 2006).

No optical afterglow was detected in images from BOOTES-1B down to the limit of $V > 19$ on a coadd of images starting 47 min after the burst and lasting for one hour (de Ugarte Postigo et al., 2005b). Considering the redshift of the GRB, V-band was likely to have suffered Lyman forest blanketting.

The burst was covered simultaneously by the All Sky Monitor at BOOTES-1 (ASM1), which provided an unfiltered limit of 9.2 (Jelínek et al., 2005b).

GRB 050509A A rather short long GRB detected by *Swift* (Hurkett et al., 2005). An optical candidate observed by NOT turned out to be an uncatalogued star (Fynbo et al., 2005b,a)

At the time of this trigger, the observatory dome was still operating independently from the rest of the system - we obtained the first image 23 s after the GRB trigger (6 s after receiving the alert), although the dome was closed due to what we consider a false reading on the rain sensor. The first useful 10 s exposure was obtained 63.8 min after the burst and has a limiting magnitude of V>14.9. A coadd of first 112×10 s exposures with an exposure mean time 88.0 min after the GRB has a limit of V>18.1.

GRB 050509B The first short duration GRB for which an accurate positional measurement was made, sufficient to locate it near to an elliptical galaxy lying at a redshift of 0.225 (Gehrels et al., 2005; Bloom et al., 2006).

Starting 62 s after the trigger, BOOTES-1B obtained one of the world-first data set of this GRB. However, bad luck caused that the location of the GRB on the sky coincided with the tip of a nearby antenna and it's signalling light. The limiting magnitude is thus seriously degraded. The first 10 s exposure has a limiting magnitude V > 11.5, a combination of the first 12×10 s exposures provides V>12.5.

GRB 050525A A bright low-redshift ($z = 0.606$) localized by *Swift* (Blustin et al., 2006). Plenty of optical data, including the signature of the associated supernova sn2005nc (Della Valle et al., 2006; Resmi et al., 2012).

GRB 050525A was the first BOOTES-1B burst for which a detection was obtained. The telescope started the first exposure 28 s after receiving the notice, 383 s after the GRB trigger. An optical afterglow with $V \simeq 16$ was detected. A weak detection of a bright GRB implied a reexamination of observing strategies employed by BOOTES.

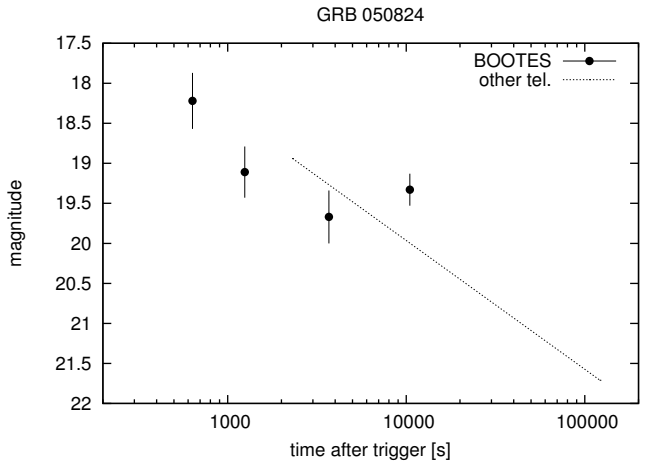

Figure 33 The optical light curve of GRB 050824 (Sollerman et al., 2007).

This burst was covered in real time by both All-Sky monitors of BOOTES (ASM1 and ASM2), providing an unfiltered limit of >9.0 (de Ugarte Postigo et al., 2005a).

GRB 050525A

$\Delta T[min]$	exp[s]	$\mathrm{mag_R}$	dmag	ref.
11.7	39×10 s	16.51	0.39	Resmi et al. (2012)

GRB 050528 A soft *Swift* burst (Cummings et al., 2005; Holland et al., 2005) with no optical afterglow detected.

BOOTES-1B started taking images 71 s after the burst and 28 s after receiving the trigger in a light twilight, setting the limit to the possible GRB counterpart to V>13.8 and I>13.0 during the first 60 s after the beginning of our observation (Jelínek et al., 2005a).

GRB 050730 A very long and bright *Swift*-localized GRB (Perri et al., 2007a). Optical afterglow with mag $R \sim 17$, redshift 3.97 (D'Elia et al., 2007).

Occurring at 19:58:23 UT, this GRB was very low above the horizon when BOOTES-1B began taking exposures 233.4 s after the GRB, but only a few images were taken before the system failed. The images did not provide detection of the 17.0 mag optical transient discovered by both *Swift*-UVOT and 1.5 m telescope at OSN (Pandey et al., 2006).

GRB 050824 A dim burst detected by *Swift*. The optical afterglow of this GRB discovered with the 1.5 m telescope at Sierra Nevada, redshift $z = 0.83$ by VLT (Sollerman et al., 2007).

BOOTES-1B was the first telescope to observe this optical transient, starting 636 s after the trigger with $R \simeq 17.5$. The weather was not stable and the focus not perfect, but BOOTES-1B worked as expected. In the end, several hours of data were obtained.

GRB 050824

$\Delta T[h]$	$\mathrm{mag_R}$	dmag	ref.
0.1763	18.22	0.35	Sollerman et al. (2007)
0.3462	19.11	0.32	Sollerman et al. (2007)
1.0249	19.67	0.33	Sollerman et al. (2007)
2.9091	19.33	0.20	Sollerman et al. (2007)

GRB050904 A very famous long and bright high-redshift GRB detected by *Swift* (Haislip et al., 2006). This was the first GRB where Ly-α blanketing had serious serious impact on optical observations – GRB was undetectable in R-band because of its redshift of $z = 6.3$.

BOOTES-1B reacted to this GRB, starting 124 s after the trigger. There was a hot pixel close to the GRB location, which made us believe we might have a detection in the R-band, which was issued in the first BOOTES-1B circular. Later, the observation revised as a limit ($R > 18.2$) which was used to compute the record redshift of this GRB (Haislip et al., 2006). The I-band camera of the 20 cm telescope, unluckily, failed.

GRB 050922C A *Swift* short and intense long burst (Norris et al., 2005; Krimm et al., 2005) that was observed also by *HETE2* (Crew et al., 2005). Optical afterglow mag ~ 15, $z = 2.198$ (Jakobsson et al., 2005).

Due to clouds, the limiting magnitude of BOOTES-1B dropped from $\sim$ 17.0 for a 30 s exposure to mere 12.9. The afterglow was eventually detected with the R-band camera (at the 30 cm telescope) during gaps between flying clouds. The first weak detection was obtained 228 s after the GRB trigger and gave $R \simeq 14.6$.

GRB 051109A A burst detected by *Swift* (Fenimore et al., 2005). Optical afterglow mag 15, redshift $z = 2.346$ (Quimby et al., 2005), optical lightcurve by Mirabal et al. (2006).

At BOOTES-1B the image acquisition started 54.8 s after the burst with the 30 cm telescope in R-band and one of the 20 cm telescopes in I-band

GRB 050922C

$\Delta T[h]$	exp[s]	$\mathrm{mag_R}$	dmag
0.0694	40	14.58	0.35
0.3752	900	17.01	0.39
0.6193	900	18.53	0.59

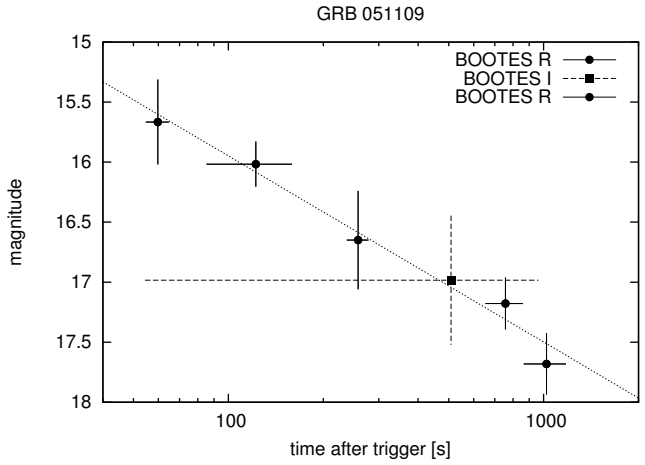

Figure 34 The optical light curve of GRB 051109. The dotted line represents the optical decay observed by Mirabal et al. (2006).

(Jelínek et al., 2005f). There were still a number of performance problems - most importantly synchronization between cameras such that when the telescope position was to be changed, both cameras had to be idle. As the 30 cm telescope was taking shorter exposures, extra exposures could have been made while waiting for the slower 20 cm to finish. The 20 cm detection is, after critical revision, only at the level of 2-σ. The R-band observation shows the object until about 20 minutes after the GRB, when it becomes too dim to measure in the vicinity of a 17.5 m nearby star. Mean decay rate observed by BOOTES is $\alpha = 0.63 \pm 0.06$.

GRB 051211A A *HETE2* burst with a single 33 s hard gamma-ray peak (Atteia et al., 2005).

The ASM-2 30 s image which starts 5 s prior to the GRB trigger sets an $R > 10$ upper limit to any possible prompt optical flash for GRB 051211A (Jelínek et al., 2005e).

GRB 051109A

$\Delta T[h]$	exp[s]	mag	dmag
	R-band		
59.7	10	15.67	0.35
122.2	74	16.02	0.19
257.9	41	16.65	0.41
756.6	205	17.18	0.22
1021.5	313	17.68	0.26
	I-band		
508.4	908	16.98	0.54

GRB 051211B A GRB detected by *INTEGRAL* (Mereghetti et al., 2005; Vianello et al., 2009).

Observation of this burst started 42 s after the burst. A 30 s R-band exposure was obtained, but the camera failed after getting this image. The 20 cm telescope acquired only useless defocused I-band images. (Jelínek et al., 2005e).

GRB 051221B Burst localized by *Swift* (Boyd et al., 2005), no optical afterglow. (GRB 051221A was a short burst with an optical afterglow.)

BOOTES-1B slewed to the position and started obtaining images 27.8 s after receiving the alert (234.8 s after the burst). We did not find any new source in our images (de Ugarte Postigo et al., 2005c).

GRB 060421 A *Swift*-localized burst with no discovered afterglow (Goad et al., 2006).

BOOTES-1B reacted to this GRB within 61 s of the trigger. Images were not of great quality, yielding a limit of R>14 for the first 10 s exposure and R>16 for the combination of 30 images (exposure mean time 547 s after the trigger).

GRB 061110B A bright GRB localized by *Swift*, notices delayed 10 min, optical afterglow by Liverpool telescope, $z = 3.44$ by VLT+FORS1 (Fox et al., 2006).

BOOTES-1B started to slew immediately after reception of the trigger, obtaining the first image 698 s after the burst (72 s after the GCN notice). When seven 60 s exposures were obtained, a communication error with the mount occurred. The communication was later restored and further 19 images were obtained starting 22:49:49 UT (0.85 h after burst). The last image was obtained at 23:36:20 (1.62 h after burst).

Combination of the first 7 images (limiting magnitude ∼17.2 mag each) with the exposure mean time 938 s after the GRB trigger was found to have a magnitude limit ∼ 18.0. Combination of 11 images obtained between 22:49:49 UT and 23:03:45 UT (lim ∼ 16.9 mag each) yields a limit of ∼ 18.2 with mean time $T_0 + 3452$ s.

GRB 071101 A rather weak and short long GRB by *Swift* (McBreen et al., 2007).

This was the first successful followup of a GRB after installation of the 30 cm telescope at the BOOTES-2 site at La Mayora, with imaging started 54.8 s after the burst (23.3 s after receiving the coordinates). No afterglow was detected, an unfiltered, *R*-band calibrated limit of W>17.0 was estimated. The GRB location was also covered by the BOOTES-ASM2 in real time (Jelínek et al., 2007).

GRB 071109 An *INTEGRAL*-detected GRB (Gotz, 2007) followed up by *Swift* without a clear identification (Perri et al., 2007b). There was an unconfirmed afterglow detected in radio (Chandra & Frail, 2007).

BOOTES followed up 58.5 s after the GRB (30.9 s after receiving the alert). Because of high altitude clouds, the telescope performance was reduced, yielding an unfiltered limit of ∼ 13.0 in the first 10 s exposure. The position was also covered by the BOOTES-ASM2 camera (de Ugarte Postigo et al., 2007).

GRB 080330 A rather bright long burst detected by *Swift* Afterglow reported to be detected by UVOT, TAROT, ROTSE-III, Liverpool Telescope and GROND. Spectroscopic redshift $z = 1.51$ by NOT (Mao et al., 2008).

This GRB happened during the first day recomissioning of BOOTES-1B after its move from the BOOTES-2 site at La Mayora. The GCN client was not yet operational and at the time of the GRB we were focusing the telescope. The first image was obtained 379 s after the GRB trigger and the optical afterglow was detected with magnitude ∼ 16.3 on the first image. A bug in the centering algorithm caused a loss of part subsequent data. Further detections were obtained starting 21 min after the GRB when the problem was fixed.

GRB 080413A A rather bright GRB detected by *Swift*, detected also by *Suzaku*-WAM, optical afterglow by ROTSE-III (Yuan et al., 2008), redshift $z = 2.433$ by VLT+UVES (Marshall et al., 2008).

BOOTES-1B started obtaining images of the GRB 080413A starting 60.7 s after the trigger (46.3 s after reception of the alert). An $R \simeq 13.3$ magnitude

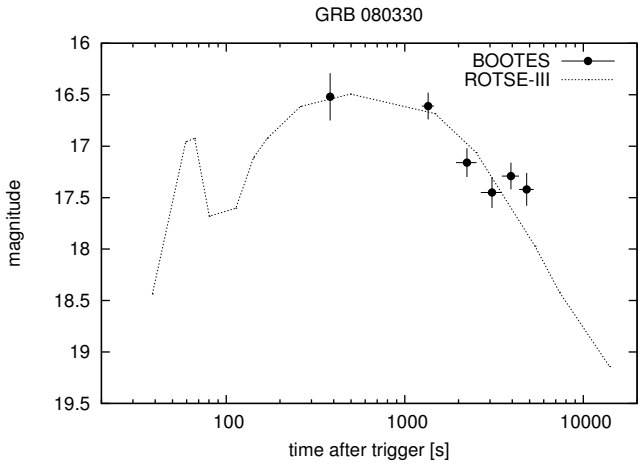

Figure 35 The optical light curve of GRB 080330. The dotted line shows how the lightcurve as seen by ROTSE-III (Yuan et al., 2008)

GRB 080330

$\Delta T[h]$	exp[s]	$\mathrm{mag_R}$	dmag
0.1061	7	16.52	0.23
0.3752	210	16.61	0.13
0.6193	588	17.16	0.14
0.8547	825	17.45	0.15
1.0915	862	17.29	0.13
1.3384	905	17.42	0.16

decaying optical afterglow was found, see. Fig. 8.3 (Kubánek et al., 2008, Jelinek et al., in prep.; and Chapter V.).

GRB 080430 A burst detected by *Swift*. It was a widely observed low-redshift $z \simeq 0.75$ optical afterglow with a slowly decaying optical afterglow (Guidorzi et al., 2008). Observed by *MAGIC* without detection (Aleksić et al., 2010).

BOOTES-1B obtained the first image of this GRB 34.4 s after the trigger. An optical transient was detected on combined unfiltered images with a magnitude $\simeq 15.5$ (Jelínek et al., 2008b; de Ugarte Postigo et al., in prep.).

GRB 080603B A long GRB localized by *Swift*, detected also by *Konus*-Wind and by *INTEGRAL* (Rau et al., 2005). Bright optical afterglow, extensive follow-up, redshift $z = 2.69$ (Mangano et al., 2008).

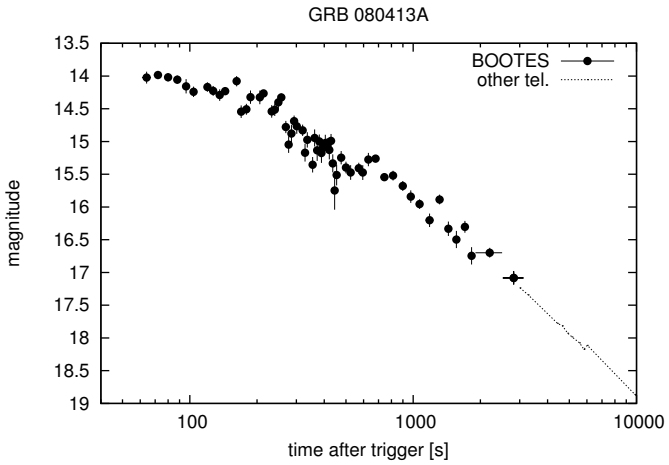

Figure 36 The optical light curve of GRB 080413.

This GRB happened in Spain during sunset. We obtained first useful images starting one hour after the trigger. An $R \simeq 17.4$ optical transient was detected with both BOOTES-1B and BOOTES-2 (Jelínek et al., 2012c).

GRB 080605 A long burst detected by *Swift* (Sbarufatti et al., 2008). The host was found to be a metal enriched star forming galaxy at redshift 1.64 (Krühler et al., 2012), and exhibits the 2175 $\mathring{A}$ extinction feature (Zafar et al., 2012).

GRB 080605 was observed by both BOOTES-1B (28 photometric points) and BOOTES-2 (5 photometric points) starting 44 s after the trigger. A rapidly decaying optical afterglow ($\alpha = 1.27 \pm 0.04$) with R = 14.7 on the first images was found (Jelínek et al., 2013), see Fig. 8.3 and Chapter VII.

GRB 081003B An *INTEGRAL*-detected GRB (Gotz et al., 2008). Undetected by *Swift*-XRT (Page & Markwardt, 2008).

BOOTES-1B started obtaining unfiltered images at 20:48:49 UT (41 s after the GRB trigger and 17.4 s after the GCN notice), single images have a detection limit of W > 14 mag. The combination of the first 32 images with an exposure mean time of 80 s after the GRB has a limit of W > 17.6 mag (calibrated against GSC2). Neither shows any new sources within the GRB errorbox (Jelínek et al., 2008a).

GRB 090313 GRB by *Swift*, no prompt X-rays (Mao et al., 2009). An optical afterglow peaking at $R \sim 15.6$. Extensive optical + infrared follow-up, the first GRB to be observed by XShooter. Also detected by various

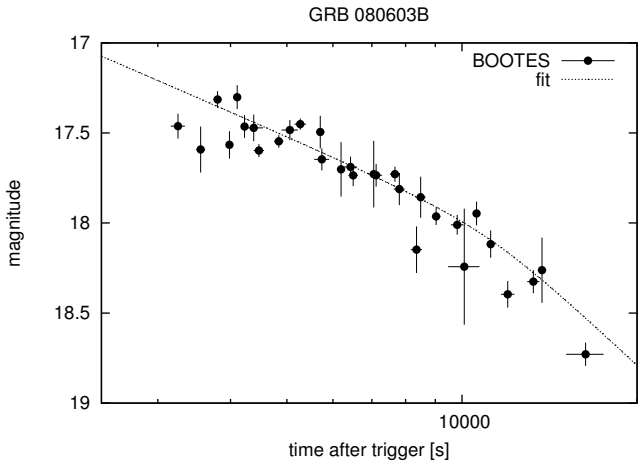

Figure 37 The optical light curve of GRB 080603B (Jelínek et al., 2012c).

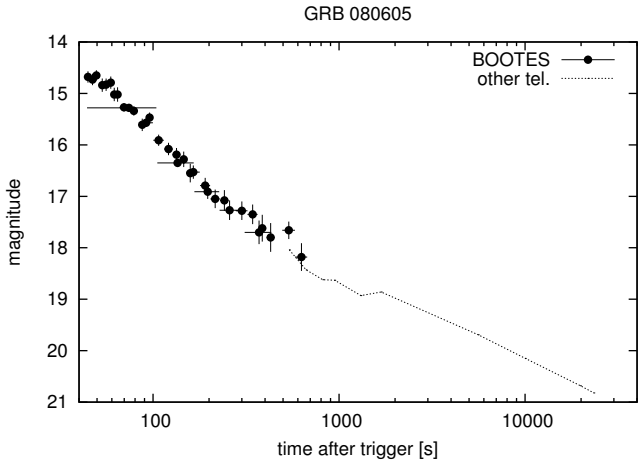

Figure 38 The optical light curve of GRB 080605 (Jelínek et al., 2013).

observatories in radio. Redshift $z = 3.375$. (de Ugarte Postigo et al., 2010a; Melandri et al., 2010)

The GRB happened during daytime for BOOTES-1B and it was followed-up manually. Due to the proximity of the Moon and limitations of then-new CCD camera driver, many 2 s exposures were taken to be combined later. The optical afterglow is detected with magnitude $\sim 18.3 \pm 0.4$ on a 635×2 s (=21 min) exposure with the mid-time 11.96 h after the GRB trigger.

GRB 090519 A rather dim burst detected by *Swift*. An $R = 22.8$ magnitude counterpart discovered ~ 20 min after the trigger at NOT + ALFOSC. Redshift of 3.85 measured by VLT + FORS (Perri et al., 2009a).

This burst was observed by BOOTES-1B starting 99 s after the trigger. The limiting magnitude was R > 17.6 and was promptly reported (Jelínek & Kubánek, 2009).

GRB 090813 A long GRB by *Swift*, suspected of being higher-z, observed also by *Konus*-Wind and *Fermi*-GBM (Cummings et al., 2009). Optical counterpart by the 1.23 m telescope at Calar Alto with a magnitude of I = 17.0 (Gorosabel et al., 2009).

BOOTES-1B started observation 53 s after the GRB, taking 10 s unfiltered exposures. The optical transient was weakly detected on a combined image of 10×10 s whose exposure mean time was 630 s after the burst. The optical counterpart was found having R = 17.9±0.3. Given that the previous and subsequent images did not show any OT detection, we might speculate about the optical emission peaking at about this time. Also the brightness is much weaker than might be expected from the detection by Gorosabel et al. (2009), supporting the high redshift origin.

GRB 090813

$\Delta T[h]$	exp[s]	$\mathrm{mag_R}$	dmag
0.175	10×10	17.9	0.3

GRB 090814A A long GRB by *Swift* (Ukwatta et al., 2009); optical afterglow $r' \sim 21$ by GROND 7 min afer the trigger (Updike et al., 2009); redshift $z = 0.696$ by VLT+FORS2 (Jakobsson et al., 2009).

BOOTES-1B observations started 172 s after the GRB trigger, a series of unfiltered 10 s images were taken, 12×10 s combined exposure with the mean time 285 s provides a magnitude limit of R > 15.8.

The burst was covered in real time by the BOOTES-ASM1 in Huelva.

GRB 090814B An *INTEGRAL* burst (Beckmann et al., 2009a), X-ray afterglow detected also by *Swift*-XRT (Evans & Baumgartner, 2009), no optical counterpart.

BOOTES-1B obtained the first image starting 53 s after the trigger. A combination of 15x10 s with mean time of 182 s after the GRB trigger provided a limit of $R > 17.5$. Single images have a limiting magnitude $R \sim 16.0$.

The burst was covered in real time by the BOOTES-ASM1 in Huelva.

GRB 090817 An *INTEGRAL* burst (Beckmann et al., 2009b), also observed by *Fermi*-GBM (Wilson-Hodge & Beckmann, 2009) and *Swift*-XRT (Evans et al., 2009). No optical afterglow. A host galaxy proposed (Holland et al., 2009), and by spectroscopy proven to be a star (Cenko et al., 2009).

BOOTES-1B started taking images during the slew. The first valid 10 s image was obtained 24 min after the GRB. A 16x10 s combined image provides a 3-σ limit of $R > 16.7$.

BOOTES-2 was by then equipped with a slow readout camera, and took a set of 40 s exposures starting 145 s after the GRB trigger, 3-sigma limit of these images is $R \sim 17.5$, a combination of first 7 images ($T_{\rm mid}$ =353 s) yielded R>18.3.

GRB 090904A Quite long and rather bright *Swift* GRB (Perri et al., 2009b). A candidate optical afterglow detected by NOT (Malesani et al., 2009).

BOOTES-2 started observations 86 s after the GRB trigger, that is, still during the gamma emision as detected by *Swift*. In particular, the third 10 s exposure covered the main peak of this GRB. The limit on any prompt emission is R>16.1 for this exposure. No counterpart was discovered in any of the images.

GRB 091127 A bright burst by *Swift*, also detected by *Fermi*-GBM, *Konus*-Wind and *Suzaku*-WAM. Bright optical afterglow, redshift $z = 0.490$, associated supernova SN 2009nz (Cobb et al., 2010; Berger et al., 2011a; Filgas et al., 2011; Vergani et al., 2011; Troja et al., 2012b).

BOOTES-2 reacted, but there were serious problems with the mount, and the telescope never reached the correct position. The burst was covered in real time by BOOTES-ASM1 in Huelva. The 3-σ limit is about 7.5 m.

GRB 091202 An *INTEGRAL* burst (Mereghetti et al., 2009), detected also by *Swift*-XRT (Vetere, 2009). A very faint and reddened optical afterglow candidate by GTC and CAHA 3.5m (de Ugarte Postigo et al., 2009).

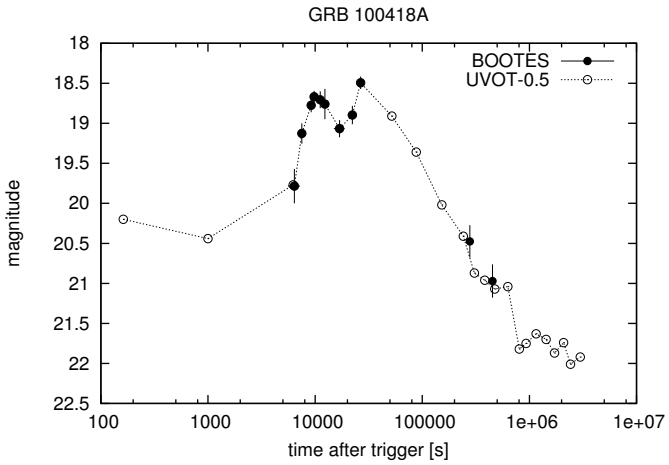

Figure 39 The optical light curve of GRB 100418A. Combination of BOOTES and UVOT data (Marshall et al., 2011). UVOT points were shifted by an arbitrary constant.

With the bright Moon, BOOTES-2 observed with a long delay of 5.5 h after the trigger due to technical problems. The 53×60 s unfiltered combined exposure with an effective exposure midtime 6 h after the GRB sets a limit of R>18.0.

The burst was covered in real time by BOOTES-ASM1 in Huelva (Pérez-Ramírez, in prep.).

GRB 100219A A rather weak long burst detected by *Swift* (Rowlinson et al., 2010). A nearby lower-redshift galaxy, the OT spectroscopically proven to be $z = 4.667$ (Thöne et al., 2013).

BOOTES-2 observed the location of the GRB yielding a limit of about 18.3 for a 30×60 s combined unfiltered exposure taken (mid) 6.32 h after the trigger.

GRB 100418A A weak long burst detected by *Swift* (Marshall et al., 2011) with a peculiar, late-peaking optical afterglow with $z = 0.6239$ (de Ugarte Postigo et al., 2011). Also detected in radio (Moin et al., 2013).

The first image of the GRB location was taken by BOOTES-2 at 21:50 UT (40 min after the GRB trigger). The rising optical afterglow was detected for the first time on an image obtained as a sum of 23 images, with an exposure mid-time 107 minutes after the GRB trigger. The optical emission peaked at magnitude R=18.7 another hour later, at an image with the mid-time 163 min after the trigger. A slow decay followed, which permitted us to detect the

optical counterpart until 8 days after the GRB.

Because of a mount problem, many images were lost (pointed somewhere else) and the potential of the telescope was not fully used. Eventually, after combining images when appropriate, 11 photometric points were obtained. A rising part of the optical afterglow was seen that way.

GRB 100418A

$\Delta T[h]$	exp[s]	$\mathrm{mag_R}$	dmag
1.78	1638	19.785	0.215
2.09	597	19.127	0.127
2.55	534	18.774	0.087
2.72	656	18.668	0.073
3.10	239	18.706	0.106
3.43	238	18.759	0.189
4.70	3908	19.067	0.108
6.19	4328	18.897	0.115
7.39	551	18.493	0.078
77.3	14830	20.475	0.202
125.6	12482	20.970	0.208

GRB 100522A A *Swift*-detected long GRB (Troja et al., 2010), also detected by *Suzaku*-WAM (Daikyuji et al., 2010) and *Konus*-Wind (Golenetskii et al., 2010a). No optical afterglow discovered.

BOOTES-2 reacted to the trigger, starting to take images 625 s after the trigger (15 s after receiving the delayed trigger). A set of 10 s unfiltered images was obtained, however the progressing twillight degraded the images (already taken at high airmass). The 120 s coadded image with an exposure mean time 735 s after the GRB provides a limit R>15.5 (Jelínek et al., 2010c).

GRB 100526A Burst detected by *Swift* (Vetere et al., 2010). Very red, most likely extinguished afterglow detected in K-band (Perley, 2010).

BOOTES-2 started to observe this GRB 4 h after the trigger with 60 s r'-filter images. Single images provided, due to the high clouds presence, a limit of $r' \simeq 14.0$. Eventually, three hours of data were taken and combined without a positive detection.

GRB 100614A A *Swift*-detected burst. No optical afterglow (D'Elia & Stratta, 2011).

BOOTES-2 observed starting 6.9 min after the onset of the GRB (18 s after the GCN notice). The co-add of 36 images (3-s each, unfiltered) obtained

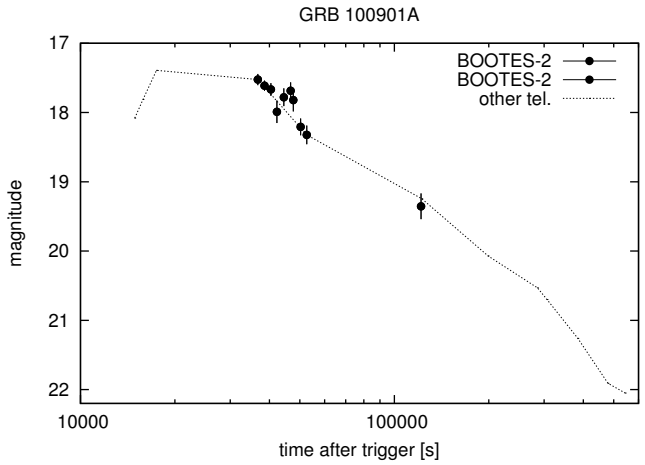

Figure 40 The optical light curve of GRB 100901A.

through cirrusses provides a limiting magnitude of R > 18 (Jelínek et al., 2010b).

GRB 100901A A long burst from *Swift*. Bright, slowly decaying optical afterglow discovered by UVOT. Redshift $z = 1.408$. Detected also by SMA in the 345 GHz band (Immler et al., 2010; Gorbovskoy et al., 2012; Hartoog et al., 2013).

The burst happened in daytime in Spain and the position became available only almost ten hours later after the sunset. The afterglow was still well detected with magniude $R \simeq 17.5$ at the beginning. BOOTES-2 had some problems with CCD cooling, and some images were useless. The afterglow was detected also the following night with $R = 19.35$.

GRB 100906A A *Swift* detected bright long GRB (Markwardt et al., 2010). Optical afterglow mag ~ 16 by UVOT. Redshift $z = 1.727$ by Gemini-N (Tanvir et al., 2010; Gorbovskoy et al., 2012).

BOOTES-1B followed-up this GRB, starting to take images 8.5 h after the GRB. The optical afterglow stays below the detection limit on a combined 100×30 s image (8.51–9.56 h after trigger), with a limit about R > 18.8.

GRB 100915A A very long and weak *Swift* burst previously classified as *likely* (Littlejohns et al., 2010).

BOOTES-2 obtained a large set of unfiltered 3 s exposures, starting 106 s after the GRB trigger. Single images have a limiting magnitude ~ 15, combined 16×3 s exposures have a limit of ~ 16.5. No optical afterglow was

GRB 100901A

$\Delta T[h]$	exp[s]	$\mathrm{mag_R}$	dmag
10.202	268	17.52	0.08
10.719	415	17.61	0.07
11.230	354	17.67	0.09
11.734	238	17.99	0.16
12.346	730	17.78	0.13
12.980	759	17.68	0.12
13.239	759	17.82	0.16
13.971	997	18.21	0.12
14.611	1101	18.32	0.14
33.791	4012	19.35	0.19

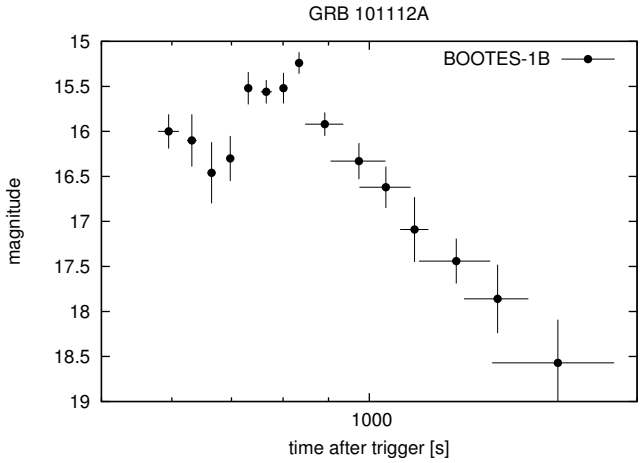

Figure 41 The optical light curve of GRB 101112A.

detected.

GRB 101020A A long long GRB by *Swift* without an optical aftergow (Saxton et al., 2010; Gorbovskoy et al., 2012).

BOOTES-2 started to observe this GRB 5.13 h after the trigger, a 40×60 s r' band combined exposure was obtained, providing a 3-sigma limit $r' > 18.0$. The effective exposure time is 05:08:14 UT, i.e. 5.46 h after the GRB trigger (Jelínek & de Ugarte Postigo, 2010).

GRB 101112A An *INTEGRAL*-localized burst (Gotz et al., 2010), also detected by *Fermi*-GBM (Goldstein, 2010), *Konus*-Wind (Golenetskii et al.,

2010b) and *Swift*-XRT (Evans & Krimm, 2010). Optical afterglow detected independently by BOOTES-2 and Liverpool Telescope (Guidorzi et al., 2010). Detected also in radio (Chandra et al., 2010).

BOOTES-2 reacted to the GRB101112A and started to observe 47 s after the GRB. A set of 3 s expoures was taken, but due to technical problems with the mount a lot of observing time was lost. An optical afterglow was discovered and reported (de Ugarte Postigo et al., 2010b). The optical lightcurve exhibits first a decay, then a suden rise to a peak at about 800 s after the trigger, followed by a surprisingly fast decay with $\alpha \simeq -4$. This behavour seems more like an optical flare than a "proper" GRB afterglow, but there does not seem to be enough data to make a firm statement.

GRB 101112A

$\Delta T[s]$	exp[s]	$\mathrm{mag_R}$	dmag
595.0	16	16.00	0.19
631.8	8	16.10	0.29
664.9	7	16.46	0.34
697.8	7	16.30	0.25
731.0	7	15.52	0.18
766.1	11	15.56	0.13
800.9	7	15.52	0.17
833.8	7	15.24	0.12
891.2	44	15.92	0.13
973.7	69	16.33	0.20
1044.0	69	16.62	0.23
1124.2	41	17.09	0.36
1252.7	115	17.44	0.25
1393.8	116	17.86	0.38
1629.5	255	18.57	0.48

GRB 110106B A *Swift*-detected GRB (Sbarufatti et al., 2011), detected also by *Fermi*-GBM (Bhat, 2011). Faint optical afterglow detected by WHT (Levan et al., 2011), galaxy redshift $z = 0.618$ (Berger et al., 2011b).

Observed by BOOTES-2, an observation done 10.3 – 12.8 min after the burst was released, the limit is $R > 16.5$ mag (Gorosabel et al., 2011).

GRB 110205A A very long and bright burst by *Swift*. Detected also by *Konus*-Wind and *Suzaku*-WAM, optical afterglow peaking at R $\sim$ 14.0, extensive multiwavelength follow-up, $z = 2.22$ *"Textbook burst"* (Zheng et al., 2012; Gendre et al., 2012).

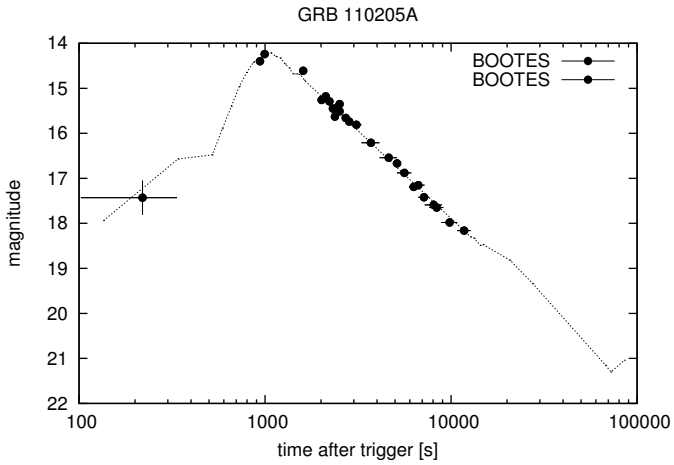

Figure 42 The optical light curve of GRB 110205A.

BOOTES-1B reacted automatically to the *Swift* trigger. First 10 s unfiltered exposure was obtained 102 s after the beginning of the GRB (with $T_{90} = 257\,s$) i.e. while the gamma-ray emission was still taking place. After taking 18 images, the observatory triggered on a false alarm from the rain detector, which caused the observation to be stopped for 20 minutes. After resuming the observation, 3×30 s images were obtained and another false alert struck over. This alert was remotely overridden by Petr, so that all 20 minutes were not lost. From then on, the observation continued until sunrise. The afterglow is well detected in the images until 2.2 hours after the GRB. 16 photometric points from combined images were eventually published.

BOOTES-2 started observations 15 min after the trigger, clearly detecting the afterglow in *R*-band until 3.2 hours after the burst. 13 photometric points were obtained. The delay was caused by technical problems (as claimed by Petr). All BOOTES data are included in the paper by Zheng et al. (2012).

GRB 110212A A faint GRB detected by *Swift*-BAT close to the Moon, no X-ray or optical afterglow (D'Elia et al., 2011a).

BOOTES-2 reacted automatically to the GRB, obtaining the first image 32.1 s after the GRB trigger (and 7.3 s after the reception of the trigger). A large number of 3-s *R*-band images was obtained. No new source was found on 40 individual images (R > 15) taken between 32 and 253 s after the GRB, nor at their 120 s (40×3 s) combination (R > 16.5) (Jelínek & Gorosabel, 2011).

BOOTES-1B also reacter, although more slowly (50 s after the GRB, 26 s

after the trigger), and the limit of the first set of 10 s exposures is of the order of 13.0. I was, however, in the middle of studying the problem with the focuser, so the images are a little out of focus.

GRB 110213A A bright burst detected by *Swift*, detected also by *Konus*-Wind and *Fermi*-GBM. Optical afterglow R $\sim$ 14.6, extensive follow-up (D'Elia et al., 2011b).

BOOTES-1B started to observe 15 hours after the GRB (the position was below horizon at the time of the trigger) and continued for an hour, eventually, 100× 30 s unfiltered images were combined, the OT brightness calibrated against USNO-A2 is 18.3±0.3 at the exposure mid-time of 15.5 h after the GRB trigger.

GRB 110213A

$\Delta T[min]$	exp[s]	$\mathrm{mag_R}$	dmag
930	100×30	18.29	0.30

GRB 110223A A faint GRB detected by *Swift* (Sakamoto et al., 2011), no optical afterglow.

At BOOTES-2 *R*-band observations began 228 s after the burst. Single images provide a limit of $\sim$ 15.4, the combination of first ten minutes has a limit of R>17.6 (Jelínek et al., 2011).

GRB 110411A A dim burst detected by *Swift* (Grupe et al., 2011). No optical counterpart: 1.5m OSN limit Sota (Sota et al., 2011).

BOOTES-1B responded during twilight, 24 s after the GRB trigger. No optical afterglow was detected on the early, bright-sky images or later imaging. In particular a combined exposure from BOOTES-1B (56×30 s), with exposure mean time 31.6 min after the GRB trigger provided an unfiltered limit of R>17.8.

GRB 111016A A very long (550 s) *Swift* GRB (Mangano et al., 2011). Faint (i′=21mag) optical afterglow detected in near-IR by the Palomar 60 inch telescope, confirmed by Gemini-N (Cenko & Evans, 2011; Cenko et al., 2011).

BOOTES-1B took 10×30 s images of the field starting 1.25 h after the trigger. The magnitude limit can be set to R>17.8 1.3 h after the burst.

GRB 120326A A *Swift*-detected burst. Afterglow discovered by TAROT. Long-lived optical emission, redshift $z = 1.78$ by GTC. Detected also by *Fermi*-GBM and *Suzaku*-WAM (Siegel et al., 2013, and references therein).

For BOOTES-1B this was a disaster, the mount failed, because of the serial port communication failure. After a manual recovery, 40 minutes after the GRB, images were taken in hope for a detection, but the counterpart with the brightness of R$\sim$19.5 was detected only at about 2σ level.

GRB 120327A A bright burst by *Swift* with an afterglow discovered by UVOT (Sbarufatti et al., 2012). Redshift $z = 2.813$ (D'Elia, 2013). Extensive optical follow-up.

BOOTES-1B reacted in 41 min (similar failure as the day before: the mount failed, because of the serial port communication failure.), obtaining a series of 20 s exposures, these images were combined to get 600 s effective exposures and premitted detection of the afterglow on six such images. The brightness was decaying from R=17.5 to R=18.6.

The all-sky camera at BOOTES-1 (ASM1) covered the event in real time and did not detect anything down to R$\sim$7.5 (Zanioni, Covino et al. in prep. 2014).

GRB 120327A

$\Delta T[min]$	exp[s]	$\mathrm{mag_R}$	dmag
57.3	654	17.50	0.12
68.4	674	17.65	0.12
80.2	748	17.82	0.13
92.0	660	18.24	0.21
103.1	673	18.17	0.21
114.3	656	18.59	0.29

GRB 120328A A rather weak burst by *Swift*. No optical emission detected (Pagani et al., 2012b).

This was 12 deg above horizon at Bootes-1B; We have 6 usable images taken between 8.6 and 17.7 min after the trigger, limit of their sum is R$\sim$17.0 at 788 s after burst, 60 s exposure total.

GRB 120514A A "long long" GRB (T_{90}=164 s) detected by *Swift* (Mangano et al., 2012). Detected also by the *Suzaku*-WAM (Akiyama et al., 2012). No optical emission detected.

BOOTES-1B reacted to GRB 120514A, the first image was taken at 01:20:20, i.e. 451 s (7.5 min) after the trigger (43 s after the notice) The limit of a single 10 s image was $R \sim 16$, but the first ten images were somehow degraded (cloud?) with limits as bad as 14.5.

GRB 120521C A bright *Swift* burst (Baumgartner et al., 2012) with a very weak optical and a radio afterglow shown by Laskar et al. (2014) to be at redshift $z \sim 6.0$.

BOOTES-1 performed clear-band observations between 11.7 and 21.5 minutes post burst. No object was detected within the *Swift*-XRT circle down to R$\sim$20.5 (Jelínek et al., 2012d).

GRB 120711B A *Swift*-detected dim burst which happened 3.5° above the galactic plane (Page et al., 2012b) (11A was an intensively followed-up bright GRB from *INTEGRAL*).

BOOTES-1B got GRB this with a 107 s delay after the GRB (27 s after recieving the GCN notice). A long series of 10 s images was acquired. No new object was detected neither on single images down to the limiting magnitude R $>$ 17.0 nor on a combined 60$\times$10 s image with a magnitude limit if 18.2.

GRB 120729A *Swift*-detected relatively bright burst with low redshift $z = 0.6$ (Ukwatta et al., 2012). Bright 13.2 mag optical counterpart by Raptor (Wren et al., 2012).

Burst happened in daytime for Spain. BOOTES-1B followed-up for about 3 hours, starting 10 h after the GRB, providing a limit of R $>$ 19.0. BOOTES-2 started 13.25 hours after the trigger and provided a limit of R $>$ 19.4 (Gorosabel et al., 2012b).

GRB 120805A GRB from *Swift* (Troja et al., 2012a). An optical afterglow discovered by CAHA 1.23m (Gorosabel et al., 2012a), and confirmed by NOT (Malesani et al., 2012).

BOOTES-2 started observing 25 minutes after the GRB. A 33$\times$60 s image with an exposure mean time 41.6 min after the GRB trigger provides a limit of R $>$ 18.5.

GRB 120816A GRB detected by *Swift* (Page et al., 2012a). Afterglow with R $\sim$ 17.8 by Rau & Kanbach (2012).

BOOTES-2 + COLORES started to observe the field about one hour after the GRB, as soon as the night started, obtaining a series of unfiltered images. In particular, a combination of 15 $\times$ 60 s frames gathered around

20:24:35 UT (i.e. $T_0 + 66$ min) provides a limit of R > 18 at the position of the reported optical counterpart (Jelínek et al., 2012e).

GRB 121001A A bright and long *Swift*-detected GRB, originally designated as possibly galactic (D'Elia et al., 2012). Afterglow discovered by Andreev et al. (2012).

BOOTES-2 observed this trigger starting 32 min after the trigger. An optical afterglow is detected in I-band with $I \sim 19.7$ (Vega) for a sum of images between 20:49 – 21:52 UT (Tello et al., 2012).

GRB 121017A A *Swift*-detected short long GRB without an optical afterglow (Grupe et al., 2012).

BOOTES-2 + COLORES started to take unfiltered images about 3 min post burst (19:26:10 UT), following the initial *Swift*-BAT position. There is no optical counterpart within the *Swift*-XRT error box down to $R = 18.5$ for a 153 s combined exposure (5 min post burst). Further exposures in i'-band (22:05 UT, 1200 s on the aggregate) set a limit of 19.5 (35 min post burst) (Jelínek et al., 2012b).

BOOTES-1B observed starting 79 s after the GRB trigger. A series of 10 s exposures with a limiting magnitude of $R \sim 17$ was obtained. A sum of the first 10 minutes of the follow-up provides a limit of $R > 19.0$.

GRB 121024A A bright *Swift*-detected GRB with a bright optical afterglow (Pagani et al., 2012a; Klotz et al., 2012). Detected also in radio (Laskar et al., 2012). Redshift $z = 2.298$ by Tanvir et al. (2012).

BOOTES-1B observed the optical afterglow of GRB 121024A. The observations started 40 minutes after the GRB trigger. The sum of 20 minutes of unfiltered images with a mean integration time 54 minutes after the GRB shows a weak detection of the optical afterglow with magnitude roughly $R = 18.2 \pm 0.5$ (Jelínek et al., 2012a).

GRB 121024A

$\Delta T[h]$	exp[s]	$\mathrm{mag_R}$	dmag
0.900	1200	18.2	0.5

GRB 121209A A GRB detected by *Swift*. At the X-ray position a weak source, proposed to be a host galaxy (Maselli et al., 2013).

BOOTES-1B responded in an unfavorable weather, getting a 41.7 s post GRB delay. A series of 10 s exposures was obtained, with varying quality due to the passing clouds. Limiting magnitude of the images varies between 14.0

an 15.0, and after 20 images taken (~ 250 s after burst) goes slowly down to 13.0, when the astrometric solution starts to fail (~ 400 s after the GRB). An image combined from 12×10 s with mean exp. time at 176.8 s has a limiting magnitude of 16.5. No GRB counterpart was found.

The all-sky camera was reading out when the GRB trigger occured, starting the new exposure at 21:59:26.9 UT, i.e. 15.5 s after the trigger. Both reactions seem to be within the 60 s long GRB "alive" period.

GRB 130122A A *Swift*-detected burst, optical afterglow by UVOT (Lien et al., 2013).

BOOTES-1B responded to this GRB with dT=28min, but due to a technical failure (Pointing was 50 arcmin away, and only eventually, the astrometry caught up and permitted the images after 03:55 UT to be centered on the GRB location.), only a limit R>18.4 for a 15 min integration could be obtained for a mid-time 4.325 h after the GRB.

GRB 130418A A bright and long burst with a well detected optical afterglow somewhat peculiarly detected after a slew by *Swift* (de Pasquale et al., 2013), observation by *Konus*-Wind shows that the burst started already 218 s before *Swift* triggered (Golenetskii et al., 2013). Redshift $z = 1.218$ by de Ugarte Postigo et al. (2013).

BOOTES-2 obtained a large set of unfiltered, r'-band and i'-band images starting 1.5 h after the trigger. The optical afterglow is well detected in the images. The lightcurve is steadily decaying with the power-law index of $\alpha = -0.93 \pm 0.06$, with the exception of the beginning, where there is a posible flaring with peak about 0.25 mag brighter than the steady power-law (Gorosabel et al., in prep.).

GRB 130505A A bright and intense GRB with a 14 mag optical afterglow detected by *Swift* (Cannizzo et al., 2013). Redshift $z = 2.27$ reported by Tanvir et al. (2013).

BOOTES-2 obtained the first image of this GRB 11.94 h after the trigger. A set of 60 s exposures was obtained. Combining the first hour of images taken, we clearly detect the optical afterglow, and using the calibration provided by Kann et al. (2013), we measure R_C=19.26±0.06.

GRB 130606A A high-redshift GRB detected by *Swift* (Ukwatta et al., 2013), optical afterglow discovered by BOOTES-2, redshift $z = 5.9$ by GTC (Castro-Tirado et al., 2013).

BOOTES-2 reaction to this GRB alert was actually a failure, the system did not respond as well as it should and it had to be manually overriden to

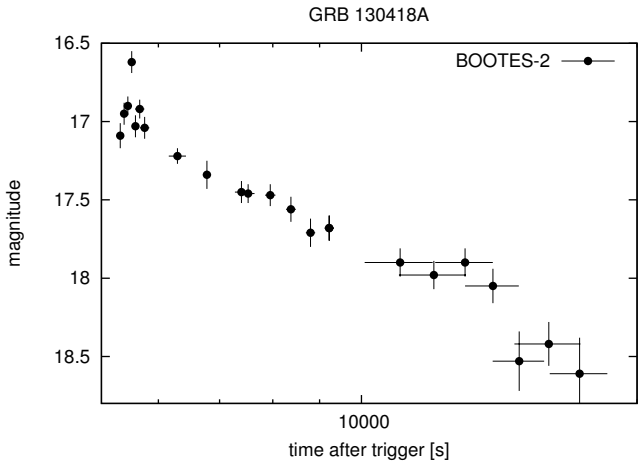

Figure 43 The optical light curve of GRB 130418A.

perform the observations. The first image has therefore been taken as late as 13 minutes after the trigger. These observations led to a discovery of a bright afterglow not seen by *Swift*-UVOT, and prompted spectroscopic observations by 10.4m GTC, which show redshift of this event to be $z = 5.9135$. Overall, 14 photometric points in i'-band and 7 in z'-band were obtained (Castro-Tirado et al., 2013).

GRB 130608A *Swift*-detected burst without a detected optical afterglow (Krimm et al., 2013).

Location of this GRB was below the local horizon at the time of reception of the notice 10 min after the trigger, and the observation had to be postponed until the position rises to be observed, first 60 s images were obtained 136 min after the GRB.

During a first epoch we combined 11 images with an unfiltered exposure of 60 seconds each that begun at 02h31m45s (136 minutes after the burst) and ended at 02h44m21s (mean time 142 minutes after the burst), and derived a limiting magnitude of R>18.8.

During a 2nd epoch we combined 22 images with an unfiltered exposure of 60 seconds each that begun at 3h00m11s (165 minutes after the burst) and ended at 3h22m08s (mean time 176 minutes after the burst) getting R>19.5 (Tello et al., 2013).

GRB 130612A A *Swift*-detected long GRB with an optical afterglow which peaked at about 90 s after the burst with V∼17.5 (Racusin et al., 2013; Trotter et al., 2013).

GRB 130418A

$\Delta T[h]$	exp[s]	$\mathrm{mag_R}$	dmag	filter
1.514	3×15 s	17.09	0.08	clear
1.529	3×15 s	16.95	0.07	clear
1.544	3×15 s	16.90	0.06	clear
1.558	3×15 s	16.62	0.07	clear
1.573	3×15 s	17.03	0.07	clear
1.590	4×15 s	16.92	0.06	clear
1.610	4×15 s	17.04	0.07	clear
1.749	7×15 s	17.22	0.05	clear
1.865	60 s	16.92	0.18	r'
1.884	4×15 s	17.34	0.09	clear
2.054	7×15 s	17.45	0.07	clear
2.089	7×15 s	17.46	0.06	clear
2.209	6×15 s	17.47	0.07	clear
2.326	6×15 s	17.56	0.08	clear
2.444	6×15 s	17.71	0.09	clear
2.562	6×15 s	17.68	0.08	clear
2.798	22×60 s	17.40	0.04	i'
3.061	15×60 s	17.90	0.09	r'
3.333	15×60 s	17.98	0.09	r'
3.604	15×60 s	17.90	0.09	r'
3.866	15×60 s	18.05	0.11	r'
4.130	15×60 s	18.53	0.19	r'
4.449	20×60 s	18.42	0.14	r'
4.808	20×60 s	18.61	0.23	r'

BOOTES-2 took the first 3 s exposure 4.8 min after the GRB, the sum of 60 such images provides a limit of R>18.6 at exp. mean time 7.7 min post trigger, the images are somewhat degraded due to technical problems with the CCD camera (analog noise).

GRB 130806A A *Swift* burst without an optical afterglow (Gompertz et al., 2013).

BOOTES-2 started taking the first image 40 s after the GRB, although it was not very well focused. Combination of all early (118×3 s) images provides a limit of R>18.3.

GRB 131202A A *Swift*-localized burst (Kocevski et al., 2013), detected also by *Fermi*-GBM (Collazzi, 2013). No optical afterglow was reported.

GRB 130505A

$\Delta T[h]$	exp[s]	$\mathrm{mag_R}$	dmag	ref.
12.488	$51 \times 60\,\mathrm{s}$	19.26	0.06	-

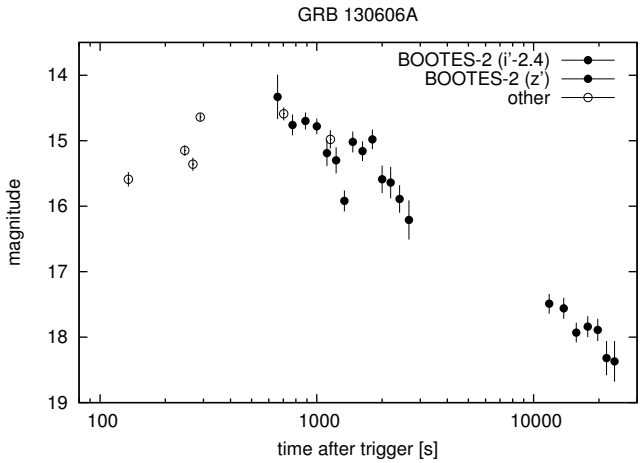

Figure 44 The optical light curve of GRB 130606A. i'-band points were shifted 2.4 mag up to match with the z'-band points.

The GRB happened in daytime in Spain, BOOTES-2 observed followed up after sunset. $58 \times 60\,\mathrm{s}$ i' band images were obtained. The exp. mean time is 19:27 UT, 4.25 h after the trigger. No optical transient was found within a limiting magnitude is $i' \sim 19.7$.

Table 10. BOOTES-1B GRBs in a table

GRB	ΔT	no. pts	result	note
030913	2 h		$? > 17.5, ? > 12$	
050215B	22 m		$V > 16.5, I > 15.0$	
050505	47 m		$V > 19$	
050509A	64 m		$V > 14.9$	
050509B	62 s		$V > 11.5$	
050525A	12 m	1	16.5 ± 0.4	> 9
050528	71 s		$V > 13.8, I > 13.0$	
050824	10 m	4	$R = 18.2 \pm 0.3$	
050904	2 m		$R > 18.2$	
050922C	4 m	3	$R = 14.6 \pm 0.4$	
051109A	55 s	6	$R = 15.7 \pm 0.4$	
051211B	42 s		$R >$	
051221B	4 m		$R >$	
060421	61 s		$R > 14$	
061110B	11 m		$R > 18$	
071101	55 s		$C > 17.0$	
071109	59 s		$C > 13.0$	
080330	6 m	6	$C = 16.5 \pm 0.2$	
080413A	61 s	*	$C \simeq 13.3$	
080430	34 s	*	$C \simeq 15.5$	
080603B	1 h	*	$C \simeq 17.4$	
080605	44 s	28	$C \simeq 14.7$	
081003B	41 s		$C > 17.6$	
090313	12 h	1	$C \simeq 18.3$	
090519	99 s		$C > 17.6$	
090813	53 s	1	$C \simeq 17.9$	
090814A	3 m		$C > 15.8$	$>$
090814B	53 s		$C > 17.5$	$>$
090817	24 m		$C > 16.7$	
100906A	106 s		$C > 16.5$	
110205A	102 s	16	C	
110212A	50 s		$C > 13.0$	
110213A	15 h	1	$C = 18.3 \pm 0.2$	
110411A	24 s		$C > 17.8$	
111016A	1.25 h		$C > 17.8$	
120326A	40 m	1	$C \sim 19.5$	
120327A	41 m	6	$C = 17.5$	> 7.5

Table 10 (cont'd)

GRB	ΔT	no. pts	result	note
120328A	7.5 m		$C > 16$	
120521C	11.7 m		$C > 20.5$	
120711B	107 s		$C > 18.2$	
120729A	10 h		$C > 19.0$	
121017A	79 s		$C > 19.0$	
121024A	40 m	1	$C = 18.2 \pm 0.5$	
121209A	42 s		$C > 16.5$	>
130122A	28 m		$C > 18.4$	

8.4 GRB follow-up efficiency

Between January 2005 until December 2008 BOOTES-1B could have received 86 GRB triggers via GCN, which could have been followed in real time or would become observable within the following two hours. Table 13 summarizes these triggers, noting, among BOOTES-1B status of the followup, also the brightness of the GRB optical counterpart, if it is known. The magnitude estimation search was done with a heavy use of GRBlog **?**. We use these data to construct a "limiting magnitude vs. likelihood of detection" graph (Fig. 45).

8.5 Implications

8.5.1 Success rate

Of the 89 triggers, 45 were processed in realtime and observed if possible, in 44 cases the system could not respond. This makes the overall failure rate quite high (50 %). 29 triggers were, however, lost due to long-term failures resulting from the telescope being struck by lightning. 8 more triggers failed during first 6 months of operation, when the system was not yet fully stable and one was lost during maintenance (and followed manually). 6 triggers out of 47 (13 %) were lost unexpectedly during the 963 nights of telescope operation if we do not count the first semester of 2005.

8.5.2 Planning

When specifying the GRB follow-up needs, the number of nights (hours) spent observing GRBs has to be estimated. Under various follow-up strategies we may derive different results.

Table 11. BOOTES-2 GRBs in a table

GRB	ΔT	no. pts	result	note
080603B		*	$R \simeq 17.4$	
080605		5	$R \simeq 14.7$	
090817	145 s		$R > 18.3$	
090904A	86 s		$R > 16.1$	
091202	5.5 h		> 18.3	
100219A	6.3 h		$C > 18.3$	
100418A	1.8 h	11	$C = 19.3$	
100522A	625 s		$C > 15.5$	
100526A	4 h		$r' > 14$	
100614A	6.9 m		$C > 18$	
100901A	6.9 m	10	$C = 17.52 \pm 0.08$	
101020A	5.1 h		$r' > 18.0$	
101112A	595 s	15	$? = 15.5$	
110106B	10.3 m		$? > 16.5$	
110205A	15 m	13	R	
110212A	32 m		$R > 16.5$	
110223A	228 s		$R > 17.6$	
120729A	13.25 h		$R > 19.4$	
120805A	25 m		$R > 18.5$	
120816A	66 m		$R > 18$	
121001A	32 m		$I > 19.7$	
121017A	3 m		$C > 18.5$, $i' > 19.5$	
130418A	1.5 h	$20+i'$	$C = 16.8 \pm 0.06$	
130606A	13 m	21	$i' = 16.7 \pm 0.3$	
130608A	2.3 h		$C > 18.8$	
130612A	4.8 m		$C > 18.6$	
130806A	40 s		$C > 18.3$	
131202A	4.25 h		$i' > 19.7$	

Due to various instrumental effects (like a passage through the South Atlantic Anomaly) related to the satellite *Swift*, an offset from the overall triggering statistic which would depend on a geographical location could be found.

In Table 13, the fourth column has the time in hours until the first set of the event location below 10° of altitude or until the Sun rises above -15° of altitude. For non-realtime events, this is the time the location spends on the night sky, for real-time triggers, it is the time between the trigger and the moment when the target becomes unobservable.

For a small telescope, we assume that once the GRB is real-time triggered, it is unlikely to detect it the following night (i.e. after ∼24 h), so we assume the following simple follow-up strategy: Let the telescope observe the GRB once it becomes accessible for the first time (which is immediately for real-time triggers) and let it observe until the GRB sets or the night ends. Do not observe any further nights. Under the given assumptions we get the following observing needs (assuming perfect weather):

Real time triggers There have been 72 real time triggers during the studied 4 years, during their first nights they accumulated 202 hours.

So if we allow only real-time followable triggers to be observed, we would need ∼ 18 triggers per year (once per 20 days) and on average 2.8 h (max. 8.0 h) of observing time per trigger, 50.5 h per year. Such a program would consume about 2 % of the telescope time.

Extended set In the extended set, we assume that GRBs that would become observable within 2 hours after the event would also be followed. We would need ∼22 triggers per year, each with an average length of 3.5 h. In total we would need 78.5 h per year, or about 3 % of the telescope time.

	Real time only	Up to 2 h
triggers/year	18	22
hours/year	50.5	78.5
hours/trigger	2.8	3.5
days/trigger	20.3	16.6

Table 12: Results of the GRB-planning statistic

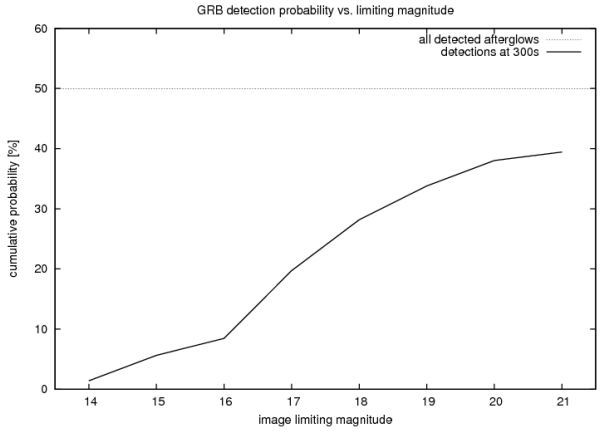

Figure 45 The graph (based on T_{300} data from Table 13), showing the likelihood of detection of an optical afterglow of a GRB as a function of the magnitude the telescope can detect (in the time interval discussed here). The dotted line delimits 50 % — the ratio of GRBs in our data for whose there was eventually discovered an optical transient.

8.5.3 Optical Afterglow Brightnesses

As a representative value of GRB optical transient brightness, important for real-time follow-up, we have chosen its magnitude at 300 s after the trigger. It turns out that it is not easy to find a uniform sample and available magnitudes and limits are a mixture of different passbands, mainly V,R and unfiltered CCD magnitudes. For a general idea of how bright an OT could be this is, however, good enough. Fig. 45 shows a cumulative probability of detecting an OT five minutes after the trigger with a telescope able to detect a given magnitude. For many GRBs the brightness at this early time is unknown, or only a limit from small telescopes has been established, so this curve is actually a slight underestimation.

For example BOOTES-1B, which could detect mag ~ 18 at an unfiltered 60 s exposure, may detect an OT in about one third of the GRB triggers.

Table 13. The Great Table of BOOTES-1B GRB triggers.

Object	Target	t_1[h]	t_{obs}[h]	m_{300}[mag]	dT	observation status
050128	-	+0.0	1.8	-	-	No link to GCN
050208	-	+0.0	4.2	-	-	No link to GCN
050215B	5064	+0.4	10.0	$\gtrsim 16^{\dagger}$	22 m	V,I limits
050306	5075	+0.2	1.8	>16	86 s	w/roof closed
050416B	5109	+0.0	2.8	-	-	`grbd` failure
050421	5112	+0.0	0.2	>18.4	-	hw problems
050502A	-	+0.0	1.8	16.3	-	`grbd` failure
050505	5123	+0.0	2.2	$-^{\dagger}$	609 s	clouds, V,I limits
050509A	5129	+0.0	2.2	>18.2	23 s	hw problems, later limit
050509B	5130	+0.0	0.0	>20.8	62 s	OK, $V > 12.5$, antenna hit!
050520	-	+0.0	3.6	>16.6	-	GCN connection lost
050525A	5136	+0.0	3.6	14.7	383 s	OK, V-band lightcurve
050714A	1037	+0.0	3.6	$-^{\dagger}$	10 m	manually, later limit
050730	50008	+1.2	1.6	17.4	1 h 40 m	limits
050805B	50015	+0.2	7.2	-	62 s	limits
050824	50032	+0.0	5.2	17.5	636 s	detection
050904	50055	+0.0	2.8	$-^{\dagger}$	124 s	R-band limit
050922C	50090	+0.0	6.2	15.5	228 s	detections between clouds
051109A	50126	+0.0	1.4	16.8	54.8 s	detection in R,I
051111	-	+0.0	4.6	14.9	-	GCN connection lost
051211A	50144	+0.0	3.2	$-^{\dagger}$	-	CCD failure
051211B	50146	+0.0	4.8	>14.0	50 s	OK, limits
051221B	50151	+0.0	3.8	>18.2		
051227	50155	+1.6	10.6	>19.2	59 m	bad weather
060111A	50162	+0.0	2.0	> 18.3	296 s	during maintenance, limit
060121	-	+0.0	7.8	$-^{\dagger}$	-	telescope OFF
060123	50171	+0.0	7.6	-	-	bad weather
060130	50173	+0.0	1.2	-	-	bad weather
060203	-	+0.0	6.2	-	-	bad weather+no GCN
060204C	-	+0.0	9.6	> 18.7	-	bad weather+no GCN
060206	-	+0.0	1.4	16.5	-	GCN connection lost
060219	50185	+1.0	6.0	>18.6	-	bad weather
060319	50190	+0.0	4.4	$>19^{\dagger}$	-	bad weather
060418	50207	+0.0	1.4	14.2	-	bad weather
060421	50208	+0.0	3.8	>16.8	61.2 s	limit
060424	-	+0.0	0.0	$-^{\dagger}$	-	hw failure
060502A	-	+0.0	1.0	18.7	-	hw failure
060507	-	+0.0	2.0	$> 15.5^{\dagger}$	-	hw failure
060512	-	+0.0	4.6	17.15	-	hw failure
060515	-	+0.0	1.4	>16.2	-	hw failure
060522	-	+0.0	1.6	19.65	-	hw failure
060602A	-	+0.0	1.2	$>15^{\dagger}$	-	hw failure
060602B	-	+0.0	3.6	-	-	hw failure
060712	-	+0.2	3.0	> 14.5	-	hw failure
060814	-	+0.0	0.8	>17.4	-	hw failure
060825	-	+0.0	1.4	>18.3	-	hw failure
060901	-	+1.6	5.2	$-^{\dagger}$	-	hw failure
060904A	-	+0.0	0.2	>19.5	-	hw failure
060904B	-	+0.0	2.2	∼17	-	hw failure
060929	50212	+0.0	1.2	>17.0	-	bad weather
061019	50220	+0.0	1.0	$>14.8^{\dagger}$	-	bad weather
061110B	50228	+0.0	2.2	$>17.8^{\dagger}$	11 m38 s	> 18.1 OK
061217	50240	+0.0	2.6	>19.2	-	mount failure
061218	50242	+0.0	2.0	>18.6	-	mount failure

8.6 Conclusions

We have shown in a small historical retrospective the evolution of the telescope of BOOTES-1B, as it developed from the wide-field survey telescope to a dedicated GRB follow-up telescope.

Eleven years of BOOTES-1B and BOOTES-2 GRB follow-up history are summarised in the textual and tabular form.

Each GRB is given a short introductory paragraph as a reminder of the basic optical properties of the event. Although we do not discuss the properties in other wavelengths, we try to include a comprehensive reference of literature relevant to each burst. One by one, we show all the successful follow-ups that these telescopes have performed during the first ten years of the *Swift*era, and the transition of the BOOTES network to the RTS-2 (Kubánek et al., 2004) observatory control system, first installed at BOOTES-2 in 2003, and made definitive during the summer of 2004.

For four years (2005-2008), an extended information was searched and the data collected are used to show the GRB trigger rate in Spain. By simply counting the triggers and the days during which they were collected, we estimate 18 triggers and about 50.5 h of telescope time per year for real time triggers. These numbers grow to about 22 triggers and 78.5 h per year if we include also the GRBs observable within 2 hours after the trigger. We also derive the likelihood of the optical afterglow detection five minutes after the GRB trigger depending on the limiting magnitude of the telescope.

References

Akiyama, M., Ohmori, N., Yamauchi, M., et al. 2012, GCN Circular, 13301
Aleksić, J., Anderhub, H., Antonelli, L. A., et al. 2010, A&A, 517, A5
Andreev, M., Sergeev, A., & Pozanenko, A. 2012, GCN Circular, 13833
Atteia, J.-L., Clergeot, H., Ricker, G., et al. 2005, GCN Circular, 4324
Barbier, L., Palmer, D., Burrows, D., et al. 2005, GCN Circular, 3296
Barthelmy, S., Barbier, L., Cummings, J., et al. 2005, GCN Circular, 3024
Barthelmy, S., Markwardt, C., Sakamoto, T., et al. 2004, GCN Circular, 2908
Baumgartner, W. H., Barthelmy, S. D., Burrows, D. N., et al. 2012, GCN Circular, 13318
Beckmann, V., Gotz, D., Mereghetti, S., et al. 2009a, GCN Circular, 9795
Beckmann, V., Gotz, D., Mereghetti, S., et al. 2009b, GCN Circular, 9815
Berger, E., Chornock, R., Holmes, T. R., et al. 2011a, ApJ, 743, 204
Berger, E., Levan, A. J., Chornock, R., & Tanvir, N. R. 2011b, GCN Circular, 11540
Berger, E., Penprase, B. E., Cenko, S. B., et al. 2006, ApJ, 642, 979
Bhat, P. N. 2011, GCN Circular, 11543
Bloom, J. S., Prochaska, J. X., Pooley, D., et al. 2006, ApJ, 638, 354
Blustin, A. J., Band, D., Barthelmy, S., et al. 2006, ApJ, 637, 901

Table 13 (cont'd)

Object	Target	t_1[h]	t_{obs}[h]	m_{300}[mag]	dT	observation status
061222B	50245	+0.0	0.6	18.0	-	mount failure
070103	50246	+0.0	2.8	>19.6	-	mount failure
070129	50253	+0.0	0.4	>19.2†	-	mount failure
070219	-	+0.0	4.8	>20.0	-	mount failure
070220	50258	+0.0	1.2	>19.6	-	mount failure
070223	50259	+0.0	4.6	>21.4†	-	mount failure
070224	50260	+1.4	8.0	>20.1†	-	mount failure
070406	50277	+0.0	4.0	-	-	mount failure
070411	-	+0.0	3.2	∼18.3	-	mount failure
070412	-	+0.0	3.2	>20.7	-	mount failure
070429A	50286	+1.6	1.0	>18.0	-	mount failure
070531	-	+0.0	1.4	>19.9	-	mount failure
070610	-	+0.4	6.2	∼19	-	mount failure
070704	-	+1.4	6.2	>21.2	-	manually disabled
070714A	50010	+0.0	1.0	-†	52 s	bad weather
071025	50033	+0.0	0.4	17.3	-	bad weather
071101	50038	+1.0	10.6	>19.7	56 s	limit
071109	50040	+0.0	1.0	>15.5	59 s	thick cirrus, limit
071112C	50044	+0.4	11.0	17.5	64 s	bad weather
080320	50076	+0.0	0.6	>20	-	bad weather
080330	50079	+0.0	1.2	16.8	400 s	manual, detection
080413A	50082	+0.0	1.6	15.0	60.7 s	detection
080430	50090	+0.8	7.4	17.5	34 s	detection
080517	50098	+0.0	2.4	>18.5	3 h 22 m	weather delay
080603B	50113	+1.6	6.4	16.5	1 h 15 m	detection
080605	50115	+0.0	3.8	17.9	43 s	detection
080727C	-	+0.0	4.8	>19.9	-	dome failure
080903	-	+0.0	4.4	19.2	-	dome failure
081001	50159	+0.0	1.4	-	-	bad weather
081003B	50167	+0.0	3.6	>17.6	41 s	OK, limit
081126	50181	+0.0	4.0	>18.0	-	bad weather
081128A	50184	+1.2	9.8	20.9	-	bad weather
081210	50188	+0.0	8.0	19.9	45 m	weather delay, out of focus
081228	50195	+0.0	2.0	19.8	-	bad weather
081230	50197	+0.0	3.2	19.1	-	bad weather

Note. — "Target" is the RTS2 target number at BOOTES-1B. t_1 is the time delay between the GRB trigger and the possible start of observation. $t_{\rm obs}$ is the amount of time for which the GRB can be followed until it sets for the first time. m_{300} is the known brightness of the GRB optical transient 300 s after the event. dT is the delay of BOOTES-1B followup.

† denotes discovered optical counterparts where there are not enough data to estimate the brightness 300 s after the GRB.

Boyd, P., Barthelmy, S., Burrows, D., et al. 2005, GCN Circular, 4376
Cannizzo, J. K., Barthelmy, S. D., Cummings, J. R., Melandri, A., & de Pasquale, M. 2013, GCN Report, 429
Castro-Tirado, A. J., Castro Cerón, J. M., Gorosabel, J., et al. 2002, A&A, 393, L55
Castro-Tirado, A. J., Jelínek, M., de Ugarte Postigo, A., et al. 2005, GCN Circular, 2961
Castro-Tirado, A. J., Sánchez-Ramírez, R., Ellison, S. L., et al. 2013, ArXiv e-prints
Cenko, S. B., Cucchiara, A., Tanvir, N. R., et al. 2011, GCN Circular, 12447
Cenko, S. B. & Evans, P. A. 2011, GCN Circular, 12444
Cenko, S. B., Walkowicz, L. M., Kasliwal, M. M., et al. 2009, GCN Circular, 9841
Chandra, P. & Frail, D. A. 2007, GCN Circular, 7049
Chandra, P., Frail, D. A., & Cenko, S. B. 2010, GCN Circular, 11404
Cobb, B. E., Bloom, J. S., Perley, D. A., et al. 2010, ApJ, 718, L150
Collazzi, A. C. 2013, GCN Circular, 15565
Crew, G., Ricker, G., Atteia, J.-L., et al. 2005, GCN Circular, 4021
Cummings, J., Barbier, L., Barthelmy, S., et al. 2005, GCN Circular, 3502
Cummings, J. R., Beardmore, A. P., & Schady, P. 2009, GCN Report, 240
Daikyuji, A., Ohmori, N., Nishioka, Y., et al. 2010, GCN Circular, 10795
de Pasquale, M., Baumgartner, W. H., Beardmore, A. P., et al. 2013, GCN Circular, 14377
de Ugarte Postigo, A. 2007, PhD thesis, Universidad de Granada
de Ugarte Postigo, A., Castro-Tirado, A. J., Gorosabel, J., et al. 2009, GCN Circular, 10247
de Ugarte Postigo, A., Goldoni, P., Thöne, C. C., et al. 2010a, A&A, 513, A42
de Ugarte Postigo, A., Guziy, S., Gorosabel, J., et al. 2004, in ESA Special Publication, Vol. 552, 5th INTEGRAL Workshop on the INTEGRAL Universe, ed. V. Schoenfelder, G. Lichti, & C. Winkler, 663
de Ugarte Postigo, A., Jelínek, M., Gorosabel, J., et al. 2005a, GCN Circular, 3480
de Ugarte Postigo, A., Jelínek, M., Gorosabel, J., et al. 2005b, GCN Circular, 3376
de Ugarte Postigo, A., Jelínek, M., Kubánek, P., Castro-Tirado, A. J., & Sabau-Graziati, L. 2007, GCN Circular, 7047
de Ugarte Postigo, A., Jelínek, M., Vítek, S., et al. 2005c, GCN Circular, 4379
de Ugarte Postigo, A., Kubánek, P., Tello, J. C., et al. 2010b, GCN Circular, 11398
de Ugarte Postigo, A., Thoene, C. C., Gorosabel, J., et al. 2013, GCN Circular, 14380
de Ugarte Postigo, A., Thöne, C. C., Goldoni, P., Fynbo, J. P. U., & X-shooter GRB Collaboration. 2011, Astronomische Nachrichten, 332, 297
D'Elia, V. 2013, in EAS Publications Series, Vol. 61, EAS Publications Series, ed. A. J. Castro-Tirado, J. Gorosabel, & I. H. Park, 247–249
D'Elia, V., Cummings, J. R., Stamatikos, M., et al. 2012, GCN Report, 392
D'Elia, V., Fiore, F., Meurs, E. J. A., et al. 2007, A&A, 467, 629
D'Elia, V., Palmer, D., Krimm, H., et al. 2011a, GCN Report, 320
D'Elia, V. & Stratta, G. 2011, A&A, 532, A48

D'Elia, V., Stratta, G., Kuin, N. P. M., et al. 2011b, GCN Report, 323
Della Valle, M., Malesani, D., Bloom, J. S., et al. 2006, ApJ, 642, L103
Donaghy, T., Suzuki, M., Lamb, D., et al. 2003, GCN Circular, 2388
Evans, P. A. & Baumgartner, W. H. 2009, GCN Circular, 9810
Evans, P. A., Guidorzi, C., & Baumgartner, W. H. 2009, GCN Circular, 9819
Evans, P. A. & Krimm, H. A. 2010, GCN Circular, 11399
Fenimore, E., Angelini, L., Barbier, L., et al. 2005, GCN Circular, 4217
Filgas, R., Greiner, J., Schady, P., et al. 2011, A&A, 535, A57
Fox, D. B., Bathelmy, S. D., Grupe, D., et al. 2006, GCN Report, 14
Fynbo, J. P. U., Jensen, B. L., Hjorth, J., et al. 2005a, GCN Circular, 3389
Fynbo, J. P. U., Jensen, B. L., Hjorth, J., et al. 2005b, GCN Circular, 3460
Gehrels, N., Sarazin, C. L., O'Brien, P. T., et al. 2005, Nature, 437, 851
Gendre, B., Atteia, J. L., Boër, M., et al. 2012, ApJ, 748, 59
Goad, M. R., Barbier, L. M., Barthelmy, S. D., et al. 2006, GCN Circular, 4985
Godet, O., Page, K. L., Osborne, J. P., et al. 2006, in American Institute of Physics Conference Series, Vol. 836, Gamma-Ray Bursts in the Swift Era, ed. S. S. Holt, N. Gehrels, & J. A. Nousek, 281–284
Goldstein, A. 2010, GCN Circular, 11403
Golenetskii, S., Aptekar, R., Frederiks, D., et al. 2010a, GCN Circular, 10796
Golenetskii, S., Aptekar, R., Frederiks, D., et al. 2010b, GCN Circular, 11400
Golenetskii, S., Aptekar, R., Frederiks, D., et al. 2013, GCN Circular, 14417
Gompertz, B. P., Burrows, D. N., Gehrels, N., et al. 2013, GCN Circular, 15071
Gorbovskoy, E. S., Lipunova, G. V., Lipunov, V. M., et al. 2012, MNRAS, 421, 1874
Gorosabel, J., Castro-Tirado, A. J., Jelínek, M., et al. 2011, GCN Circular, 11552
Gorosabel, J., Huelamo, N., Sanchez-Ramirez, R., et al. 2012a, GCN Circular, 13591
Gorosabel, J., Jelínek, M., Wang, C., et al. 2012b, GCN Circular, 13550
Gorosabel, J., Terron, V., Fernandez, M., et al. 2009, GCN Circular, 9782
Gotz, D. 2007, GCN Circular, 7048
Gotz, D., Mereghetti, S., Paizis, A., et al. 2010, GCN Circular, 11396
Gotz, D., Mereghetti, S., Paizis, A., et al. 2008, GCN Circular, 8317
Grupe, D., Kuin, P., Cummings, J. R., et al. 2011, GCN Report, 330
Grupe, D., Ukwatta, T. N., Breeveld, A., et al. 2012, GCN Report, 398
Guidorzi, C., Smith, R. J., Mundell, C. G., et al. 2010, GCN Circular, 11397
Guidorzi, C., Stamatikos, M., Landsman, W., et al. 2008, GCN Report, 139
Haislip, J. B., Nysewander, M. C., Reichart, D. E., et al. 2006, Nature, 440, 181
Hartoog, O. E., Wiersema, K., Vreeswijk, P. M., et al. 2013, MNRAS, 430, 2739
Hascoët, R., Uhm, Z. L., Mochkovitch, R., & Daigne, F. 2011, A&A, 534, A104
Holland, S. T., Band, D., Barthelmy, S., et al. 2005, GCN Circular, 3496
Holland, S. T., Breeveld, A., & Baumgartner, W. 2009, GCN Circular, 9831
Hurkett, C., Rol, E., Barbier, L., et al. 2005, GCN Circular, 3379
Hurkett, C. P., Osborne, J. P., Page, K. L., et al. 2006, MNRAS, 368, 1101
Immler, S., Sakamoto, T., Page, K. L., et al. 2010, GCN Report, 304
Jakobsson, P., de Ugarte Postigo, A., Gorosabel, J., et al. 2009, GCN Circular,

9797
Jakobsson, P., Fynbo, J. P. U., Paraficz, D., et al. 2005, GCN Circular, 4029
Jelinek, M. & Castro-Tirado, A. 2014, In prep.
Jelínek, M., Castro-Tirado, A. J., de Ugarte Postigo, A., et al. 2010a, Advances in Astronomy, 2010
Jelínek, M., Castro-Tirado, A. J., de Ugarte Postigo, A., et al. 2005a, GCN Circular, 3500
Jelínek, M., Castro-Tirado, A. J., de Ugarte Postigo, A., et al. 2004, GCN Circular, 2822
Jelínek, M., Castro-Tirado, A. J., & Gorosabel, J. 2012a, GCN Circular, 13888
Jelínek, M., Castro-Tirado, A. J., Gorosabel, J., et al. 2005b, GCN Circular, 3373
Jelínek, M., Castro-Tirado, A. J., Gorosabel, J., et al. 2005c, GCN Circular, 3029
Jelínek, M., Castro-Tirado, A. J., Gorosabel, J., et al. 2005d, GCN Circular, 3298
Jelínek, M., Castro-Tirado, A. J., Gorosabel, J., & Guziy, S. 2012b, GCN Circular, 13876
Jelínek, M., Castro-Tirado, A. J., Kubánek, P., & de Ugarte Postigo, A. 2010b, GCN Circular, 10839
Jelínek, M., Castro-Tirado, A. J., Vítek, S., et al. 2005e, GCN Circular, 4333
Jelínek, M. & de Ugarte Postigo, A. 2010, GCN Circular, 11360
Jelínek, M., de Ugarte Postigo, A., Castro-Tirado, A. J., et al. 2005f, GCN Circular, 4227
Jelínek, M., de Ugarte Postigo, A., Kubánek, P., & Castro-Tirado, A. J. 2011, GCN Circular, 11755
Jelínek, M., Gómez Gauna, E., & Castro-Tirado, A. J. 2013, in EAS Publications Series, Vol. 61, EAS Publications Series, ed. A. J. Castro-Tirado, J. Gorosabel, & I. H. Park, 475–477
Jelínek, M. & Gorosabel, J. 2011, GCN Circular, 11701
Jelínek, M., Gorosabel, J., Aceituno, F., Castro-Tirado, A., & de Ugarte Postigo, A. 2008a, GCN Circular, 8320
Jelínek, M., Gorosabel, J., Castro-Tirado, A. J., et al. 2012c, Acta Polytechnica, 52, 010000
Jelínek, M., Gorosabel, J., Castro-Tirado, A. J., et al. 2005g, GCN Circular, 3023
Jelínek, M. & Kubánek, P. 2009, GCN Circular, 9404
Jelínek, M., Kubánek, P., & Castro-Tirado, A. J. 2010c, GCN Circular, 10785
Jelínek, M., Kubánek, P., Castro-Tirado, A. J., & Gorosabel, J. 2012d, GCN Circular, 13323
Jelínek, M., Kubánek, P., Gorosabel, J., et al. 2008b, GCN Circular, 7648
Jelínek, M., Kubanek, P., Vitek, S., Castro-Tirado, A. J., & Sabau-Graziati, L. 2007, GCN Circular, 7032
Jelínek, M., Tello, J. C., Gorosabel, J., & Castro-Tirado, A. J. 2012e, GCN Circular, 13658
Kann, D. A., Stecklum, B., & Ludwig, F. 2013, GCN Circular, 14593
Klotz, A., Gendre, B., Boer, M., & Atteia, J. L. 2012, GCN Circular, 13887
Kocevski, D., Barthelmy, S. D., Baumgartner, W. H., et al. 2013, GCN Circular, 15559

Krimm, H. A., Melandri, A., & Holland, S. T. 2013, GCN Report, 434
Krimm, H., Barbier, L., Barthelmy, S., et al. 2005, GCN Circular, 4020
Krimm, H., Palmer, D., Barthelmy, S., et al. 2004, GCN Circular, 2914
Krühler, T., Fynbo, J. P. U., Geier, S., et al. 2012, A&A, 546, A8
Kubánek, P., Jelínek, M., Gorosabel, J., et al. 2008, GCN Circular, 7603
Kubánek, P., Jelínek, M., Nekola, M., et al. 2004, in AIP Conf. Proc. 727: Gamma-Ray Bursts: 30 Years of Discovery
Laskar, T., Berger, E., Tanvir, N., et al. 2014, ApJ, 781
Laskar, T., Zauderer, A., & Berger, E. 2012, GCN Circular, 13903
Levan, A. J., Tanvir, N. R., Wiersema, K., & Coccato, L. 2011, GCN Circular, 11534
Lien, A. Y., Sakamoto, T., Palmer, D. M., et al. 2013, GCN Report, 438
Littlejohns, O. M., Markwardt, C. B., Baumgartner, W. H., et al. 2010, GCN Report, 302
Malesani, D., Jakobsson, P., Tanvir, N., & Ilyin, I. 2009, GCN Circular, 9884
Malesani, D., Kruehler, T., de Ugarte Postigo, A., et al. 2012, GCN Circular, 13639
Mangano, V., Barthelmy, S. D., Burrows, D. N., et al. 2011, GCN Circular, 12439
Mangano, V., Maselli, A., Krimm, H. A., et al. 2012, GCN Report, 397
Mangano, V., Parsons, A., Sakamoto, T., et al. 2008, GCN Report, 144
Mao, J., Guidorzi, C., Markwardt, C., et al. 2008, GCN Report, 132
Mao, J., Margutti, R., Sakamoto, T., et al. 2009, GCN Report, 204
Markwardt, C. B., Barthelmy, S. D., Beardmore, A. P., et al. 2010, GCN Circular, 11227
Marshall, F. E., Antonelli, L. A., Burrows, D. N., et al. 2011, ApJ, 727, 132
Marshall, F. E., Barthelmy, S. D., Burrows, D. N., et al. 2008, GCN Report, 129
Maselli, A., Mangano, V., Ukwatta, T. N., et al. 2013, GCN Report, 422
Mason, K., Schady, P., Ivanushkina, M., et al. 2005, GCN Circular, 3037
McBreen, S., Godet, O., Ukwatta, T., et al. 2007, GCN Report, 101
Mereghetti, S., Gotz, D., Mowlavi, N., et al. 2005, GCN Circular, 4327
Melandri, A., Kobayashi, S., Mundell, C. G., et al. 2010, ApJ, 723, 1331
Mereghetti, S., Paizis, A., Gotz, D., et al. 2009, GCN Circular, 10234
Mirabal, N., Halpern, J. P., Tonnesen, S., et al. 2006, in American Astronomical Society Meeting Abstracts, Vol. 207, American Astronomical Society Meeting Abstracts, 210.02
Moin, A., Chandra, P., Miller-Jones, J. C. A., et al. 2013, ApJ, 779, 105
Nakagawa, Y., Ricker, G., Atteia, J.-L., et al. 2005, GCN Circular, 3053
Norris, J., Barbier, L., Burrows, D., et al. 2005, GCN Circular, 4013
Pagani, C., Barthelmy, S. D., Baumgartner, W. H., et al. 2012a, GCN Circular, 13886
Pagani, C., Baumgartner, W. H., Gehrels, N., et al. 2012b, GCN Circular, 13147
Page, K. L. & Markwardt, C. B. 2008, GCN Circular, 8324
Page, K. L., Palmer, D. M., Immler, S., et al. 2012a, GCN Report, 381
Page, M. J., Baumgartner, W. H., Burrows, D. N., et al. 2012b, GCN Circular, 13431

Pandey, S. B., Castro-Tirado, A. J., McBreen, S., et al. 2006, A&A, 460, 415
Perley, D. A. 2010, GCN Circular, 10806
Perri, M., D'Elia, V., Krimm, H. A., et al. 2009a, GCN Report, 219
Perri, M., D'Elia, V., Palmer, D. M., et al. 2009b, GCN Report, 245
Perri, M., Guetta, D., Antonelli, L. A., et al. 2007a, A&A, 471, 83
Perri, M., Stratta, G., Kuin, N. P. M., et al. 2007b, GCN Report, 102
Quimby, R., Fox, D., Hoeflich, P., Roman, B., & Wheeler, J. C. 2005, GCN Circular, 4221
Rabaza, O., Jelínek, M., Castro-Tirado, A., et al. 2013, Review of Scientific Instruments, 84, 114501
Racusin, J. L., Cummings, J. R., Gehrels, N., et al. 2013, GCN Circular, 14874
Rau, A. & Kanbach, G. 2012, GCN Circular, 13657
Rau, A., Kienlin, A. V., Hurley, K., & Lichti, G. G. 2005, A&A, 438, 1175
Resmi, L., Misra, K., Castro-Tirado, A. J., et al. 2012, MNRAS, 427
Rowlinson, A., Barthelmy, S. D., Baumgartner, W. H., et al. 2010, GCN Circular, 10430
Sakamoto, T., Barbier, L., Barthelmy, S., et al. 2005, GCN Circular, 3305
Sakamoto, T., Barthelmy, S. D., Baumgartner, W. H., et al. 2011, GCN Circular, 11753
Saxton, C. J., Baumgartner, W. H., Beardmore, A. P., et al. 2010, GCN Circular, 11357
Sbarufatti, B., Barthelmy, S. D., Baumgartner, W. H., et al. 2011, GCN Circular, 11525
Sbarufatti, B., Barthelmy, S. D., Gehrels, N., et al. 2012, GCN Circular, 13123
Sbarufatti, B., Parsons, A., Sakamoto, T., et al. 2008, GCN Report, 142
Siegel, M. H., Kuin, N. P. M., Holland, S., et al. 2013, GCN Report, 409
Sollerman, J., Fynbo, J. P. U., Gorosabel, J., et al. 2007, A&A, 466, 839
Sota, A., Gorosabel, J., & Jelínek, M. 2011, GCN Circular, 11928
Tanvir, N., Pak, S., Priddey, R., et al. 2005, GCN Circular, 3031
Tanvir, N. R., Fynbo, J. P. U., Melandri, A., et al. 2012, GCN Circular, 13890
Tanvir, N. R., Levan, A. J., Matulonis, T., & Smith, A. B. 2013, GCN Circular, 14567
Tanvir, N. R., Wiersema, K., & Levan, A. J. 2010, GCN Circular, 11230
Tello, J. C., Gimeno, R., Gorosabel, J., et al. 2012, GCN Circular, 13835
Tello, J. C., Jelínek, M., Gorosabel, J., Castro-Tirado, A. J., & Sanchez-Ramirez, R. 2013, GCN Circular, 14829
Thöne, C. C., Fynbo, J. P. U., Goldoni, P., et al. 2013, MNRAS, 428, 3590
Troja, E., Barthelmy, S. D., Beardmore, A. P., et al. 2012a, GCN Circular, 13588
Troja, E., Krimm, H., Beardmore, A. P., et al. 2010, GCN Report, 286
Troja, E., Sakamoto, T., Guidorzi, C., et al. 2012b, ApJ, 761, 50
Trotter, A., Hailslip, J., Reichart, D., et al. 2013, GCN Circular, 14877
Ukwatta, T. N., Krimm, H. A., Page, K. L., et al. 2009, GCN Report, 238
Ukwatta, T. N., Krimm, H. A., Palmer, D. M., et al. 2012, GCN Report, 384
Ukwatta, T. N., Stamatikos, M., Maselli, A., et al. 2013, GCN Report, 444
Updike, A., Olivares, F., Afonso, P., Yoldas, A., & Greiner, J. 2009, GCN Circular,

9794
Vergani, S. D., Flores, H., Covino, S., et al. 2011, A&A, 535, A127
Vetere, L. 2009, GCN Circular, 10243
Vetere, L., Campana, S., Cummings, J. R., et al. 2010, GCN Circular, 10797
Vianello, G., Götz, D., & Mereghetti, S. 2009, A&A, 495, 1005
Wilson-Hodge, C. A. & Beckmann, V. 2009, GCN Circular, 9823
Wren, J., Wozniak, P., Davis, H., & Vestrand, W. T. 2012, GCN Circular, 13545
Yuan, F., Rykoff, E. S., Schaefer, B. E., et al. 2008, in American Institute of Physics Conference Series, Vol. 1065, American Institute of Physics Conference Series, ed. Y.-F. Huang, Z.-G. Dai, & B. Zhang, 103–106
Zafar, T., Watson, D., Elíasdóttir, Á., et al. 2012, ApJ, 753, 82
Zheng, W., Shen, R. F., Sakamoto, T., et al. 2012, ApJ, 751, 90

IX. Spectrograph COLORES

COLORES stands for Compact Low Resolution Spectrograph. It is a spectrograph designed to be lightweight enough to be carried by the high-speed robotic telescope 60cm BOOTES-2/Telma. The instrument makes use of a high speed Electron Multiplying CCD, which permits up to 10 full frames per second. The primary scientific target of the spectrograph is a prompt GRB followup, particularly the estimation of redshift.

The system is a miniaturized FOSC (faint object spectrograph and camera), a multi-mode instrument that can switch from imaging a field (target selection and precise pointing) to spectroscopy by rotating wheel-mounted grisms, slits and filters within an otherwise fixed optical system.

The filters and the grisms (only one is mounted at the moment) are located in standard filter wheels and the optical design is comprised of a four-element refractive collimator and an identical four-element refractive camera. As a spectroscope, the instrument can use different slits to match

Table 14 COLORES at BOOTES-2 basic specifications

focal ratio	f/8
CCD resolution	1024×1024, 13 μm
CCD pixel scale	0.56″
field of view	$10' \times 10'$
magnitude limit	R>18 mag in 60 s
spectral scale	7.8 Å/pixel
slits	25/50/75/100 μm
dispersion ($\lambda/\delta\lambda$)	400/200/150/100 @ 6000 Å
spectral resolution	15/30/45/60 Å
wavelength range	3800 – 11500 Å
magnitude limit	15.5 mag in 300 s
spectrograph weight	12 kg
seeing at BOOTES-2	2” in 50%, 3” in 90%

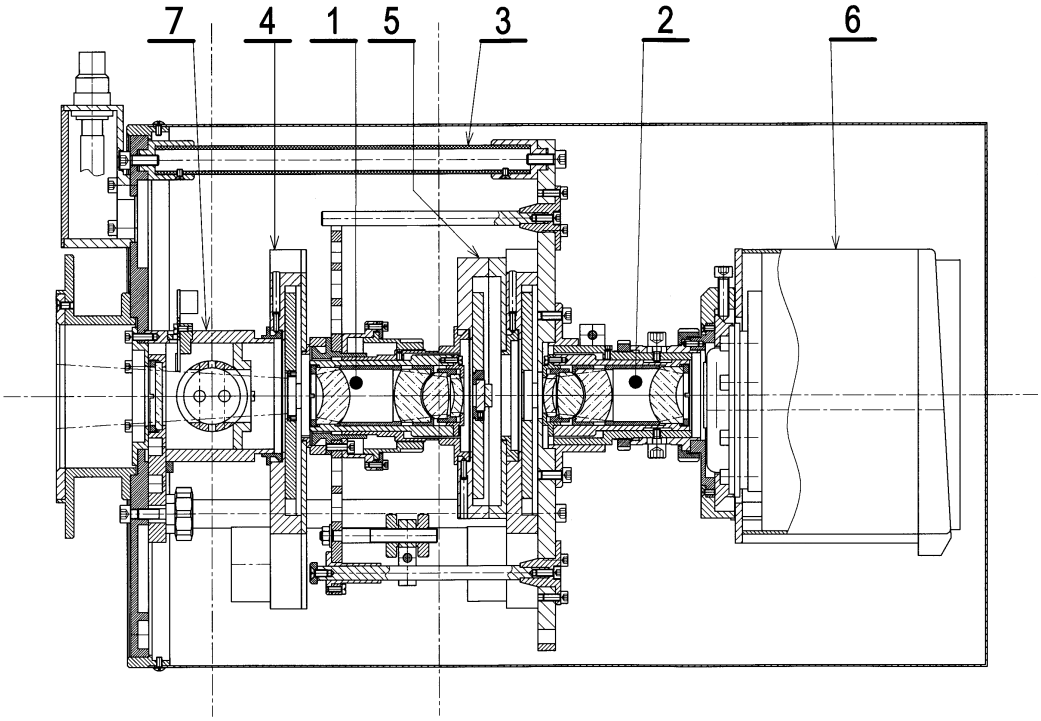

Figure 46 Schematic of COLORES: 1. collimator optics 2. camera optics 3. carbon fibre supporting structure 4. aperture wheel 5. grism and filter wheels 6. CCD camera 7. calibration lamps.

the atmospheric seeing, and different grisms in order to select the spectral resolution according to the need of the observation. The current detector is a 10241024 pixels device, with 13 micron pixels, but a different device (larger chip or different QE curve) could easily be installed to cover a different spectral range. The telescope is a rapid and lightweight design, and a low instrument weight was a significant constraint in the design as well as the need to be automatic and autonomous. See Table 14 for the principal parameters of the system. Rabaza et al. (2013) provides more insight into the optical layout of the spectrograph.

9.1 Observing with COLORES

IMAGING Simple imaging with COLORES is done the same way as with any other telescope equipped with RTS2. The user creates a target (**rts2-newtarget** on the command line) and assigns a script to it via **rts2-target**. One requirement specific to COLORES has to be mentioned, however: as it has three filter wheels, as the default position of the aperture wheel is closed,

and as the positions of the other wheels cannot always be 100a 300 s exposure in R-band:

```
rts2-target -c andor3 -s 'FILTA=open FILTB=open FILTC=R E 300' 1109
```

The camera is fringing-sensive, so actions have to be taken to get rid of it when observing in i', Z and Y. RTS2 provides a way to make a random position dithering, as ilustrated in the following chunk of a script:

```
for 5 { B2.WOFFS=(rand(-0.03,0.03),rand(-0.03,0.03)) E 180 }
```

This will take five 3 min exposure will be taken with a random 1.8′ dithering. After reduction, a median of these images would reperesent their fringing pattern, which then can be subtracted.

SPECTROSCOPY The preferred way to observe with COLORES is to pass **rts2-executor** a python script that uses the high-level programming of the spectrograph provided by colores.py, which in turn uses rts2comm to communicate with rts2.

A simple example of this is an all-in-one spectrum acquisition script **acquire.py**, which obtains a bias frame, the slit position, switches on a calibration lamp, waits for it to warm up, takes a λ calibration frame, ensures the focus is correct, identifies the field, re-centers the requested position on the slit, obtains a through-slit image and begins taking 5 minute spectroscopic exposures until terminated. Acquire.py and the underlying class colores.py are at this moment rather rudimentary reference implementations, but are expected to evolve into a complete observing tool as more experience is gained.

The target would get configured for spectroscopy by associating a script 'exe /etc/rts2/acquire.py' to it, for example the following way:

Table 15 COLORES overheads

Action	duration
16 bit full frame readout	1.250 s
14 bit full frame readout	0.532 s
filter change	0.4 s – 2.2 s (0.1 s + 0.3 s × dist.)
HgAr lamp warm-up	∼ 90 s
telescope slew	∼ 6 s or 10 s (no flip/flip)
telescope dither/correction	∼ 1 s

```
rts2-target -c andor3 -s 'exe /etc/rts2/acquire.py' 1109
```

for the target 1109. Then, the target has to be executed, by one of the many ways provided by RTS2, for example by **now** or **next** commands to the executor, or by including in a queue.

OVERHEADS When computing the time needed for different actions, a table of overheads may be handy, see table 15. RTS2 assures that some of these actions can be taken simultaneously under certain conditions, i.e. CCD readout and telescope dither or filter change are performed simultaneously. The CCD readout times may change substantially depending on the CCD camera setup. Recorded ones are those taken without any further changes in the configuration.

DARK AND FLAT FIELDS Dark frames and flat fields are obtained automatically at the beginning and end of the observing session, and typically the user does not need to take care of them. In case of some special needs - typical darkframes with an unusual exposure time, these can be done in daytime with $rts2 - scriptexec$, although care must be taken to first cool down the camera, as the cooling is usually switched off for daytime.

9.2 RTS2 interface

The spectrograph's electronics are represented in RTS-2 as a set of low level *devices*, summarised in Table 16. A script can control these individually.

Table 16 Different devices which represent the spectrograph in RTS2.

Name	function
COLORES	the spectrograph's microcontroller, which handles the calibration mirror, provides light levels, reports device temperatures, and can reset filter wheels
COLLAMP	a second microcontroller in the control computer, which controls the calibration lamps, can reset the focuser, and provides the dome ambient temperature
COLSLTW	the aperture (slits) wheel
COLGRSW	the grism wheel
COLFLTW	the filter wheel
andor3	the Andor iXon CCD camera
F0	the Optec focuser on the telescope's M2

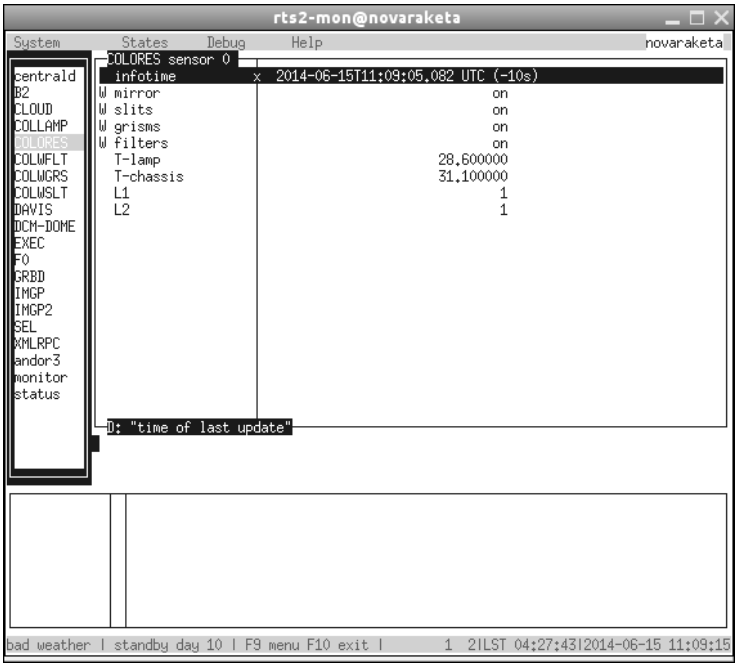

Figure 47 Rts2-mon with COLORES devices.

Two of these devices, COLORES and COLLAMP, are specific to COLORES, the others are standard RTS2 drivers for commercial components: the filter wheels are FLI filter wheel drivers **rts2-filterd-fli**, the camera is an Andor driver **rts2-camd-andor**, the focuser is an Optec TCF-2 driver, **rts2-focusd-optec**. How COLORES appears in the BOOTES-2 **rts2-mon** low-level device monitor is shown in Fig 47.

COLORES BOARD What is known as "COLORES" to RTS2, is an arduino-based microcontroller, responsible for internal management of the device. The driver binary is called **rts2-sensor-colores** and has been added to the RTS2 distribution. It is controlled via USB and provides access to reset lines for the filter wheels (so that they can be effectively turned off and on in software), has a stepper motor driver that moves the calibration mirror in and out of the optical path. It has two light-level sensors: at the instrument entrance window and inside the calibration lamp chamber; and two temperature sensors: on the physical structure of the grism wheel assembly, and on the calibration lamp chamber.

The device also provides 12 V for the CCD-cooling fan. The 12 V power is drawn from the computer, via a relay controlled by COLLAMP, and while the arduino is alive without this power, the filter wheels, calibration mirror,

Table 17 COLORES (device) programming interface

property	function
mirror	calibration mirror control. (on=sky, off=calib)
slits	slit wheel control. (on/off)
grisms	grism wheel control. (on/off)
filters	filter wheel control. (on/off)
T-lamp	temp chamber temperature
T-chassis	chassis temperature
L1	light level at the spectrograph entrance
L2	light level inside the lamp chamber

and CCD fan can all be turned off. The programming interface is given in the table 17.

COLLAMP BOARD This is another *arduino*-based board, inside the control computer, presented in RTS2 as COLLAMP. It operates an array of 8× 240 V triacs, to turn on and off the power to different subsystems: the calibration lamps, the focuser (to permit remote reset), 12V for the spectrograph electronics, and a halogen lamp mounted inside the dome. See table 18. The binary is called **rts2-sensor-colamp**. It also provides a measurement of the dome temperature.

IMAGE ORIENTATION As installed on BOOTES-2, COLORES images are oriented with the north-south axis horizontal and the east-west vertical, i.e. they come out rotated ±90° depending on the mount position. In this position, the system's weight is naturally symmetric on the optical tube and further weight compensation is avoided.

There is no derotator and the dispersion orientation is fixed along the horizontal (sky meridional) axis of the CCD and the slits are always vertical (equatorial).

For partial readouts of Andor EMCCD, readout time scales with the number of horizontal lines read, and is independent of the number of pixels read per line. So, for time-resolved spectroscopy it is advantageous to use a vertical slit and a horizontally oriented grism. However, this means that any column trap or bad column will cut always cross the horizontal spectrum and leave some wavelength bins useless, and is the reason why most instruments use a vertical spectrum, requiring only to position the star on a good column. In our case, we chose horizontal spectrum for high time resolution, with a supporting argument being that if one would expect instability

while pointing, it would be rather on the equatorial than the meridional axis. Mechanically, there is nothing to prevent a change of the spectrograph to a different configuration of either the CCD or the spectroscopic elements.

FILTERS The optical filter set consists of 28 mm diameter round filters. The table below shows the complete filter set with filter names, central wavelengths, FWHM and transmission at maximum.

APERTURES COLORES has 4 slits with different widhts: 25, 50, 75 and 100 μm, which translates into 1.2, 2.4, 3.6 and 4.8 arc seconds. There is also a 25 μm pinhole, presumably to be used while aligning the grism, but available to any possible application. Also, there is a hartmann mask, basically to perform optics testing. One position in the aprture wheel must be always left empty to provide an optical path for imaging (and pre-spectroscopy centering, as no spectroscopy can be done without imaging capability with COLORES). One other position is occupied by a blank, to allow for dark frames, as the CCD camera has no physical shutter.

9.3 Data reduction

WAVELENGTH CALIBRATION To perform the wavelength calibration, lines from the Hg/Ar calibration lamp are used (see Fig. 20). The response fits well with a second order polynomial,

$$\lambda = A + B \times (x_0) + C * \times (x - x_0)^2$$

yielding a centre wavelength $A = 782.44 \pm 0.05\, nm$, with dispersion at the centre $B = (0.7643 \pm 0.0003)\, nm/pixel$, and the change of the dispersion

Table 18 COLLAMP (device) programming interface

property	function
colores	12 V supply for the onboard electronics, (see COLORES device).
H	Hg/Ar lamp on/off
K	Kr lamp on/off
halogen	in-dome halogen lamp for dome flats
focuser	power for the optec focuser
dometemp	ambient temperature in the dome
switch[6-8]	currently unused triacs

Table 19 COLORES filter set

ID	Name	Cenwave (nm)	FWHM (nm)	Tmax[%]
1	SDSS g'	480	145	∼90
2	SDSS r'	620	140	∼90
3	SDSS i'	770	160	∼90
4	Bessel R	650	130	∼90
5	UKIRT Z	880	100	∼90
6	UKIRT Y	1020	200	∼50

along the X-axis $C = (53 \pm 1) \times 10^{-6}\, nm/pixel^2$. i.e. the resolution varies linearly from $\sim 0.71 - -0.79\, nm/pixel$ along the X-axis, being larger for longer wavelengths.

Given the dispersion and the width of the narrowest slit (25um = 1.923 pixels) we obtain the spectral resolution of the spectrograph of about 1.5nm. I.e. a doublet of 1.5nm separation should be just about distinguishable.

The slit position, and therefore also the position of the spectrum on the CCD is not perfectly stable due to mechanical deformation of the instrument. Further work is needed to find out how serious problem this is, but it is not expected to have more than a linear effect, i.e. the spectrum linearly shifts on the CCD.

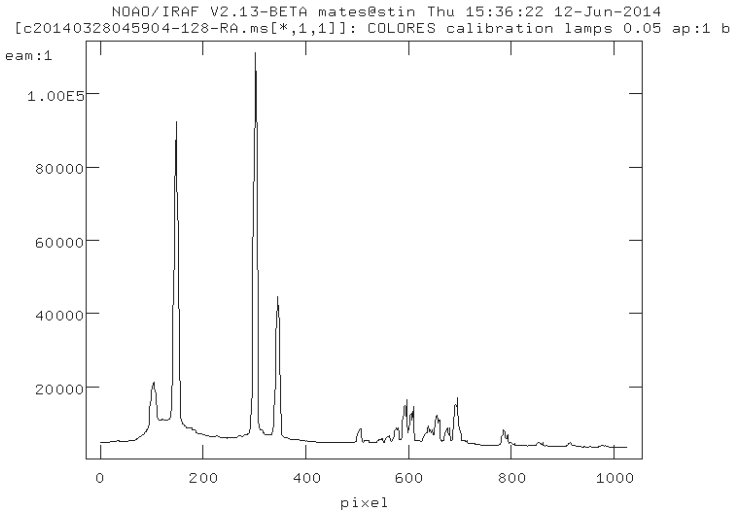

Figure 48 IRAF: Calibration spectrum of the mercury-argon lamp.

IRAF DATA REDUCTION For routine reduction we use IRAF, and the package **apextract**. The steps involved in reducing the spectrum are relatively straightforward. A good introduction on how to process the data is given in Massey et al. (1992), while this text provides a summary of relevant changes needed for COLORES data compared to the default **apextract** behaviour.

The first of these is the dispersion direction (horizontal vs. vertical), so **dispaxi=1** must be set to reflect this.

The second is that IRAF does not seem to provide a Hg/Ar lamp calibration spectrum, so an optimized set of calibration lines is provided in the file **/etc/rts2/hgar** on the BOOTES-2 computer.

There is an ongoing effort to implement a quick-lookup pipeline for BOOTES-2, which would provide real-time reduction of the obtained data.

Table 20 Lines used to do the grism wavelength calibration, lines used now in IRAF. Particular case of identification of image 20140328045904-128.fits.

CCD x-coordinate	Fitted λ	Lab λ	note
102.9	4046.7	4046.563	HgI
147.2	4358.0	4358.33	HgI
301.5	5462.8	5460.735	HgI
345.2	5778.8	5781.088	HgId
505.8	6963.7	6965.431	ArI
519.3	7066.0	7067.218	ArI
547.3	7279.7	7272.94	Ar
561.6	7389.2	7383.98	Ar
577.7	7513.3	7514.652	Ar
592.7	7629.1	7635.106	Ar
604.6	7721.3	7723.761	ArI
638.7	7986.4	-	2nd order HgI 4046
654.9	8112.4	8115.311	ArI
674.7	8266.4	8264.522	ArI
693.6	8413.6	-	2nd order HgI 4358
707.8	8524.4	8521.442	ArI
785.4	9123.5	9122.966	ArI
798.4	9223.3	9224.498	ArI
853.4	9649.2	-	2nd order Hg 5460 / refl.
914.1	10139.8	10139.76	HgI
977.4	10695.4	-	2nd order Hg 5460 / refl.

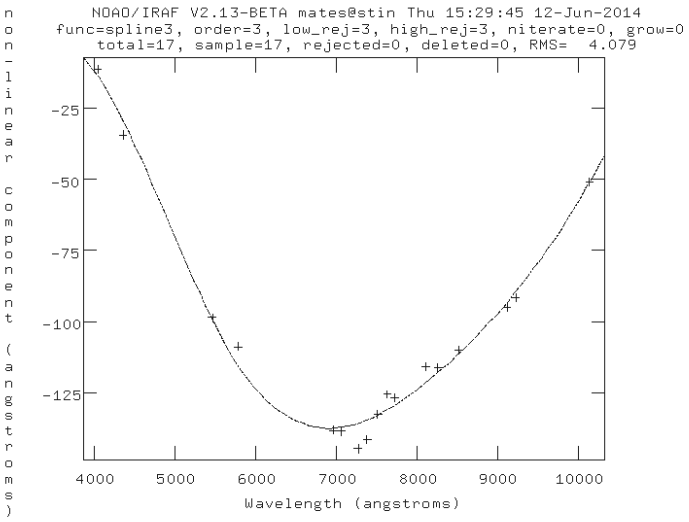

Figure 49 IRAF: nonlinear residuals of the dispersion fitting.

EMCCD CAMERA NON-LINEARITY A question has been raised about how non-linear is COLORES' CCD (an e2v CCD201-20). I tested this, using the capabilities of COLORES, and experience with the CCD. The challenge in this case is that the CCD response is reduced when all or most of the pixels have high counts than with a mostly dark field such as a star image - a psuedo-saturation effect, but we also cannot use a stellar image, as the stars are unstable due to atmosphere. The solution was to use the pinhole in the slit wheel with the HgAr calibration lamp, but with the mirror withdrawn (i.e. in the sky-observing, not the calibration, position). In this way we get a stable image with a constant brightness. The absolute brightness can then be controlled via filters in the filter wheel (I used no filter for non-EM and z' filter for electron multiplying mode. In theory CCD non-linearity should not depend on wavelength, as the effect occurs after charge production). I obtained 100 exposures from 0 to 1.0 s and used them as a base for a linear fit.

Results for the non-em mode are at fig. 51, where the CCD is linear within errors almost up to saturation. Then an effect (possibly related to saturation of a nearby pixel) is observed, and then saturation occurs. The CCD is reliably linear up to some 18000 counts.

The electron multiplying mode results are shown in fig. 50, the CCD is obviously non-linear, with the onset of non-linearity occurring at about 3500

counts. The non-linear part of the response curve can be fitted as

$$y = x * \left[1 + Bf\left(\frac{x}{ct}\right)^{\beta}\right]$$

where $f(x) = 0$ when $x < 1$ and $f(x) = x - 1$ otherwise. Least squares fitting provides the following values: $\beta = 1.55 \pm 0.28$ and $B = 0.26 \pm 0.17$ and the onset of nonlinearity $ct = 3490 \pm 730$.

9.4 Instrument maintenance and calibration

This section describes how to prepare the spectrograph for observation after mounting it: focusing the camera, focusing the slit, aligning the CCD withr respect to the sky, and finally aligning the slit(s) and grism(s) to the CCD chip. The calibrations are described in the order in which they are normally done after assembly. In certain situations, only some of the steps need to be performed.

OPENING AND CLOSING THE SPECTRGRAPH The spectrograph is enclosed in an aluminium bucket to protect it from mechanical and elemental damage, and which is held in position by two thumbscrews on the circumference of the base plate. To open the spectrograph, loosen (but do not remove) the thumbscrews and rotate the bucket clockwise for about 15 mm when it will be released and can be gently pulled off the device. Be careful when doing this, as there are many things inside that are easy to damage.

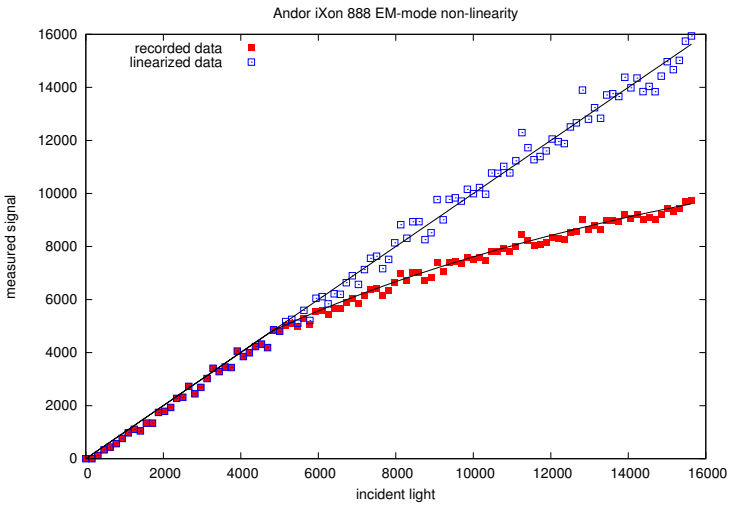

Figure 50 Andor CCD non-linearity in EM mode.

DISMOUNTING AND MOUNTING TO THE TELESCOPE Before dismounting the spectrograph, the telescope should be pointed to the zenith, switched off, and the counterweight supported. The last point is extremely important, as the loss of balance will cause the telescope to swing uncontrollably upwards even with the brakes on. The spectrograph is mounted to the telescope via six screws, requiring a number 10 hex key.

The six screws are for symmetry, but as one is normally inaccessible behind the instrument's connectors, it is therefore left untightened. The screws never need to be removed, as they pass through keyhole slots in the instrument's base, and the spectrograph is dismounted by by gently rotating it until the screw heads can be slid through the keyholes.

CAMERA CENTERING The spectrograph is equipped with the possibility of recentering the CCD chip on the optical axis, by adjusting the three screws which hold the CCD camera on the projecting lens. A practical way to do this is to place the spectrograph vertically on a table, pointing down, but permitting some light into the entrance (using spacers, say, two chopsticks). The screws holding the CCD camera (no. 6 on fig. 52) can then be released, and the CCD can then be be freely moved perpendicular to the optical axis, either by hand, or using the screws. We use the pinhole to define the optical axis, and the hartmann mask as a measure of point source distortion. The CCD is set to make images, while we search for an optimum camera position. When a satisfactory position is achieved, we tighten the adjustment screws well.

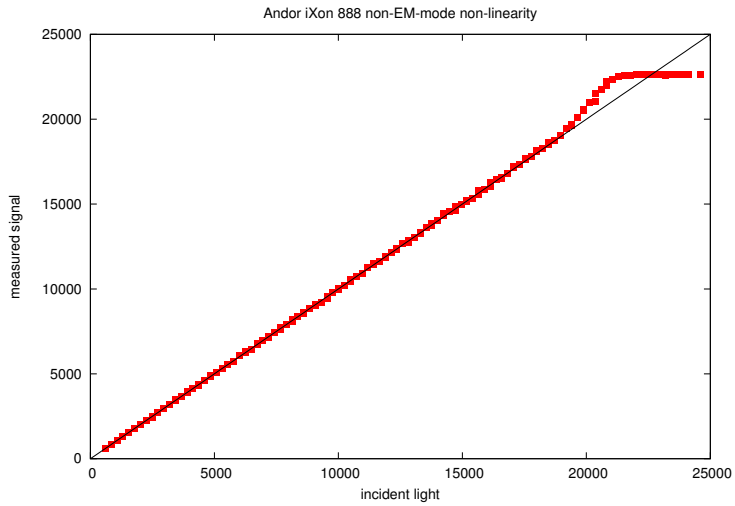

Figure 51 Andor CCD in non-EM mode is linear within errors.

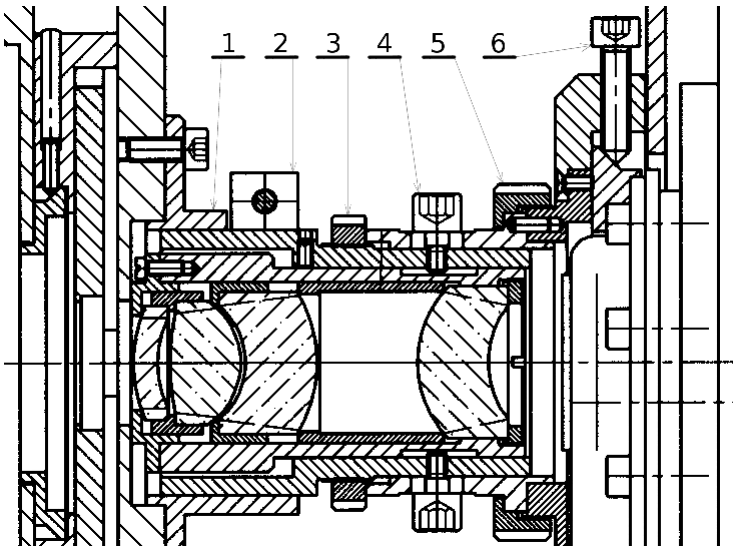

Figure 52 Detail of COLORES camera: 1. grism assembly extension tube 2. camera fixing ring + screw 3. adjustment ring 4. aretation screw 5. CCD mounting ring 6. CCD centering screw

CAMERA FOCUS The lens which projects the collimated beam to the CCD has to be focused to infinity. There are two and a half ways to do this.

One way is to point it to the sky and achieving the focus to stars. The other way is to use a test pattern and collimator, which is essentially the same technique but no stars are needed. A special case of the latter, the extra half way, is possible when we have not touched the collimator of COLORES, so that we may replace the camera and focus to a test pattern (hartmann mask) installed in the slit wheel.

When focusing the camera we first have to release it from the grism wheel assembly by relaxing the ring holding the camera and optics (no. 2 on fig. 52). This is a potentially dangerous operation if the instrument is pointing upwards, as the camera and optics may fall off. For this reason, a preferred way to focus using COLORES' own collimator is the same technique as described in *camera centering*, on a laboratory table, pointing down. The optical assembly barrel is fixed in place by two relatively large steel screws (no. 4 on fig. 52) on its circumference. When released, the optics can be moved in one direction (away from the CCD) by rotating the adjustment ring, in the other direction it has to be pushed by hand. When focused, the camera unit has to be reinstalled to the spectrograph such that the camera lens barrel touches its respective counterpart in the grism wheel assembly.

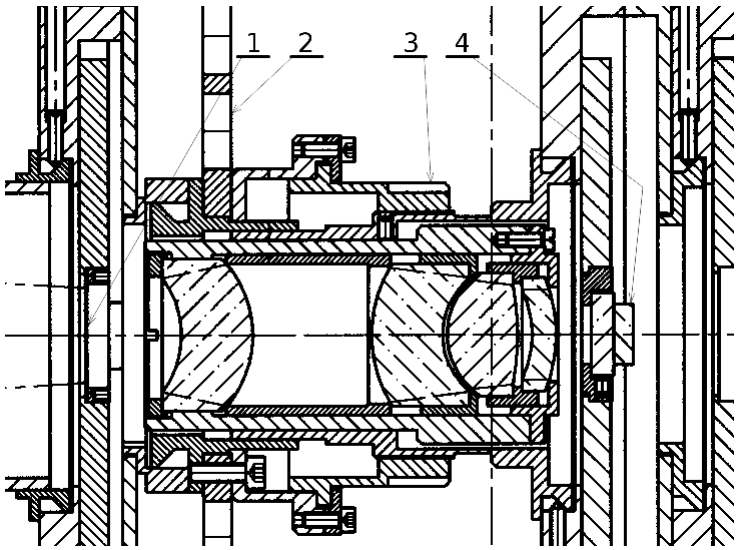

Figure 53 Detail of COLORES colimator: 1. aperture (slit), 2. support structure, 3. adjustment ring, 4. grism

SLIT FOCUS The spectrograph has a capacity to move the slit wheel against the collimator, which is fixed with respect to the grism assembly. The adjustment is done by the adjustment ring, which provides, similarly to the camera focusing, one-direction, i.e. push adjustment only. The pull is not provided and when passing through the focus, the slit wheel must be helped manually.

CAMERA ROTATION To adjust the rotation of the CCD camera with respect to the sky, the camera can be rotated without changing focus if the camera fixing screw (no. 2 on fig. 52) is relaxed. When in the desired position, it can be dismounted (e.g. for maintenance) by releasing the CCD mounting ring. It can then be returned to the spectrograph without loss of focus or set-up rotation angle, thanks to a position pin in the camera mount (no. 5 on fig. 52).

FILTER WHEELS The filters, slits, grisms and other optical elements may be exchanged and/or manipulated in the filter wheels without dismounting the instrument thanks to openings available on the rear side of each of the filter wheels. After unscrewing the cover, the filter which is on the opposite side to the optical axis, i.e. active position ±4, is available. The first wheel is in the optical plane of the telescope and is meant primarily for slits, it holds also a hartmann mask, a pinhole, and one empty space should lways

kept free for imaging purposes. This filter wheel is not for filters, by being so close to the focus, any imperfection in the filter would have a dramatic impact on the image quality. The second wheel is for filters, it can also hold a low dispersion, order separating, prism. The third, "grism" wheel has some extra space to permit for a longer grism, but is otherwise identical to the wheel which holds filters and can be used to hold more filters as well. The second and third filter wheel are in the parallel beam, so there should not be any need for refocus when changing filters during observations.

SLIT SETUP The slits are located in the first filter wheel and their rotation can be adjusted after slightly loosening their mounting screws using the holes in their mount. The spectrograph has a tool available for rotating them. Achieving the correct slit position is tedious work, done by trial-and-error, rotating the filter wheel 180 degrees between iterations.

GRISM SETUP The grism can be accessed behind the cover on the grism wheel. The filter wheel has to be rotated 180 degrees with respect to the position when the grism is in the optical path. Like the slits, the grism mount has small holes in the circumference of its mount and its rotation can be adjusted using the tool provided. To do this we place the pinhole into the slit wheel and adjust the grism until the spectrum produced is perpendicular to the slit. The mounting screws should be somewhat relaxed before, and tightened after, performing this action. Both slit and grism orientation can be adjusted in the laboratory.

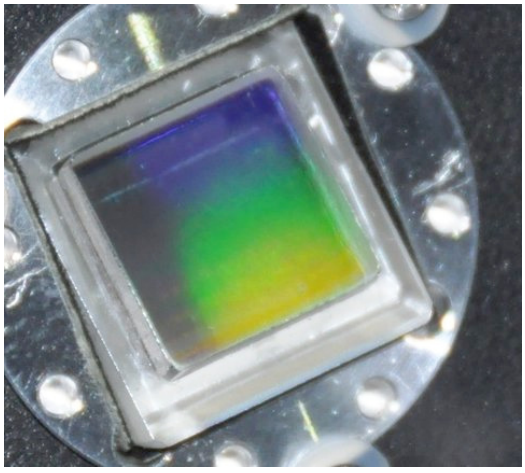

Figure 54 The Grism with its mount inside the filter wheel. Note the holes in the circumference of the mount to allow for rotation.

ENTRANCE WINDOW The spectrograph is equipped with an entrance window, which is fixed by one screw, and can be removed for cleaning by pulling it out with its mount.

9.5 Known issues

OPTICAL AXIS OFFSET During observation it was discovered that the optical axis seems to be shifted towards one side of the CCD chip and that the CCD camera mounting needs to be slightly modified, especially in the future versions of the instruments (considering this is a prototype).

GRISM MOUNT FAILURE During observations on X.X.2012, the grism was released from its socket and fell onto the fist collimator lens, and the grating surface of the grism was damaged. It was concluded that any future grism should be glued into their sockets. It was also decided to design and build two new grisms based on efficiency curves obtained from the first.

BENDING Although the spectrograph was carefully designed and constructed to be very stiff, an observable bending is present.

THERMAL STABILITY COLORES was originally designed with steel bars supporting the construction, but these were changed for carbon-fiber rods to reduce weight. No observation of thermal instability has been noted during the operation of the instrument.

LIQUID COOLING The spectrograph was constructed to use liquid cooling, both for the camera and the calibration lamp housing. This cooling was operating during the first summer, until the water pump failed. While waiting for a replacement, a large fan was installed to the rear of the CCD camera, which turned out to handle the heat well. Later the rear wall of the camera was replaced with one that fits the large fan permanently. As the calibration lamps also do not suffer from overheating, there does not appear to be any need for the water cooling.

GRISM EFFICIENCY We performed a simple test of the grism first order efficiency. The setup consisted of a 550nm green laser beaming through the grism, being diffracted into orders. A solar panel connected to an ammeter was used as a detector. We obtained an efficiency measurement of slightly above 50% for the grism only. A very similar result (55%) was obtained by comparing the signal level received with and without the grism inserted into the optical path while pointing to a standard star.

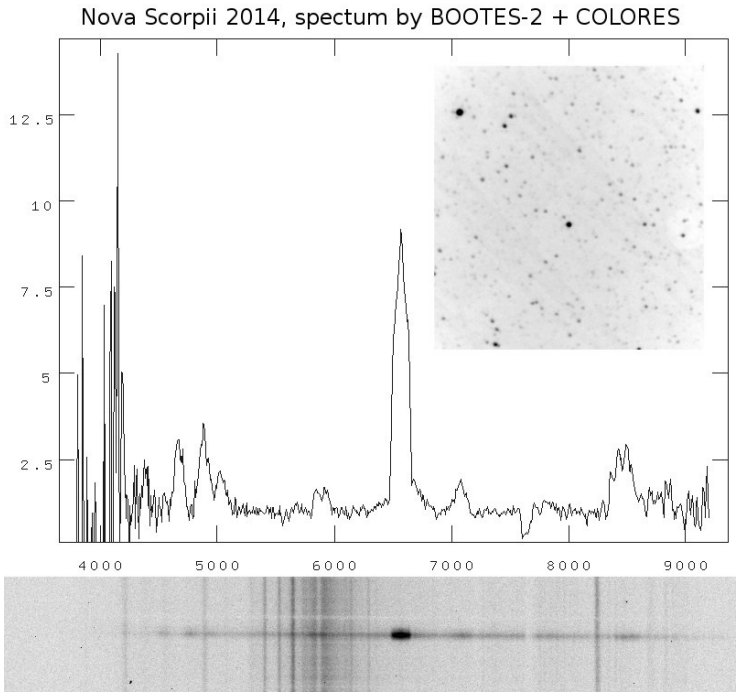

Figure 55 Nova Scorpii 2014 as observed by COLORES

9.6 Selected results

NOVA SCO 2014 We used COLORES to observe and confirm the nature of an apparent object on Scorpius discovered reported on March 27, 2014 by Koichi Nishiyama and Fujio Kabashima (via the IAU CBAT TOCP page), the spectrum shows emission lines of Balmer series, He I 501.6, 587.8, 706.5, and probably of O I 844.6, suggesting a nova in early phase (Nova Scorpius 2014) thus confirming the earlier suggestion by Ayani and Maeno (CBAT Transient Object Follow-up Reports). , see fig. 55 (Jelinek et al., 2014).

9.7 History

The idea of using a spectrograph on a GRB follow-up telescope must have occurred together with the first follow-up telescopes themselves. The 30 cm telescope BOOTES-1B was equipped with a field (slitless) spectrograph (de Ugarte Postigo, 2007). This device could now be considered a pathfinder to COLORES.

The definitive proposal "to try and build" a spectrograph for BOOTES-2 came when it was clear that a new 60 cm telescope (called TELMA, "Telescopio Malaga") would be installed at the BOOTES-2 station in about 2007.

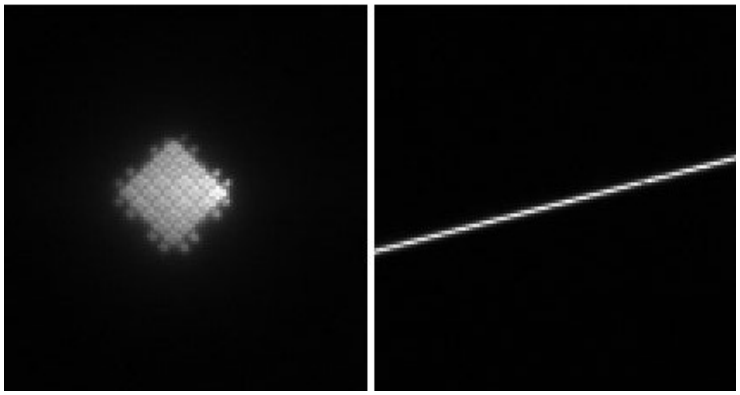

Figure 56 Two of the first images taken with COLORES while assembling it in the Turnov optical workshop. Left: the test pattern of the collimator used to focus the camera. Right: the narrowest 25um slit after focusing the system.

The idea was proposed by Alberto Castro-Tirado on the group meeting, Ovidio Rabaza offered to design the optics, and René Hudec with Jiří Zeman later agreed to support it and to do the mechanical design.

The optical and mechanical design eventually took 4 years to complete. COLORES was not a project bound by any specific terms and the design cycles were often interrupted by other works that had higher priority. Eventually in mid-2010 the mechanical design was complete. Manufacturing of the mechanical parts was started, but it was not finished until about June 2011, because of low capacity of the workshop and because of other projects taking priority occasionally.

During the Spring BART Workshop, the electronics, internal sensors and other important details were discussed in depth and the final shape of the onboard electronics was fixed.

In June 2011 the spectrograph was finally assembled for the first time, still without anodizing.

By the end of July the spectrograph was finally completed (without optics) after anodizing, and delivered to Soběslav for Martin Kákona to equip it with the onboard electronics.

The following week, the already-complete spectrograph was taken to the optical workshop in Turnov, where the optics were already prepared and the system was put in focus - the camera was focused on a testing pattern projected by a collimator, and the slit was simply illuminated and put into the focus. Also the filters were cleaned and installed in the system.

The spectrograph was by then missing the last part – the grism.

Somehow during the completation of the spectrograph the grism was al-

Figure 57 The finished optical assemblies for COLORES in the Turnov optical workshop. (left: camera, right: collimator).

ways put aside and so it eventually happened that it was finished last. The mount was done in Ondřejov, and the prism with the grating were glued in Turnov.

OSN 90 CM TELESCOPE Because of a failure of the BOOTES-2 mount, we searched for an alternative telescope to test the spectrograph, and we obtained technical time on the 90 cm telescope of the Sierra Nevada Observatory (OSN) during May 2012. The spectrograph was installed on May 4, and after two days of waiting for good weather, the night from May 6 to May 7, 2012 was the night when the first astronomical light was taken by COLORES.

COLORES AT BOOTES-2 COLORES was definitively installed onto BOOTES-2 in July 2012, when the telescope arrived from factory-refurbishment in ASTELCO.

References

A. de Ugarte Postigo. *GRBs, Universe and Everything.* PhD thesis, Universidad de Granada, 2007.

M. Jelinek, R. Cunniffe, A. J. Castro-Tirado, O. Rabaza, and R. Hudec. TCP J17154683-3128303 = Nova Scorpius 2014. *The Astronomer's Telegram*, 6025: 1, Mar. 2014.

P. Massey, J. Valdes, and J. Barnes. A user's guide to reducing slit spectra with iraf. *IRAF online spectroscopy documentation*, 1992.

O. Rabaza, M. Jelínek, A. Castro-Tirado, R. Cunniffe, J. Zeman, R. Hudec, and L. Sabau-Graziati. Compact low resolution spectrograph (colores), an imaging and long slit spectrograph for robotic telescopes. *Review of Scientific Instruments*, 84:114501, 2013.

X. Conclusions

This thesis is largely composed of selected results I have obtained or worked on during the past ten years. Six chapters contain studies of individual GRBs, one chapter traces the peroformance of BOOTES and the last chapter is an observing manual and technical documentation for spectrograph COLORES.

GRB 051028 was a burst discovered by HETE-2, observed also by *Swift*-/XRT. The optical afterglow was discovered by the author on images taken by the Himalayan Chandra Telescope 2.0m telescope. Based on the combined optical and X-ray data, we conclude that the reason for the optical dimness is not extra absorption in the host galaxy, but rather the GRB taking place at high-redshift. The non-detection of the host galaxy down to $R = 25.1$ is also consistent with the burst arising at high redshift, compatible with the published pseudo-z of 3.7 ± 1.8.

GRB 060117 was one of the brightest (both optically and in gamma-rays) busts ever to have been observed. The robotic telescope FRAM obtained unique optical data which show a peak brightness $R = 10.1$ mag and an unexpectedly rapid further decay. We present an interpretation featuring a relatively steep electron-distribution parameter $p \simeq 3.0$ and providing a straightforward solution for the overall fast decay of this optical transient as a transition between reverse and forward shock.

For the GRB 060904B a very interesting optical lightcurve is available, thanks to our high-resolution data obtained with the OSN 1.5m. It permits testing of distinct fireball model scenarios. The fast changes and well resolved behaviour seen in the lightcurve remains unexplained by the energy injections model.

GRB 080413A is a GRB observed by BOOTES-1B with a very short burst-to-image delay of $\sim$40 s. we use lightcurve modelling to propose the most likely scenario. In addition, this GRB seems to have happened in a large and bright galaxy, which we studied spectroscopically, the star forming rate was derived from both Ly-α and UV continuum, a comparison to an existing set of GRB-hosting galaxies shows this to be one of the brightest and metal-poorest galaxies to host a GRB.

GRB 080603B was a burst observed in colors by both BOOTES-1B and BOOTES-2, we study the spectral energy distribution and a break in the

lightcurve that happened during our observation. Our fit of the obained data provides the decay parameters $\alpha_2 = 1.23 \pm 0.22$ and $\beta = -0.53 \pm 0.06$, which suggest a slow cooling expansion into a stellar wind.

GRB 080605 was a GRB detected by BOOTES-1B and BOOTES-2. BOOTES detected a relatively steep decay index $\alpha = 1.27$ during the first 10 minutes after the trigger, in contrast to other observatories, which observed the optical emission later, between 1.5 and 6.5 h after the trigger, with a shallower decay rate of $\alpha_{\mathrm{late}} = 0.72$.

The penultimate chapter is a summary of all GRBs successfully observed by BOOTES-1B and BOOTES-2. It presents a total of 71 observations and 21 detections. Follow-ups by BOOTES-1B from 2005 to 2008 were given a special attention, and are used to study the efficiency of the system.

Th work concludes with a chapter dedicated to the spectrograph COLORES built for BOOTES-2. The chapter is concieved as a user's manual (which we hope this chapter would give base for), but provides also througher explications and deeper insight.

XI. Conclusiones

Esta tesis se compone en gran medida de los resultados seleccionados que he obtenido o trabajado durante los últimos diez años. Los GRBs son unos fenómenos más energéticos del Unverso, consecuencia en la mayor parte de a formación de un agujero negro en galaxias remotas. Seis de los capítulos que componen esta tesis contienen estudios de GRBs individuales, un capítulo detalla los resultados de BOOTES en la última década y el último capítulo es de caracter más técnico para el espectrógrafo COLORES, desarrollado por el docrorando.

GRB 051028 fue una explosión descubierta por HETE-2, observada también por *Swift*/XRT. La postluminiscencia óptica fue descubierta por el autor en las imágenes tomadas por el telescopio de 2.0m HCT en el Himalaya. Basándonos en la combinación de los datos ópticos y los datos de rayos X, llegamos a la conclusión de que el motivo para la baja emisión en el óptico no es la absorción extra en la galaxia anfitriona, sino más bien el alto corrimiento rojo (redshift) del GRB. La no detección de la galaxia anfitriona a $R = 25.1$ también es consistente con la explosión que surgió a alto corrimiento rojo, compatible con el publicado pseudo z de 3.7 ± 1.8.

GRB 060117 fue uno de los estallidos más brillantes (tanto ópticamente como de rayos gamma) que se hayan detectado. El telescopio robótico FRAM en Argentina obtuvo datos ópticos únicos que muestran un pico de brillo $R = 10.1$ mag y una caída de flujo inesperadamente rápida. Presentamos una interpretación que utiliza el parámetro de distribución de electrones relativamente alto $p \simeq 3.0$ y que proporciona una sencilla solución para el decaimiento rápido general de esta transición óptica a una transición entre las dos ondas cd choque ("forward shock" y "reverse shock").

Para el GRB 060904B se dispone de una curva de luz óptica muy interesante gracias a nuestros datos de alta resolución obtenidos con el telescopio de 1.5m del OSN en España. Permite testear los distintos escenarios contemplados en el modelo bola de fuego. Se pueden observar variaciones con alta resolución y la curva de luz no encaja bien con el modelo de las inyecciones de energía.

GRB 080413A es un GRB observado por BOOTES-1B sólo 40 s tras la emisión de rayos gamma. Utilizamos la curva de luz de modelado para pro-

poner el escenario más probable. Además, este GRB parece haber sucedido en una galaxia masiva y luminosa, la cual estudiamos espectroscópicamente. La tasa de formación de estrellas se deriva tanto de la línea Ly-α como del continuo UV. Una comparación con un conjunto existente de galaxias anfitrionas muestra que es una de las galaxias más pobres en metales y una de las más brillantes que albergan un GRB.

GRB 080603B fue una explosión observada en distintos filtros por ambos BOOTES-1B y BOOTES-2. Podemos estudiar su distribución espectral espectral así como un cambio de pendiente en la curva de luz que sucedido durante nuestra observación. Nuestro ajuste de los datos obtenidos ofrece un decaimiento con parámetros $\alpha_2 = 1.23 \pm 0.22$ y $\beta = -0.53 \pm 0.06$, lo que sugiere una expansión fría y lenta en un viento estelar, tras el colapso grvitacional de la estrella progenitora.

GRB 080605 era un GRB detectado por BOOTES-1B y BOOTES-2. BOOTES detecta un relativamente alto índice de decaimiento $\alpha = 1.27$ durante los primeros 10 minutos después del estallido, en contraste con otros observatorios, que observaron la emisión óptica más tarde, entre

El penúltimo capítulo es un resumen de todos los GRBs observados con éxito por BOOTES-1B y BOOTES-2. Se presenta un total de 71 observaciones y 21 detecciones. Los seguimientos por BOOTES-1B durante el período 2005 – 2008 tuvieron una atención especial, y la estadística más detallada se utilizó para estudiar la eficiencia del sistema.

Este trabajo de tesis concluye con un capítulo dedicado al espectrógrafo COLORES desarrollado por este doctorando para BOOTES-2. Con un enfoque más técnico mostrando un primer resultado cientifico lo que prueba la calidad del mismo.